For Reference

NOT TO BE TAKEN FROM THIS ROOM

University of Alberta
Department of Chemical and Petroleum Engineering

Flow of Clay - Water Slurries

II Design and Construction of a Concentric Cylinder Viscometer

J. F. Villiers-Fisher

August 9, 1951

Ex libris
universitatis
albertaensis

UNIVERSITY OF ALBERTA
QUAECUMQUE VERA

UNIVERSITY OF ALBERTA
LIBRARY

Regulations Regarding Theses and Dissertations

Typescript copies of theses and dissertations for Master's and Doctor's degrees deposited in the University of Alberta Library, as the Official Copy of the Faculty of Graduate Studies, may be consulted in the Reference Reading Room only.

A second copy is on deposit in the Department under whose supervision the work was done. Some Departments are willing to loan their copy to libraries, through the interlibrary loan service of the University of Alberta Library.

These theses and dissertations are to be used only with due regard to priority rights of the author. Written permission of the author and of the Department must be obtained through the University of Alberta Library when extended passages are used. When permission has been granted, credit must appear in the published work.

This thesis or dissertation has been used in accordance with the above regulations by the persons listed below. The borrowing library is obligated to secure the signature of each user.

Please sign below:

Date	Signature	Institution

Digitized by the Internet Archive
in 2017 with funding from
University of Alberta Libraries

https://archive.org/details/flowofclaywaters00jfvi

Thesis
1951
#65

THE UNIVERSITY OF ALBERTA

FLOW OF CLAY - WATER SLURRIES

II DESIGN AND CONSTRUCTION OF A CONCENTRIC CYLINDER VISCOMETER

A DISSERTATION
SUBMITTED TO THE SCHOOL OF GRADUATE STUDIES
IN PARTIAL FULFILMENT OF THE REQUIREMENTS FOR THE
DEGREE OF MASTER OF ~~APPLIED~~ SCIENCE

FACULTY OF ENGINEERING
DEPARTMENT OF CHEMICAL
AND PETROLEUM ENGINEERING

by

J. F. Villiers-Fisher
EDMONTON, ALBERTA,
DATE August 9, 1951.

ACKNOWLEDGEMENT

The author is grateful to Dr. G. W. Govier for his advice and criticism throughout this project.

The assistance, with the details of the design of the new viscometer, given by Mr. R. MacDonald is gratefully acknowledged.

The author appreciates the continued sponsorship of this project by the National Research Council of Canada, and by the Department of Chemical and Petroleum Engineering of the University of Alberta.

A note of thanks is due the many others whose advice has contributed so much to this project.

THE PROBLEM

The problem undertaken, to which this thesis is a partial solution, was the accurate determination of the rheological properties of certain clay - water slurries used in previous studies of the flow of non-Newtonian fluids. More specifically, the problem became:

1. A critical analysis of the suitability of both commercial and research type viscometers for the determination of the rheological properties of clay - water slurries and similar non-Newtonian fluids.

2. As a result of this analysis, to design, construct, and test a rotational viscometer suitable for the determination of the absolute consistency curves of any non-Newtonian fluids in the "viscosity" range of the aforementioned clay slurries.

3. Finally, to compare the consistency curves obtained with the new viscometer with,

(a) new data obtained with a modern Stormer viscometer, and (b) previously obtained data from an older model of this type of Stormer viscometer.

TABLE OF CONTENTS

PAGE NO.

Table of Contents

Lists of Illustrations

The Problem

Summary

I INTRODUCTION 1

II LITERATURE SURVEY 4

The Flow of non-Newtonian Fluids 4

Characteristics of flow in pipes at, or near, the onset of motion 4

Region of laminar flow in pipes 5

Region of turbulent flow in pipes 5

Laminar flow in a concentric cylinder rotational viscometer 6

Viscometers suitable for the Determination of the Rheological Properties of non-Newtonian Fluids 7

The capilliary tube viscometer 8

The theory of flow in the capilliary tube viscometer 9

The advantages and disadvantages of the capilliary tube viscometer 13

Analysis of the more important capilliary tube viscometers 14

The rotational viscometer 17

The geometry of the fluid boundaries 18

Table of contents continued

PAGE NO.

The onset of turbulence 22

The measurement of angular velocity and torque 24

Alignment of the cylinders 28

Desirable features of a rotational viscometer 29

The existing or proposed rotational viscometers for research and industrial control 31

III A SUITABLE VISCOMETER 41

Rheology 41

Suitable Type of Viscometer 41

Adaptability of available Viscometers 43

IV MECHANICAL DESIGN OF THE NEW VISCOMETER 44

Noteworthy Mechanical Features of some Rotational Viscometers 46

Final Design of the Viscometer 46

Mechanical Details of the New Viscometer 49

V OPERATION OF THE VISCOMETER 56

Alignment of the Viscometer 56

Filling and Cleaning the Viscometer 57

Measurement of the Rotor Speed 58

VI EXPERIMENTAL DATA WITH THE NEW VISCOMETER 60

Behavior with Newtonian Fluids 60

Calibration of the torsion wires 60

Behavior of Newtonian fluids between rotating concentric cylinders 73

Damping the oscillations 75

Table of contents continued PAGE NO.

Behavior with Clay - Water Slurries 78

Measurement of the rheological properties of clay-water slurries 78

Determination of the torque per inch of immersion 78

Measurement of the consistency curve 80

Interpretation of the consistency curve 82

Smoothing the data 83

Stability of the stator 88

VII EXPERIMENTAL DATA WITH THE STORMER VISCOMETER 89

Behavior with Newtonian Fluids 89

Calibration of the Stormer viscometer 89

Magnitude of the friction forces 91

Behavior with Clay - Water Slurries 93

The form of the flow boundaries 93

The consistency curves of the clay - water slurries 93

Smoothing the data 97

Comparison of the consistency curves of the new viscometer and the Stormer viscometer 99

Comparison of present and previous Stormer data 102

CONCLUSIONS 107

RECOMMENDATIONS 109

BIBLIOGRAPHY 110

Theoretical Derivations

APPENDIX A Analysis of Laminar Flow in a Straight Circular Tube A1

Table of contents continued PAGE NO.

APPENDIX B Kinetic Energy Correction in Capilliary Tubes B1

APPENDIX C Laminar Flow in a Rotational Viscometer C1

APPENDIX D Measurement of the Torque on the Base of the Inner Cylinder D1

APPENDIX E Calculation of the Volumetric Rate of Flow through straight tubes from the Absolute Consistency Curve E1

APPENDIX F Analysis of Torque - Angular Velocity Data for Bingham plastics F1

APPENDIX G Approximate Mechanical Force Balance on the Stormer Viscometer G1

Experimental Data

APPENDIX H Data from Rotational Viscometer H1

APPENDIX I Data from Stormer Viscometer I1

NOMENCLATURE (at end of Appendices)

LISTS OF ILLUSTRATIONS

FIGURE NO.	ILLUSTRATION	PAGE NO.
A	Cross-section of concentric cylinder rotational viscometer	47
B	Rotational viscometer	48
1	Calibration of Graham variable speed drive	59
2	Calibration of torsion wire #32	62
3	Calibration of torsion wire #32	63
4	Calibration of torsion wire #30	64
5	Calibration of torsion wire #28	65
6	Calibration of torsion wire #24	66
7	Calibration of torsion wire #22	67
8	Calibration of torsion wire #20	68
9	Determination of height equivalent to end effect	69
10	Determination of torsion wire constants from relative immersion	71
11	Torsion wire diameter as function of torsion wire constant	74
12	Settling as a function of torque and time	79
13	Torque - angular velocity curves for clay slurries	81
14	Yield value and mobility as function of percent solids	85
15	Yield value and mobility as function of percent solids	86
16	Yield value and mobility as function of percent solids	87
17	Viscosity as a function of load and speed for Stormer viscometer	90

FIGURE NO.	ILLUSTRATION	PAGE NO.
18	Viscosity as a function of load per revolution per second for Stormer viscometer	92
19	Correlation of flow boundaries with torque - speed data	94
20	Torque - speed curves for clay slurries for Stormer viscometer	95
21	Stormer yield value and mobility as functions of percent solids	98
22	Stormer yield value and mobility as functions of percent solids	100
23	Stormer yield value and mobility as functions of percent solids	101
24	Magnitude of friction in old model Stormer viscometer	104
25	Comparison of consistency curves	105
26	Effects of ratios of cylinder diameters on torque - speed curves	F3

Blue Prints (see notes on last page)

27	Cross-section of rotational viscometer	
28	Stator assembly	
29	Elevator assembly	
30	Rotor assembly	
31	Part #1 of main framework	
32	Part #2 of main framework	

DIAGRAM NO.	ILLUSTRATION	PAGE NO.
1	Capilliary tube viscometer	10
2	The onset of turbulence	25
3	Regions of safe operation of new viscometer	76

SKETCH NO.		
1	Typical consistency curves	2
2	Forms of conical bases	19
3	Delay in the onset of turbulence with increasing effective height to diameter ratio	22
4	Maximum wall thickness for over damping	27
5	Laminar flow in a circular tube	A1
6	Velocity distributions in a capilliary tube as a result of pressure gradients P and $P+dP$	A5
7	Plot of $\frac{Q}{\pi R^3}$ against $\frac{PR}{2}$	A6
8	Flow through a tube	B1
9	Laminar flow in a concentric cylinder rotational viscometer	C1
10	Relations between torque and angular velocity in a concentric cylinder rotational viscometer	C3
11	Shear stresses and velocity gradients across the annulus	C4
12	Surfaces of constant angular velocity in a rotational viscometer	D3
13	An absolute consistency curve	E2
14	Power per unit volume at radius R in a pipe	E3

SKETCH NO.	ILLUSTRATION	PAGE NO.
15	Evaluation of volumetric rate of flow	E3
16	Evaluation of volumetric rate of flow of a Bingham plastic	E4
17	Effect of annulus width on the torque - angular velocity curves for a Bingham plastic	F4
18	Absolute consistency curve and corresponding torque - angular velocity curve for a Bingham plastic	F4

SUMMARY

Further study of the characteristics of the type of Stormer viscometer, used in the previous investigations(10) of the flow properties of clay-water slurries, cast some doubt on the completeness of the data and the validity of its interpretation. Consequently, a detailed study was made of the suitability of other commercial and research type viscometers for the determination of the absolute consistency curves of this type of non-Newtonian fluid. The study indicated that none of the presently available viscometers would be entirely suitable for the clay-water slurries used in this investigation or those materials likely to be used in future investigations. A new viscometer was designed and constructed. This instrument is of the concentric cylinder rotational type employing a freely suspended inner cylinder, and designed to use a differential height technique to evaluate the end effects.

The behavior of the new instrument with calibrated Newtonian oils between 5 and 500 centipoises appears to be in good agreement with existing theories. The early onset of turbulence at the lower viscosities suggests that the annulus width may be too great. The elimination of the unpredictable onset of an oscillatory motion of the stator at higher rates of shear will almost certainly require some modifications to the design.

The data from the clay slurries also indicates that a narrower annulus would be advantageous since it is difficult to determine whether the more concentrated slurries should be treated as Bingham plastics. The onset of the oscillatory motion occurs much earlier with these fluids than with Newtonians.

The data, obtained with the new instrument, on the clay-water slurries is believed to be fairly reliable. Some modifications to the instrument, and possibly to the technique, will probably be required if more complete and more accurate data are desired.

A comparison of the data obtained with the new viscometer and a modern Stormer viscometer confirms the original concern over the interpretation of such Stormer data.

A comparison of the new data with that obtained in the previous investigation indicates the probable presence of important but indeterminate frictional effects in the old model Stormer.

I INTRODUCTION

The determination of the flow properties of Non-Newtonian fluids is of considerable theoretical and practical interest. The measurement of the absolute consistency curve of the fluid is a primary method of investigating the effects of particle size and composition on the quality of printing inks (11), and the effects of various additives on the gel strengths and flow properties of drilling muds used in the oil and gas industry (18). Another application of the absolute consistency curve is the prediction of the flow rates through pipes. The flow of slimes and tailings in the mining industry, of cement slurries in the construction industry, and of muds in the oil and gas industry, are probably the most commonly encountered applications. Methods of predicting the flow rates in the laminar flow region have been developed for those fluids whose shear stress is a unique function of the velocity gradient (Appendices C & E). However, no really satisfactory method of predicting, from the absolute consistency curves, the flow rates in the turbulent region has, as yet, been developed.

The long term object of this research program is to develop a satisfactory method of predicting the flow rates of non-Newtonian fluids in both the laminar and turbulent flow regions. In the initial investigation (10) the consistency curves of the slurries were determined by an old standard Stormer viscometer. A reinvestigation of the characteristics of the Stormer viscometer cast doubt on the validity of the interpretations placed on its data. Therefore, it was decided to find some indisputable method of determining the absolute consistency curves of these slurries, and to compare these data from the new instrument with the data

from the Stormer viscometer. This thesis is a partial solution of this problem.

Nomenclature:

In view of the general lack of uniformity of usage of the terms describing the various forms of consistency curves, it seems advisable to outline the definitions which will be used.

A consistency curve is a plot of the tangentially applied shearing stresses against their corresponding rates of shear, or velocity gradients, in the fluid. The forms of consistency curves which will be encountered are illustrated in Sketch #1 and are defined below.

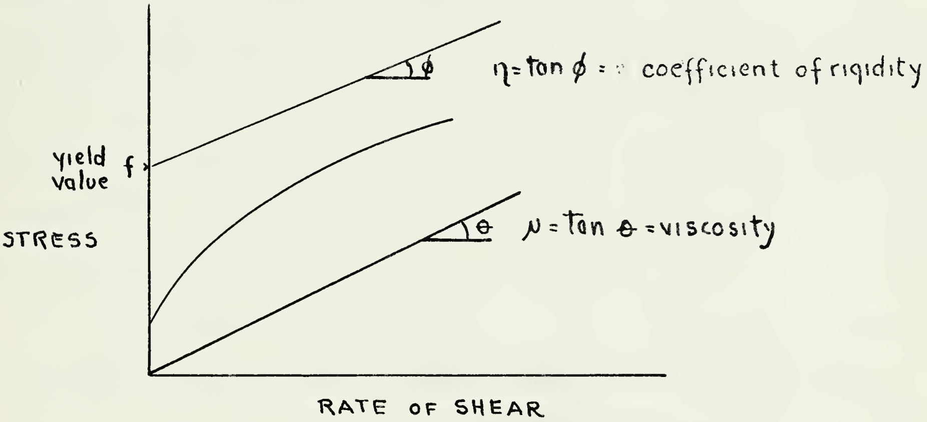

SKETCH #1. TYPICAL CONSISTENCY CURVES.

A Newtonian fluid is one which shows a linear relationship between stress and rate of shear, the plot of this curve passing through the origin. The slope, μ , of this line, as illustrated in Sketch #1, is called the viscosity.

The term non-Newtonian will be used generically to define any consistency curve which does not agree with Newton's hypothesis, defined above.

A Bingham plastic is a fluid which requires a definite stress, the yield value f, to initiate motion and thereafter shows a linear relationship between stress and rate of shear. The slope, η, of this line is called the coefficient of rigidity (3). The reciprocal of the slope of this line is called the mobility.

A plastic fluid is one which may, or may not, require a definite stress to initiate motion but the relationship, illustrated in Sketch #1, between the stress and the rate of shear is non-linear.

A thixiotropic fluid is any fluid whose shearing stress is an isothermal reversible function of the rate of shear history (11)

Anomalous behavior is, as the name implies, any deviation from the behavior assumed for the class.

II LITERATURE SURVEY

THE FLOW OF NON-NEWTONIAN FLUIDS.

The following experimental evidence, of the flow of materials approximating a Bingham plastic, is presented in order to illustrate the patterns of flow of such fluids in pipes and between rotating concentric cylinders and to indicate a few of the abnormalities which may be encountered in such fluids.

Characteristics of Flow in Pipes at, or near the Onset of Motion.

Green (11) examined, by means of a microscope, the flow characteristics of a number of suspensions in a capilliary tube. The majority of suspensions behave, at high concentrations, somewhat like Bingham plastics. At the onset of motion, which required a definite applied force, the whole mass moved as a solid plug. At the wall of the tube, an extremely narrow layer was found to be in laminar motion but, at times, the carrier fluid acted as a lubricant between the plug and the tube wall.

Green and Halsam (12) measured the relationships between the pressure drop and the volumetric rate of flow through capilliary tubes for about eighty different suspensions. They found that the plots of these variables never extrapolated through the origin, indicating that any lubricating action of the carrier fluid is incomplete. Scott-Blair and Crowther (29) found that etching the tube wall materially reduced the degree of this lubricating action. They also found that the relative magnitude of this wall effect became negligible with wide capilliaries at higher flow rates.

The Region of Laminar Flow in Pipes.

Green (11) with the aid of a microscope, and Pichot (21) by chronophotography, measured the velocity distributions of plastic fluids in capilliary tubes. They found the velocity distribution to be parabolic becoming asymptotic to a zone of constant velocity near the axis of the tube. This general velocity distribution agrees with that predicted by Buckinghams equations (7) for the flow of a Bingham plastic through a pipe.

Green (11) tested Buckinghams equations experimentally and found excellent agreement. He emphasizes the mechanical difficulty of interpreting the pressure drop-rate of flow data in terms of yield value and mobility.

The Turbulent Flow Region in Pipes.

No investigations similar to Reynolds classical experiments appear to have been reported on the turbulent flow of Non-Newtonian fluids. However, a number of attempts have been made to correlate the pressure drop-rate of flow data for Bingham Plastics in turbulent flow.

Babbitt and Caldwell (3) defined the apparent viscosity, μ', of the fluid as the viscosity found from Poiseuilles equation if the fluid is assumed to be Newtonian. This apparent viscosity is then substituted into Buckinghams equation (7) to yield the relationship $\mu' \simeq \frac{Df}{6V} + \eta$ where V is the average velocity and D is the pipe diameter. They then assume a critical Reynolds number, $\frac{DV_c\rho}{\mu'}$, of about 2500, where V_c is the critical velocity and ρ is the fluid density. The critical velocity is obtained by solving these equations for V_c. For flow in the turbulent region they defined a friction factor, F, equal to $\frac{PD}{2V^2\rho}$, where P is the pressure gradient. Then, for a

given fluid, a "turbulent viscosity" is found by experiment which yields a value of F equal to the Fanning friction factor for Newtonian fluids. Their data on suspensions appears to confirm these theories. They found that the "turbulent viscosity" of their sludges was the viscosity of the carrier fluid, water.

However, others (4, 22) have reported "turbulent viscosities" ranging between 2 and 12 centipoises for water based muds. Beck, Nuss and Dunn (4) found that better agreement could be obtained if a Reynolds number of $\frac{3{\cdot}2DV\rho}{\eta}$ was used in the turbulent region.

Govier and Winning (12) used dimensional analysis to obtain the relationship $\frac{PD}{V^2\rho} = \phi\left(\frac{Df}{V\eta}, \frac{DV\rho}{\eta}\right)$ between the measured variables. Their plots of these variables, from the data for a series of clay - water slurries, shows a rather strikingly symmetrical pattern. However, the validity of their consistency curves is doubtful.

All the above mentioned workers found that the effects of the yield value disappear at high velocities.

Laminar Flow in a Concentric Cylinder Rotational Viscometer.

The geometrical form of the flow between two rotating coaxial cylinders, which is dissimilar to that of the flow through a pipe, has proven amenable to mathematical analysis (Appendix C). At equilibrium, a torque balance on the system shows that the stress on any cylinder of fluid, coaxial with the rotating cylinder, varies inversely as the distance from the axis of the system. Now, Since stress is proportional to the velocity gradient, it would be expected that more and more fluid, for a Bingham plastic, would undergo laminar flow as the velocity of the rotating cylinder increases This has been confirmed by many workers(25, 26, 36).

Probably the simplest method of illustrating this effect is that suggested by Roller and Stoddard (26). They poured a line of charcoal dust across the surface of the fluid in an annulus, and examined its motion as the velocity of the inner cylinder was increased. At one speed, the inner portion of the fluid caused rapid diffusion of the dust around the inner cylinder, while the portion adjacent to the outer cylinder remained undistorted. As the velocity increased, the length of the undistorted line decreased until, finally, all the dust was dispersed over the surface of the fluid.

VISCOMETERS SUITABLE FOR THE DETERMINATION OF THE RHEOLOGICAL PROPERTIES OF NON-NEWTONIAN FLUIDS

If, in a given system, an applied force acts to produce a shearing stress in a fluid, and this applied force and the resultant rates of shear can be determined directly, or by inference, from the reactions of the system, then, in theory, this system may be used as a viscometer. The variety of types which have been used is confirmation of this statement. In practice, however, only a few simple geometric patterns have proven amenable to mathematical analysis - a prerequisite for their use in measuring the absolute consistency curves of non-Newtonian fluids.

The Geometric Forms Presently Amenable to Mathematical Analysis.

If a fluid exhibits neither thixiotropic nor anomalous behavior, the consistency curves may be evaluated from the data obtained with the following instruments: straight tubes of constant circular cross-section; rotating coaxial concentric

cylinders; under certain conditions rotating concentric cones with a common apex; and, for Bingham Plastics only, rotating parallel discs if the ratio of the clearance to the diameter approaches zero. If the fluid exhibits thixiotropic behavior, the only practical means is the rotating concentric cylinder viscometer, with or without concentric cones, in which the ratio of the annulus width to the radius is very small.

The Capilliary Tube Viscometer

The capilliary tube viscometer will be treated first since it is the oldest and most widely used of all the types of viscometers. It was in just such an instrument that Poiseuille experimentally confirmed Newtons' hypothesis that the velocity gradient is directly proportional to the shear stress. It was also in such an instrument that Bingham (5) investigated the flow properties of suspensions, and brought to general attention the fact that this class of fluids does not obey Newtons hypothesis.

Since a great deal of the research on the rheology of fluids has been done with capilliary tubes, the principles and techniques of their operation have been thoroughly worked out. This continuous study of the instrument has led to the development of simple forms which eliminate, or render negligible, such extraneous effects as: entrance and end effects, surface tension errors, and variable driving forces. It has also led to the development of a number of industrial instruments, such as the Saybolt, which are, mechanically, very closely reproducible but whose use is limited to very specific applications.

In order to determine which types of capilliary tube viscometers are suitable for the measurement of the absolute

consistency curves of Non-Newtonian fluids, a general understanding of the theory of flow in such instruments is essential.

The Theory of Flow in a Capilliary Tube Viscometer.

It has been shown (Appendix A) that it is possible to evaluate the consistency curve of any fluid, which exhibits neither thixiotropic nor anomalous behavior, from the measurements of pressure drops and the corresponding volumetric rates of flow through tubes of known dimensions, a minimum of two different diameters being necessary to distinguish anomalous or thixiotropic behavior.

In practical capilliary tube viscometers, the measured pressure drop includes such errors as entrance effects, kinetic energy losses, and surface tension effects; and the measured volumetric rate of flow may be subject to the effects of drainage errors, and, in some cases, uneven surfaces.

Consider the case of a capilliary tube viscometer in which the driving force is the fluid head and the measurement of the volumetric rate of flow is accomplished by determining the time for the liquid, in either resevoir, to move between two known points.

In the capilliary tube viscometer, illustrated in Diagram #1, the overall driving force is the differential fluid head. The pressure gradient along the capilliary will therefore vary with time. This variation will be modified somewhat by the net lifting force caused by surface tension and by the portion of the driving force which corresponds to the kinetic energy of the fluid travelling through the capilliary, which energy is ultimately degraded to thermal energy in the lower resevoir. Corrections for these modifications are greatly complicated in this instrument

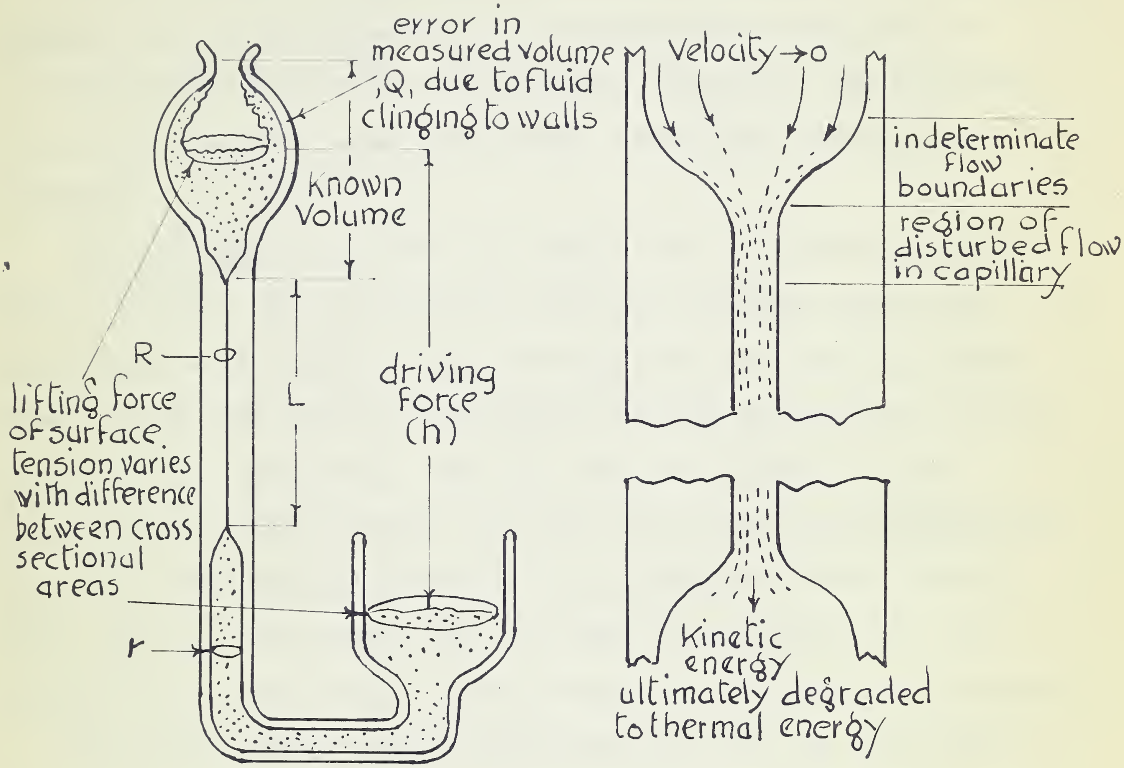
error in measured volume ,Q, due to fluid clinging to walls
Known Volume
R
L
driving force (h)
lifting force of surface tension varies with difference between cross sectional areas
r
Velocity→0
indeterminate flow boundaries
region of disturbed flow in capillary
kinetic energy ultimately degraded to thermal energy

1(a)

1(b)

DIAGRAM #1 A CAPILLARY TUBE VISCOMETER

by their variation with time.

If the effects of surface tension and kinetic energy may be neglected, the average driving force may be determined, for Newtonian fluids, from the basic equation of flow $dQ = \frac{\pi R^4 h g \rho}{8 \mu L} dt$ (14). The solution of this equation requires a knowledge of the relationship between the volume, Q , and the height, h . It is impractical to evaluate this equation for non-Newtonian fluids since the solution depends on the knowledge of the relationship between the shear stress and the velocity gradient.

In any case, assume for the moment that the average fluid head is known. Then the desired pressure gradient along the capilliary is the ratio of the driving force of the fluid head minus the surface tension and kinetic energy corrections, to the length of the capilliary. But the effective length of the capilliary is indeterminate. In the first place, the flared ends represent some unknown length of capilliary, and in the second place some unknown length must be added to compensate for the region of disturbed flow, Diagram #1b, at the capilliary entrance.

Returning again to the Diagram #1a, it will be seen that a layer of fluid remains on the walls of the upper resevoir. With plastic fluids having an appreciable yield value, this layer may be so thick that it introduces a very appreciable error into the measurement of the volume passing through the capilliary.

In the light of the foregoing discussion, it will be seen that a good capilliary tube viscometer for non-Newtonians should possess the following features:

a) Ideally, the net fluid head over the period of the run should approach zero. In any case, the average fluid head should

be a small portion of the driving force. Both of these methods require some external drive such as compressed air, but the problem of providing constant pressure air is simple compared with the problem of evaluating the mean driving force for non-Newtonian fluids.

b) The resevoirs should be so shaped that the surface tension forces are always equal and opposite.

c) The ratio of the volumetric rate of flow to the driving force should sufficiently small that the kinetic energy correction is unimportant (Appendix B)

d) The entrance and exit of the capilliary tube should be as nearly square ended as possible so that its length may be accurately measured. Admittedly this does not solve the problem of the length equivalent to the distorted flow at the entrance, but the system is at least reproducible.

e) The volume of the fluid passing through the capilliary should be measured in the receiving resevoir. If the fluid is opaque this is important, even with Newtonians.

Several other factors must be considered in the selection of a suitable capilliary tube viscometer. Since the theory of flow only holds in the laminar region, the diameter of the capilliary must be small. However it must be very much larger than the largest particle in the fluid. With dilute, or coarse suspensions, the effects of settling may be large. In this case, the relationship between the driving force, the tube diameter, and the resevoir size must be such that settling is negligible over the period of the run. Finally, the ratio of the capilliary length to its radius must be so large that entrance effects are negligible. In other words, a set of the above described capilliary tube viscometers having different capilliary lengths and

length to diameter ratios is advisable for non-Newtonian fluids.

The Advantages and Disadvantages of the Capilliary Tube Viscometer.

For fluids whose velocity gradient is a unique function of the shear stress, that is for fluids which exhibit no thixiotropic behavior, no appreciable settling and no anomalous effects at the wall, the capilliary tube viscometer, if well designed, is the most precise instrument available. It is, of course, of little value for thixiotropic fluids or for suspensions with high settling rates since the pressure gradient - rate of flow data cannot be interpreted mathematically.

When made of glass, the usual case, its resistance to abrasion and corrosion is far superior to that of the other types of viscometers.

When time is not an important factor, the great advantage of low cost is a most important asset. When, however, such instruments are in continuous use, the cost of labour may far outweigh the initial savings.

This instrument is unfortunately rather fragile, though it is somewhat more rugged than a good rotational viscometer. In view of the fact that the average person is more careless with a cheap instrument than with a very expensive one, this advantage may not be realized.

As with all instruments, certain types have their own peculiar advantages and disadvantages for their specific tasks. The question is, which of the available or proposed capilliary tube viscometers would be the most suitable instrument in which to measure the absolute consistency curves of the clay slurries in question.

An Analysis of the More Important Capilliary Tube Viscometers.

The capilliary tube viscometer has long been recognized as the standard means of measuring viscosities. Some, particularly the Bingham Plastometer, are capable of measuring this property to a high degree of accuracy since the errors, outlined previously, have been reduced to negligible quantities. Others, such as the Saybolt viscometer, are only valuable under restricted conditions since all the aforementioned errors are present to a high degree. The remainder of this section will be devoted to a more detailed analysis of these and other capilliary viscometers.

(a) The Bingham Plastometer. (14)

This viscometer practically eliminates all the normal errors encountered. The fluid resevoirs, which have the form of identical truncated cones joined at their bases, are level with each other so that the net fluid head by the end of the run approaches zero. As well, the free surfaces of the fluid are always identical, cancelling the surface tension effects. The almost square ends of the capilliary permit accurate measurement of its length. With the large length to diameter ratio normally employed, the entrance effect is negligible. The only correction necessary is therefore the kinetic energy correction.

With plastic fluids having an appreciable yield value a small net fluid head may exist since one resevoir must be slightly overfilled to account for the fluid holdup on its walls. The narrow taper at the resevoir apex is most advantageous with this type of fluid since it minimizes any irregularities of the fluid surface and reduces the chance of voids occuring at this point.

b) The Ubbelohde "Suspended Level" Viscometer. (35)

In this capilliary tube viscometer, the driving force may be either the head of fluid in the spherical glass resevoir or this augmented by compressed air. The capilliary exit is so designed that the fluid leaving the capilliary will flow out and around the walls of the lower resevoir in such a manner that the net effect of surface tension approaches zero. Whether this is the case for plastic fluids is questionable. The length to diameter ratio is high and the capilliary ends are nearly square.

While it is an excellent instrument for most Newtonian fluids, it is not so suitable for non-Newtonians. The main disadvantages are the variable fluid head, whose effect may be minimized by the use of compressed air, and the measurement, by the change in fluid level in the upper resevoir, of the volume discharged.

c) The Ostwald Type Viscometer. (4)

This name has become almost generic for a certain class of viscometer employing only a differential fluid head and a relatively short capilliary tube. This differential, variable, fluid head coupled with the short capilliary, with its tapered entrance and exit, and the unsymmetrical fluid resevoir prohibit its use with non-Newtonians. Indeed, it must be comparatively calibrated for use with Newtonians. The equation which relates this calibration with the relative viscosity of the unknown fluid is

$\mu' = \left(\frac{\mu}{\rho T}\right) \rho' T'$ (14). where μ is the known viscosity, ρ the density and T the time of efflux of the standard fluid, and where the superscripts refer to the unknown fluid.

The main value, and use, of this instrument is for control in which case it is a simple, cheap, and rapid instrument, particularly where the density term may be ignored.

d) The Efflux Type Viscometers

The efflux type of viscometer is a class which employs a capilliary tube which is so short that it might be better described as a short tube or an orifice. The relative magnitudes of the kinetic energy and the entrance effects are so large that, even if the variable fluid head could be neglected, the use of these viscometers with non-Newtonians would be questionable. Even with Newtonians, they are only suitable for measuring relative viscosities. However, their importance in certain industrial applications warrants more than passing mention.

Three of this class, the Saybolt (2, 14), the Redwood (14), and the Engler (14), are so closely standardized mechanically that individual calibration is not really essential. As well, for the petroleum hydrocarbons wherein they find their widest application, charts are available which correlate the kinematic viscosity with temperature over a wide range of these variables. The choice between the types is really one of tradition, the Saybolt being peculiar to North America, the Redwood to the British Isles, and the Engler to Germany. Hatschek (14) gives a short table correlating the kinematic viscosities measured by the respective types.

The Marsh Funnel (6), widely used in the oil and gas drilling industry to give a semi-quantitive measurement of the consistencies of drilling fluids, is another of this class. It consists of a metal cone, holding about a quart of fluid, whose apex is sufficiently truncated to recieve a 2 in. length of 3/16 in. I.D. copper tube. In practice no corrections are made for the mud density. Indeed, the muds are often so highly thixiotropic that such a correction is unwarranted. Its great advantages are its low cost, ruggedness,

and the wide capilliary which is not particularly affected by the presence of small cuttings.

e) Rising Column Viscometer (30)

This novel viscometer was primarily designed for Newtonians between 10^3 and 10^5 poises. The fluid is driven up the capilliary by compressed air. The rate of rise of the free surface in the capilliary is determined by a cathetometer capable of measuring a rise of 2 mm. within 0.5%. An excellent outline of the theory and method of designing such an instrument is given in the afore designated reference. Unfortunately, the theory is valid for Newtonians only.

The chief advantages of the instrument are the ease with which gas bubbles may be removed from the sample - an important consideration at these viscosities; the ease of temperature control (which should be kept within 0.02 deg. C. to hold the viscosity constant within 2% (30); and the very small sample required. The great disadvantage is the restriction to very low shear rates.

The Rotational Viscometer

The versatility, ease of operation, compactness, and ruggedness, of the rotational viscometer has led to its widespread use as an industrial control instrument. The disadvantage of its inherently high cost is often outweighed by its speed of operation and by the fact that, suitably designed, it is the only instrument capable of determining the absolute consistency curve of almost any type of fluid.

To date, the theory of the flow of Non-Newtonian fluids in this instrument is restricted to the case of laminar flow in the

annulus between rotating coaxial cylinders and, or, rotating coaxial cones having a common apex, providing, in both cases, the width of the annulus is small compared to the radius of the rotor (Appendix C). An approximate analysis is possible, for certain fluids, in the case of rotating parallel discs if the ratio of the clearance to the radius is very small.

In those types where the flow boundaries are too complicated for mathematical analysis, which covers the majority of the industrial viscometers, the instrument is often calibrated with Newtonian fluids and the apparent viscosity of the fluid is then determined at some arbitrary angular velocity or velocities. While such techniques may yield an idea of the characteristics of the fluid, it is doubtful whether such data would be of much value in predicting pressure drop - rate of flow relationships in pipes.

The remainder of this section will be devoted to an analysis of the general features of those rotational viscometers which may be used to determine the absolute consistency curves of non-Newtonian fluids. It is also designed to serve as a background for the analyses of the characteristics of a number of research and industrial viscometers.

The Geometry of the Fluid Boundaries.

Since the theory for the rotating parallel discs is confined to Bingham plastics and Newtonian fluids, and since it is not only difficult to interpret the data for other than Newtonians but it is also difficult to build such an instrument, the remainder of the discussion will be confined to the concentric cylinder and the coaxial cone forms of the boundaries.

Where it may be employed, the conicylindrical form is the most convenient since it reduces the number of measurements required to determine the consistency curve of the fluid, and it has the added advantage of providing a lower bearing to the system. The chief disadvantage of this form is the added expense of providing for precise location in the vertical plane, since the cones must have a common apex.

There are three general forms of the conical base. The first employs a truncated cone, the second employs a needle point bearing on a jeweled or hardened surface, and the third employs the apex of the inner cone as the needle point bearing. These three forms are illustrated in Sketch #2.

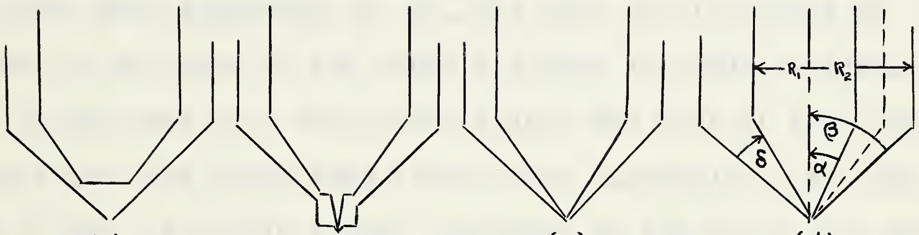

(a) Truncated cone (b) needle point (c) common apex (d) critical dimensions

SKETCH #2. FORMS OF CONICAL BASES.

In all cases the angle δ is so chosen that the rate of shear between the cones is nearly equal to that in the annulus. Mooney and Ewart (19) have shown that this will be the case when:

$$\delta = (\beta-\theta)2 = (\theta-\alpha)2 = \frac{R_2^2-R_1^2}{R_2^2+R_1^2}\sin\theta + \left(\frac{R_2^2-R_1^2}{R_2^2+R_1^2}\right)\left(\frac{3}{8}\sin^3\theta-\frac{1}{2}\sin\theta\right)$$

where θ is any arbitrarily chosen and convenient angle. The height of the cylinder equivalent to the torque on the base is then

$$\frac{R_2-R_1}{2}\left(\frac{1-\cos\theta}{\sin\theta}\right) \qquad (2)$$

While method (a), in Sketch #2, eliminates the friction at

the base, it necessitates provision for accurate, reproducible, location of the inner cylinder. Method (b) is almost frictionless and is not affected by the presence of a few small particles in the bearing, but it is very fragile and rather difficult to construct. Method (c) produces a rather large amount of friction and is, as well, very difficult to construct. This method is particularly sensitive to the presence of any small particles.

The simple cylindrical system is, at present, the most popular form of the instrument since it is much cheaper and inherently more rugged than the conicylindrical system. Admittedly, it may necessitate an extra set of measurements to evaluate the end effect. The evaluation of this end effect is the main problem with this system.

It has been suggested (8, 16, 20) that an air bubble be entrapped in the base of the inner cylinder in order to reduce the torque on the base to a negligible value. Now most of this torque is developed near the outer edge of the base (Appendix D) but the volume of the air bubble varies inversely as the fluid head and the surface tension and will therefore contract from the outer edge as these variables increase. Consequently the edges of the basin must be sharp and the volume of the air bubble must be very small. Even under these conditions, it has been found (15) that the entrapped air bubble may only reduce the torque by about 30%, in which case its value is questionable.

Two basic methods of applying the differential height technique, to evaluate the torque on the base, are available. The first method varies only the height of the fluid in the annulus. Under these conditions the torque on the base, at constant rate of shear, is a constant. Therefore, at constant rate of shear,

the net torque is the torque due only to the shear stresses in the annulus acting over the net depth of immersion. With the second method, the relative depth of immersion of the inner cylinder is the only variable. This method is based on the experimental fact, (11, 15, 20) that the torque on the base asymptotically approaches a constant value as the clearance between the bases increases beyond some small value. Therefore the net torque is very nearly the torque due to the shear stresses in the annulus acting over the net depth of immersion.

The first method may be accomplished either by filling the annulus to different heights - a troublesome procedure at best - or by using two outer cylinders of different lengths and filling the annulus completely. This is the more accurate method.

The second method may be accomplished by providing some means of raising and lowering the inner cylinder along the axis of the outer cylinder.

Lindsley and Fischer (15) found that the fractional value of the torque on the base remained constant if the clearance exceeded 1.3 cm.; Nissan, Clark and Nash (20) recommend a clearance of 1.5 cm.; and Green (11) used a clearance of 1 cm., the diameters of the inner cylinders being in all cases between 2 and 3 cm.

Lindsley and Fischer (15) also found that, while the relative end effect remained constant at all viscosities when the clearance was greater than 1 cm., the relative end effect increased exponentially as the viscosities fell below below one poise, when the clearance was about 0.2 cm. They give no explanation of this data. The explanation may lie in the onset of some form of turbulence between the bases. If this is the case, then, as will be shown later, the clearance should be fairly large since it is essential to delay the onset of turbulence as much as possible.

The Onset of Turbulence.

The theory of the rotational viscometer is limited to the laminar flow region and experiment has shown that laminar flow can always be achieved by using a low enough angular velocity. However, this approach is not necessarily the desirable one. Witness Weltmans discovery (37) that some high viscosity lubricating oils, while Newtonian at low rates of shear, exhibit thixiotropic behavior at high rates of shear. The general approach is to obtain the highest possible rate of shear consistent with laminar flow.

Mallock (16) made one of the first detailed investigations of the factors which induced turbulence in rotational viscometers. His experiments showed that the onset of turbulence is delayed to a much greater degree when the outer cylinder rotates than in in the opposite case. They also indicated that turbulence initiated in the base of the instrument and not in the annulus.

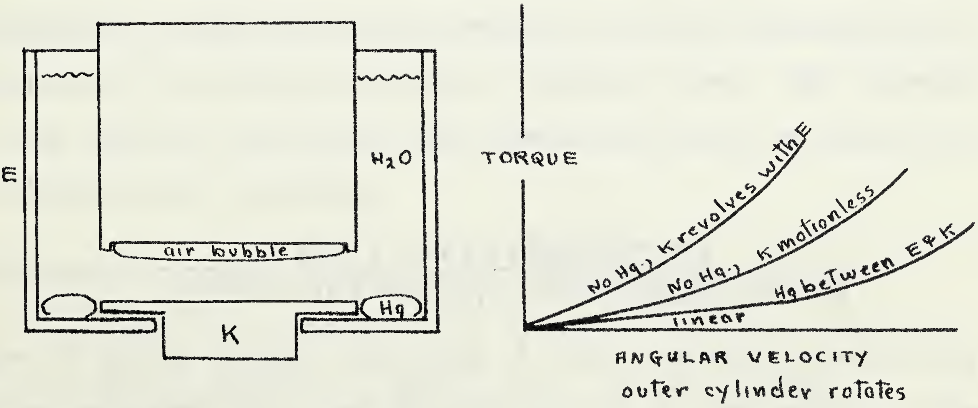

SKETCH #3. THE DELAY IN THE ONSET OF TURBULENCE WITH INCREASING EFFECTIVE HEIGHT TO DIAMETER RATIO.

If, as illustrated in Sketch #3, mercury is placed between E and K, and K is fixed, then it may be shown that the velocity

gradient in the mercury is the same as that in the water in the annulus. Under these conditions, the flow patterns approach the case when the water is between infinitely long cylinders. A study of the torque - angular velocity data, in Sketch #3b, shows that the onset of turbulence is delayed as this condition is approached. Not shown above is the data showing that turbulence was in evidence, with water, under all conditions when the inner cylinder rotated.

Taylor (31) made a detailed experimental investigation of the onset of turbulence in a system which approximated the infinite height to diameter case. The points of the onset of turbulence and the patterns of turbulence were determined with the aid of a dye injected into the water. He found that, within the limits of his equipment, no turbulence occured when the inner cylinder was fixed. However, when the inner cylinder rotated, three stable types of turbulence occured in the transition region between laminar and turbulent flow. The form of the turbulence depended on the past rate of shear history. The onset of turbulence agreed within 5% of that predicted from his mathematical analysis of the infinite height to diameter case. The criteria for the onset of turbulence with Newtonian fluids is then, for a motionless outer cylinder,

$$\Omega_{\text{critical}} = \frac{\pi^4 \nu^2 \left[1-0.652\left(\frac{R_2-R_1}{R_1}\right)\right]\left[R_2-R_1\right]}{2R_1^2(R_2-R_1)^3\left[0.0571\left\{1-0.652\left(\frac{R_2-R_1}{R_1}\right)\right\}^2+0.00056\right]}$$

where Ω is the angular velocity, ν is the kinematic viscosity, R_2 The radius of the outer cylinder and R_1 is the radius of the inner cylinder.

This formula shows that for rigid cylinders with an infinite height to diameter ratio, the onset of turbulence is delayed as the ratio of the annulus width to the diameter is reduced, and

that for a given annulus width, the average rate of shear at which turbulence onsets is nearly independent of the radius. Plots illustrating these rules are shown in Diagram #2.

The most important point brought out in Taylor's analysis is that, when the inner cylinder rotates, centrifugal forces induce turbulence, but, when the inner cylinder is fixed, the centrifugal forces stabilize the laminar flow pattern.

Green (11) found that very high rates of shear could be obtained in the laminar flow region if the annulus width was very small and the inner cylinder fixed, even though no provision was made to eliminate end effects.

Wilhelm and Wroughton (40) found that, for a concentric cylinder viscometer with a stationary outer cylinder, the torque rate of shear curves in the transition region were a function of the past rate of shear history.

In general then, the onset of turbulence will be delayed as far as practical if a fair clearance exists between the bases of the cylinders, if the outer cylinder rotates, and if the ratio of the annulus width to the diameter is small. This latter fact is important since it is also the criterion for maximum torque at a given angular velocity, an important point with low viscosity fluids.

The Measurement of Angular Velocity and Torque.

When rapidity of measurement is not important, it is a relatively simple matter to measure the respective angular velocities and torques. The angular velocity can be determined by eye up to about 120 rpm. Speeds up to about 300 or 400 rpm. can be measured by touch, for example, by providing some mechanism which will give the finger a sharp, light tap every revolution.

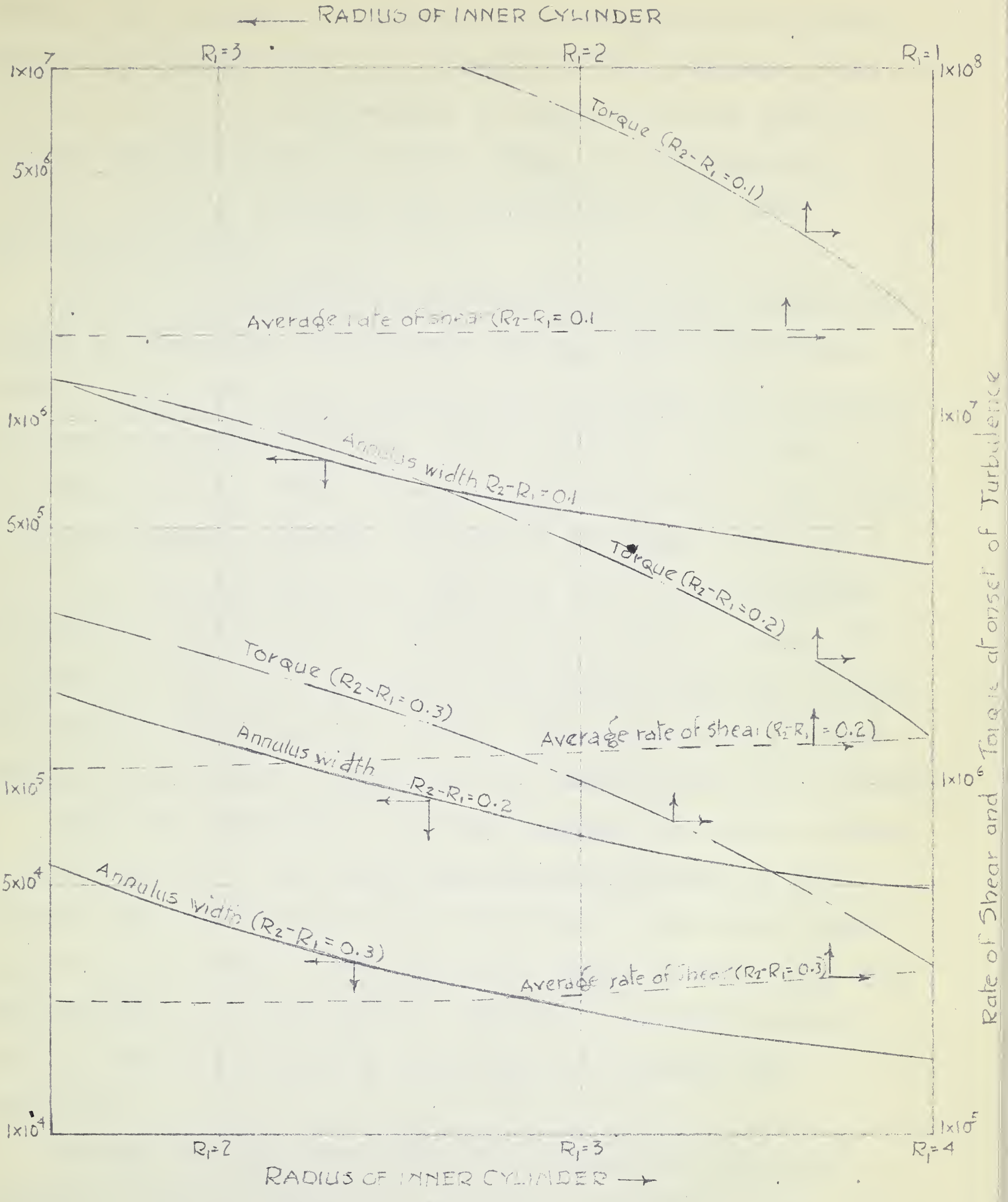

a.) The outer cylinder is stationary

b.) The ratio of the height to the diameter is infinite

DIAGRAM #2. THE ONSET OF TURBULENCE

Beyond these speeds it is advisable to use a revolution counter. When the measuring element is suspended between bearings, it is possible to use suspended weights or chain, or to use either a torsion wire or spring or a strain gauge. If the measuring element is freely suspended, the torsion wire is the only satisfactory method.

If the fluid properties are a function of time, thixiotropic fluids or suspensions which settle rapidly, special provisions must be made. The angular velocity can be measured by a calibrated tachometer, preferably the electric generator type since it is not subject to the effects of wear. The measurement of the torque is a more difficult problem. The use of suspended weights is a trial and error method and is inherently slow. The chainomatic principle is quicker but is, in many cases, still too slow. The torsion wire is, under the proper conditions, a rapid and continuous means of determining the torque. Such a system is a torsion pendulum whose motion is damped by the viscous forces of the fluid.

Under the conditions of critical damping, the system reaches a given fraction of its stable equilibrium deflection in the minimum time. Unfortunately, if the system is critically damped at one rate of shear, it will not be so damped at some other rate. Underdamping is characterized by continued oscillatory motion. In this case it is likely to be difficult to estimate the deflection.

Weltman (38) has shown that, if the moment of inertia of the fluid is small compared to the moment of inertia of the measuring system, the usual case, then the time required for the system to reach 99% of its equilibrium value is, for critical damping,

$$t \approx \frac{2IS(6.64)}{\eta} = \frac{6.64\pi\eta}{360KS} \tag{3}$$

and for overdamping the criteria are

$$\frac{\mu^2}{4I^2S} > \frac{360K}{2\pi I} \qquad 4$$

where μ is the viscosity, I is the moment of inertia of the measuring element, K is the torque per radian of deflection, and S is equal to $\frac{4\pi h R_2^2 R_1^2}{R_2^2 - R_1^2}$ where h is the depth of immersion, and R_2 and R_1 are the radii of the outer and inner cylinders respectively.

For viscosities less than 5 poises, it is very difficult to construct a system which will not be underdamped over the greater portion of the instruments range. Sketch 4 shows the effects of annular width, viscosity, and radius of the measuring element, on the maximum permissible wall thickness for overdamping. It is based on the assumptions that the deflection of the measuring means will be 100 deg. at 200 rpm. and that the moment of inertia of the system approaches the limiting case where it is due only to the walls of a steel cylinder.

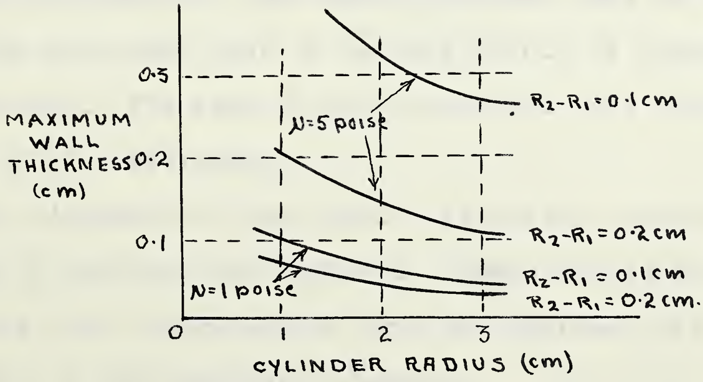

SKETCH #4. MAXIMUM WALL THICKNESS FOR OVERDAMPING.

Therefore, for an instrument designed to measure "viscosities"

of less than 5 poises, it is easier to accept the fact that the system will be underdamped and to provide additional damping by some means. The use of a dash pot in conjunction with a freely suspended system may be dangerous since surface tension may pull the system to one side if the clearances are small.

Regardless of whether the system is critically damped, or otherwise, it is inherently incapable of following any transient effect whose period is less than the quarter period of oscillation of the system which is $\frac{\pi}{2}\sqrt{\frac{IL}{K}}$ where L is the length of the torsion wire (23).

There is still one system of measurement remaining which might be successfully used for low viscosity fluids, that is, the strain gauge. The enormous increase in the permissible value of the torsion wire constant, K , permits a great increase in the moment of inertia before the system becomes underdamped.

A dynamometer might prove useful if bearings with a sufficiently low friction can be obtained.

Alignment of the Cylinders.

The alignment of the conicylindrical form is a mechanical operation which may have to be carried out in properly equipped machine shop. The ease of this operation will depend on the design of the instrument.

The alignment of the simple cylindrical system presents no problem if bearings are employed. There should be no problem to designing this instrument so that the operator will be able to align it - a very desirable feature.

The alignment of the freely suspended system can be a very difficult problem. Freely suspended systems employing heavy torsion wires are not advisable since any bend in the wire will

throw the system off axis, nor are they necessary since bearings can be employed without causing appreciable error. The mass of the measuring element will usually straighten out a fine torsion wire, so there is no problem here. The intermediate range is another matter. Since one of the desirable characteristics of the rotational viscometer is a wide viscosity range, some consideration must be given to the intermediate range. The writers experiences suggest that irrotational universal couplings should be included with the chucks so that, regardless of the shape of the wire, the measuring element will hang true.

The literature gives two criteria for coaxiality, first Gurney (13) quotes Couette as having shown that the point of minimum torque is the criterion for coaxiality; and second, Green (11) says that the liquid rides high in the direction in which the inner cylinder is off axis. A feeler gauge, whose width is a thousandth of an inch or so smaller than the annulus, may also prove satisfactory.

Desirable Features of a Rotational Viscometer.

In the light of the foregoing discussion, certain features are seen to be essential for the satisfactory operation of the instrument. These features are:

a) The outer cylinder should be the rotor, at least for fluids below a few poises.

b) The ratio of the annulus width to the radius should be as small as practical since: turbulence is delayed; the permissible moment of inertia of the stator is increased; the ratio of the torque to the angular velocity is increased, an important point where bearings are employed; and the shear stresses across the annulus are more nearly constant permitting a more accurate

calculation of the average shear stress and the velocity gradient.

c) The clearance between the bases of the cylinders should be about 1.5 cm. when the simple cylindrical system is used.

d) The height to diameter ratio of the stator should be large so that any errors in determining the end effects will be relatively small.

e) The mass of the stator should be as small as possible. This will reduce the friction if bearings are employed. It will also permit the use of finer torsion wires, with the freely suspended system, and thereby increase the viscosity range.

f) Bearings should be employed if at all possible.

g) Where bearings may be employed and where the fluid properties will not be a function of time the torque may be measured by means of suspended weights or chain or by torsion wires, a strain gauge or a dynamometer. Which of these will be the most suitable in the long run is debatable.

h) If the fluid properties are likely to be a function of time, some method of continuously measuring the torque and the speed should be employed. All of the continuous means of measuring the torque, torsion wire, strain gauge, or dynamometer, require as low a moment of inertia as possible if their full potentialities are to be realized.

This outline of the desirable features of a rotational viscometer shows that the major problem in their design is a mechanical one. The following section will review the characteristics of a number of rotational viscometers. Particular attention will be given to any important mechanical features which may prove of value in the event that it becomes necessary to build a rotational viscometer.

The Existing or Proposed Rotational Viscometers for Research and Industrial Control.

a) The Ambrose and Loomis Viscometer (1).

This is one of the early concentric cylinder rotational viscometers. The chief characteristic of this instrument is the provision of special shields, above and below the torque sensitive element, the freely suspended inner cylinder, which, by entrapping air bubbles, act to reduce the torque on the upper and lower surfaces of the stator to a minimum. The further addition of mercury between the outer cylinder and the lower screening plate yields a close approach to the infinite height to diameter case.

Since the stator is freely suspended it is suitable for relatively "low viscosity" fluids only. The complex screening system could prove difficult to align and will certainly greatly increase the time required to disassemble, clean, and reassemble the system.

Though not used with non-Newtonians, the writer can see no reason why it could not be used to determine their absolute consistency curves.

b) The Mooney and Ewart Viscometer (19)

This is the instrument Mooney and Ewart used to demonstrate the validity of their theoretical analysis of the conicylindrical form of the instrument. The stator, or inner cylinder, is located between needle bearings acting on hardened steel pivots, the lower needle point projecting from the conical base of the stator. Unfortunately, the authors give no indication of the techniques employed to align the apices of the concentric cones

forming the rotor and stator bases - the major stumbling block in employing concentric cones.

The torque developed on the stator is counterbalanced by equal weights on opposite sides of the shaft. The use of opposing, equal, weights reduces the side thrust, and therefore the friction on the bearings, to a minimum. However this procedure is rather slow.

The small annulus to diameter ratio, about 0.05, permitted a satisfactory measurement of the viscosity of water, the flow being stable to one rpm. Whether the use of concentric cones had any effect on this stability is not known.

On the whole, while the instrument is easy to operate and capable of determining absolute consistency curves, its operation is time consuming, it is rather fragile, and it is probably difficult to align. Its use with solid suspensions is rather questionable.

c) The Nissan, Clark, and Nash Viscometer (20).

The torque sensitive element, the inner cylinder, of this instrument is a solid, freely suspended cylinder with a shallow, sharp edged, basin in the base which holds an entrapped air bubble. The rotor system combines a constant temperature bath with the outer cylinder, which is readily detachable from this assembly. The outer cylinder has a sharp edged trough, to hold any overflow, with a raised outer lip to prevent any inward splashing of the fluid from the constant temperature bath.

The authors do not specify the relative end effect with the entrapped air bubble. However, they emphasize the necessity of a shallow, sharp edged, basin and mention that this technique is unreliable at large depths of immersion, so that it may be

presumed that this effect is negligible. They also recommend a clearance greater than 1.5 cm. between the rotor and stator bases.

On the whole, this is a practical, well designed, instrument suitable for measuring the absolute consistency curves of non-Newtonian fluids. A reduction in the mass of the inner cylinder would improve its damping characteristics, but it will probably lower its maximum "viscosity" range.

d) The Green and Weltman Viscometer (11).

The following description of this instrument concerns the model described by Green (11) and not the recent commercial version put out by Precision Scientific Co. The instrument has proven satisfactory for all types of fluids with "viscosities" between 1 and 2500 poises.

The stator, the inner cylinder, is suspended between ball bearings. The friction of these ball bearings is negligible over this operating range. The torque is counterbalanced by a coiled spring which permits a large deflection with a relatively short torsion element - a particularly important point at the higher viscosities.

The rotor is contained within a large stationary constant temperature bath which is capable of holding a number of samples as well. This method of construction reduces the complexity of the necessary circulating systems.

The driving mechanism, a 1/4 hp. synchronous motor coupled through a Graham variable speed transmission, combines a continuously variable output speed, 0 - 400 rpm., with a large reserve of power.

This model has no special provision for elevating the stator though it can be done. Green (11) indicates that the relative

end effect determined with Newtonians is also good for non-Newtonians, therefore, once the machine has been calibrated, there will be no further need for the differential height technique. The commercial model appears to have provision for easy elevation of the stator, thereby facilitating the use of the differential height technique.

The outer cylinder is readily removable from the drive. As well, the base of the outer cylinder may be screwed out, which simplifies the cleaning.

As far as the present problem is concerned, the commercial model is not satisfactory for the present task because the bearings are not suitable for low visconsity fluids and the cost is too high.

e) The Cardwell Viscometer (8).

This viscometer was designed for drilling muds. The stator, the inner cylinder, is suspended between opposing torsion wires which serve both to measure the torque and to hold the inner cylinder in alignment. The use of this twin torsion wire suspension necessitates a rather complex mechanical system which appears to be inconvenient to dismantle and reassemble. In view of the size of the air bubble in the base of the stator, it is doubtful if it reduces the end effect to a negligible value.

The unusual feature of the rotor is the inclusion of a filling tube extending into the space below the stator. This is reported to simplify filling the instrument.

Except for the possibility of an appreciable end effect, the instrument should be capable of measuring absolute consistency curves.

f) The Beck, Nuss, and Dunn Viscometer (4).

This is another instrument designed for use with drilling muds. The rotor, the inner cylinder, is suspended from a drill press mechanism, the normal motor being replaced by a Graham variable speed drive with a speed range of 0 - 800 rpm.

The stator is suspended between bearings, details of which are not given, the vertical load on the bearings being compensated by floating the lower portion of the stator in mercury. The chainomatic principle is used to measure the torque.

No estimate of the friction in the bearings is given, nor is any mention made of the large "surface rigidity" inherent with the use of mercury*. Also, no information is given about the onset of turbulence. It appears that the instrument may not have been tested with Newtonian oils.

Theoretically, the instrument is capable of measuring absolute consistency curves, but its application to fluids below 20 centipoises is questionable.

g) The Traxler Viscometer (34).

This conicylindrical viscometer was developed for the measurement of the viscosities of cold asphalts, and is suitable over a range of 10^3 to 10^9 poises. The very low shear rates, up

---

*The writers' experiments with mercury show that a film develops, on the mercury surface even under oil, which acts as a solid surface. This film, acting on a one inch shaft, would cause a large error in measuring 5 centipoise oils. The term "surface rigidity" is used by anolagy to Gurneys (13) discovery of a somewhat similar effect on water.

to 6 rpm., and the large variation of the stresses across the annulus, 40%, may not be too great a disadvantage since the majority of asphalts do not appear to differ very much from Newtonians.

The stator, the inner cylinder, has cones at either end of the cylinder to permit calculation of the otherwise large end effects. A ball bearing is used to locate the upper portion and a needle bearing is used to locate the lower portion of the stator. The interesting feature of both the rotor and the stator is the use of cross-engraved surfaces to prevent slippage of the asphalt. A cover plate is used to hold the fluid in the system.

The torque is counterbalanced by a lever arm and weight, the torque on which is transmitted through a gear to a very long pitch thread on the stator shaft.

While it is unquestionably a useful instrument in its special field, it has no application in the present problem. However, cross engraving the surfaces may be a means of eliminating wall effects.

h) The Stormer Viscometer (43).

This is a widely used control instrument. Its relatively low cost, ease of operation, and ability to withstand minor abuse, are its chief advantages.

The torque sensitive element, the inner cylinder, is driven by falling weights. Under normal conditions, acceleration may be neglected so the torque on the rotor is directly proportional to the applied load. The complex flow boundaries which result from the use of baffles in the stationary outer cylinder eliminate it, at present, from use as a means of measuring absolute consistency curves. The limited time of application of the shear

stresses seriously restricts its application with thixiotropic fluids.

Lindsley and Fischers modification (15), which can be carried out in any machine shop at little cost, will permit its use as a means of measuring absolute consistency curves of those fluids whose shearing stress is not dependent on the past history of the rate of shear. Even with this modification it is doubtful whether the data would be accurate to better than 5%, and whether the instrument could be used satisfactorily below 20 centipoises. A more detailed analysis of this instrument appears later in this paper.

i) The MacMichael Viscometer (42)

This rotational viscometer employs a freely suspended torque sensitive element. This stator may be either a narrow cylinder or a large flat disc. The rotor may be either a cylinder or a flat bottomed bowl, depending on the form of the stator.

The clearances between the rotor stator are too large to permit calculation of an average rate of shear for materials which behave much differently than Newtonians. This disadvantage is accentuated by the low speed range, 9 to 40 rpm. With fluids having an appreciable yield value the system is indeterminate since laminar flow will not take place across the entire annulus. The mechanical precision of the system is low, tolerances in the rotor assembly being as high as 1/64 in.

As a control instrument, however, it will give an idea of the fluid properties over the range between 1 and 10^4 centipoises.

j) The Brookfield Syncro-lectric Viscometer (41)

This is the most convenient industrial control viscometer

presently available. It may be held in, and operated with, one hand. A convenient cable extension to the torque sensitive element permits operation of the instrument at a distance of several feet from the surface of the fluid. A combination of spindles and speeds permit its use as a multipoint instrument. It can develop continuous shear, but it must be stopped to be read. It is very rugged and not liable to overranging.

The writers very limited experience with this instrument indicates that it would be very difficult, if not impossible, to modify it for use in measuring absolute consistency curves.

k) The Mooney Viscometer (32)

This parallel plate, or "shearing disc", viscometer is a standard throughout the rubber industries for measuring the consistencies of raw rubbers. The stator is a horizontal plate, and the rotor, the outer cylinder, is a totally enclosed, shallow cylinder. All the surfaces are cross-engraved to prevent slippage. The clearances are sufficiently small to permit an approximate analysis of the average stress and rate of shear.

Since it is virtually impossible to fill a system with raw rubber, or materials like it, without entrapping air, the outer cylinder is in two parts, the upper part being held down by strong springs. This pressure holds the rubber in place and assists the working free of any entrapped air.

The instrument has proven an excellent one for its specific purpose. The chief disadvantage is the variable rate of shear across the rotor.

l) The Texaco Viscometer (9).

This instrument was developed for use with drilling muds.

The inner cylinder, the rotor, is driven, by a synchronous motor, via a gear train which provides for five speeds between 100 and 900 rpm. The outer cylinder is freely suspended between torsion wires, the system being so designed that the operator may eliminate the torque due to the lower torsion wire. No provision is made for the use of a differential height technique so the end effects are unknown. The suspended assembly has such a high moment of inertia that a special dashpot is provided. In addition, the large mass of the stator requires a heavy torsion wire so that the sensitivity of the system is greatly reduced.

While it seems that the instrument was not intended to measure absolute consistency curves, the writer can see no reason why it could not be modified to do this job. The chief disadvantages of the instrument for this purpose are: the need for stopping the motor before changing gears, the use of the rotating inner cylinder if low viscosity fluids are likely to be encountered, and the low sensitivity at low viscosities.

m) The Fann V-G Meter (19)

This is a single point continuous shear viscometer for drilling fluids. It is the best instrument of its type the writer has encountered, being moderately priced, very simple to operate, compact, and rugged.

Mechanically, it is a distinct departure from the normal run. The rotor, stator, and motor drive are integral with the adjustable overhead frame. The net result is that the rotor and stator are automatically aligned on assembly, the outer cylinder rotates and the inner cylinder is stationary. The inner cylinder is located by a needle bearing at the upper end of its shaft and by a ball bearing of some type between the rotor and the stator. The torque

on the stator is counterbalanced by variable weights. The friction of this system is fairly low.

The writers brief experiments with this instrument showed that the torque - angular velocity relationship is very nearly linear over the range investigated, 2 to 150 centipoises, and that the speed held constant within 1% at 600 rpm. throughout this range. The torque is reproducible to within somewhat less than 5% for viscosities greater than 5 centipoises.

The writer can see no reason why this instrument cannot be adapted to measure absolute consistency curves. Melrose and Lilienthal (18) report a simple, satisfactory, method of converting it to a multi-speed unit.

III A SUITABLE VISCOMETER

Rheology.

The clay slurries, used in the previous investigation (10), range from the viscosity of water to about 5 "poises" at 100 rpm. All the material passes 200 mesh. However, it settles fairly rapidly at concentrations below about 20% solids. The slurries appear to be inert.

The present pipe line equipment is not suitable for slurries above about 35% solids (10). Therefore, if a reasonable range of the fluid properties is to be covered, the low concentration range will have to be investigated.

Long range plans envisage the use of the instrument with drilling muds containing rock cuttings. The temperatures may reach 150 deg F.

A Suitable Type of Viscometer

The use of a capilliary tube viscometer is not advisable in view of the high settling rates of the clay slurries over part of the concentration range of interest. It is not practical with thixiotropic fluids such as most drilling muds.

Both the high settling rates of the present slurries and the thixiotropic properties of drilling muds demand an instrument which delivers continuous shear at constant rates and which provides for the continuous measurement of the torque. The proposed investigation of the rheology of muds carrying rock cuttings suggests a large annulus width. The use of the coni-cylindrical form is debatable since the clearances between the cones become rather small.

Assuming that only the material passing 35 mesh is used and that the annulus width should be about five times the size of the largest particle, the annulus should be about 1/8 in. wide.

It is desirable to be able to investigate the effects of concentration, over a wide range, on the fluid properties. Since the carrier fluid of most drilling muds is water, the friction in the measuring system must be extremely small if this limit is to be reached. The only bearings with sufficiently low friction are the very precise ball bearings, such as those used in gyroscopes, or the magnetic type of bearing. The ball bearing is very fragile and sensitive to dust. The magnetic bearing is rugged and is not affected by dirt. However, little data are available on its other characteristics. A freely suspended system is frictionless. While the opposed torsion wire type is relatively rigid and easy to align, its sensitivity is apt to be rather low. As well, the present systems may prove rather inconvenient in operation. Unfortunately, the system in which the stator hangs free may prove difficult to align.

Since very low "viscosities are likely to be encountered, the outer cylinder should be the rotor.

Therefore, the most satisfactory instrument is a concentric cylinder rotational viscometer employing some form of the differential height technique. The outer cylinder should be the rotor. The annulus must be 1/8 in. or wider. The stator system must be practically frictionless. The drive must deliver a wide range of constant speeds. Some means of continuously measuring the torque is essential.

The Adaptability of the Available Viscometers.

Of the simple concentric cylinder rotational viscometers currently in production, only the Green and Weltman, the Texaco, and the MacMichael appear to offer any promise. While they are not, in their present form, entirely suitable for this project they might be modified to do the job. No satisfactory method of modifying the other instruments has presented itself.

The initial cost of the Green and Weltman Viscometer is prohibitive as far as this project is concerned.

The Texaco viscometer is, in its present form, too insensitive for use with water. The use of a rotating inner cylinder in conjunction with a wide annulus is not advisable, particularly at low viscosities. The use of temperatures much above room temperature may prove impractical if the water bath assembly is removed to permit the use of finer torsion wires. The present drive has an insufficient speed range.

The MacMichaels' speed range is far too low. The present annulus is wide enough but the ratio of the annulus width to the diameter is too large. The mechanical precision of the instrument is low.

In view of the initial cost of either of these instruments and the extra cost of the necessary modifications, the best approach, in the long run, is to build an instrument specially designed for the tasks at hand.

Since the problem has been reduced to the mechanical design of a new viscometer, a review of the noteworthy mechanical features of the available and proposed viscometers is in order.

IV THE MECHANICAL DESIGN OF THE NEW VISCOMETER

Noteworthy Mechanical Features of Some Rotational Viscometers.

It is evident that a number of basically different approaches to the solution of the mechanical design problem are open. The following review is confined to those approaches which were considered promising.

a) The torque sensitive element

The Ambrose and Loomis; the Nissan, Clark and Nash; and the MacMichael viscometers employ a stationary inner cylinder freely supported by a single torsion wire. The Nissan, Clark and the Nash viscometer employ micro-chucks. However, micro-chucks have a limited torsion wire range. A pin vise has a wide torsion wire range but it is likely to damage the finer torsion wires. However, it is a great deal cheaper than a set of micro-chucks.

The Cardwell and the Texaco viscometers employ opposed torsion wires, but these instruments are not convenient to operate.

The Green and Weltman viscometer uses the torsion principle, but it locates the stator shaft by ball bearings. Ball bearings suitable for this project are not generally available.

On the basis of easy operation and simple construction, the single torsion wire is the better solution. There is no reason why the instrument cannot be so designed that bearings can be added at a later date.

b) Drive mechanisms

The use of gear trains, as in the Texaco viscometer, limits the flexibility of the speed range and generally necessitates stopping the instrument before changing gears. The use of continuously variable-speed transmissions, as in the Green and

Weltman and the Beck, Nuss and Dunn viscometers, greatly simplifies the operation of the system and opens the possibility of using the transmission control as the speed indicator.

c) Filling and cleaning the instrument

The majority of the viscometers employ detachable outer cylinders. This approach permits rapid filling and cleaning of the cylinder. The Green and Weltman viscometer uses a detachable cylinder base which further simplifies the cleaning. The cardwell viscometer employs a "fixed" outer cylinder and uses a special filling tube. Suitably designed, the use of such a filling tube may also solve the cleaning problem when the outer cylinder is integral with the drive.

Both the Nissan, Clark and Nash and the Green and Weltman viscometers have an overflow trough attached to the outer cylinder. This facilitates leveling the fluid in the annulus and prevents contamination of the constant temperature system by the fluids. The sharp inner edge and the raised outer lip of the Nissan, Clark and Nash viscometer is the better approach.

d) Temperature control

The Nissan, Clark and Nash, the MacMichael, and the Texaco viscometers combine the constant temperature bath with the outer cylinder. Designing such a system to operate under conditions combining high angular velocities and low temperatures may prove rather difficult. The Green and Weltman viscometer immerses the outer cylinder in a large constant temperature bath which can handle a number of samples as well. This system is very convenient, is suitable over a wide temperature range, and simplifies the flow circuit somewhat. It also complicates the drive system.

e) Miscellaneous

Both the Mooney and the Traxler viscometers use engraved

surfaces to reduce slippage at the wall. Green (10) has found it unnecessary with the more usual suspensions. However, paper pulp suspensions, and similar ones, might require such engraving.

The Final Design of the Viscometer.

The following is a brief description of the important features of the new viscometer. A detailed description of the components and the factors governing their selection appears in the next section. The reader is refered to the illustrations on pages 47 and 48 and to the blueprints in Appendix I.

The instrument is a concentric cylinder rotational viscometer employing a differential height technique to evaluate the end effects.

The rotor, the outer cylinder, is integral with the drive. A hole is drilled through the rotor shaft to simplify cleaning and filling the system. An overflow trough is included.

The measuring element is freely suspended from a single torsion wire. Provision is made for the future application of a bearing to this element. The torque is measured by a five inch protractor which is readable to about a quarter of a degree.

The upper suspension point of the torsion wire is attached to a sliding tube. Special provision for aligning the axis of the sliding tube to the rotor axis is included. Therefore, the stator may be easily raised and lowered along the rotor axis.

The resultant differential height technique depends on the experimental evidence that, beyond a small initial clearance between the bases, the relative torque on the base is nearly independent of this clearance.

The rotor is driven by a belt from a Graham Variable Speed Transmission powered by a synchronous motor.

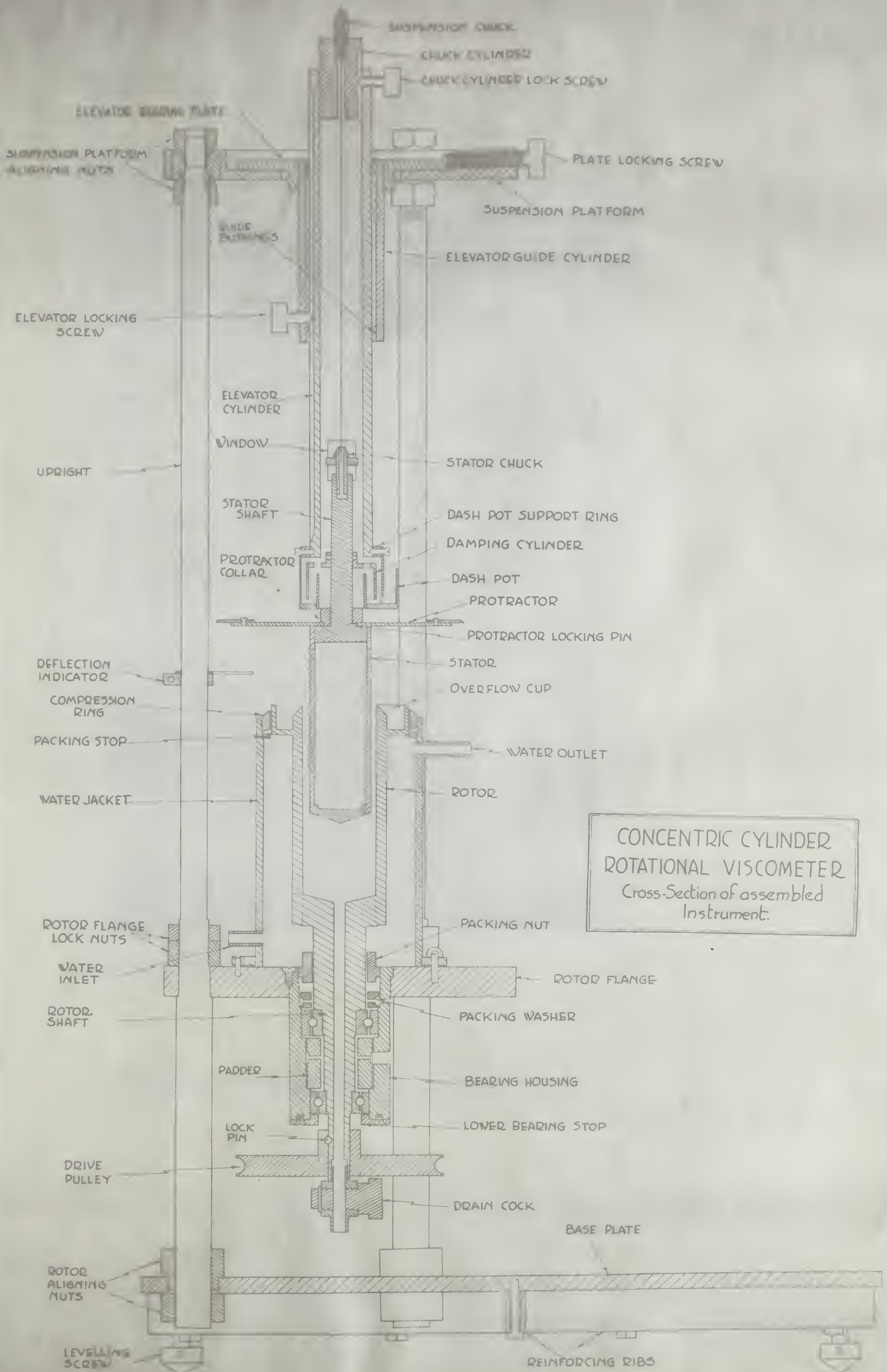

CONCENTRIC CYLINDER
ROTATIONAL VISCOMETER
Cross-Section of assembled
Instrument.

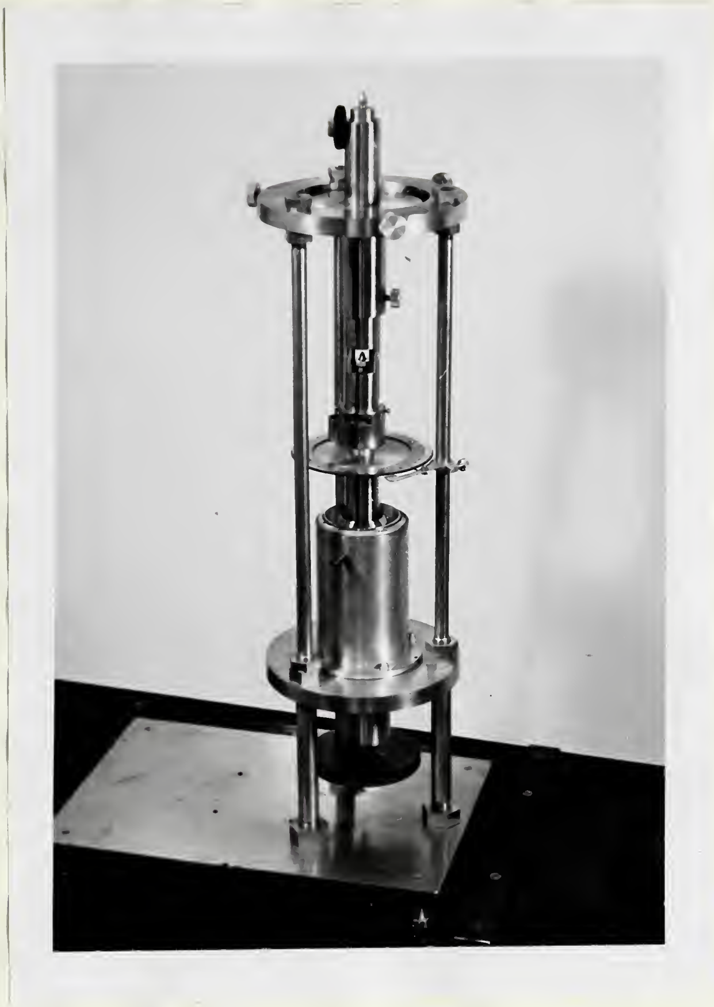

FIGURE #B THE ROTATIONAL VISCOMETER

The temperature of the rotor is controlled by a water jacket connected to a constant temperature bath.

The Mechanical Details of the New Viscometer.

This section combines a general description of the mechanical features embodied in the new instrument with, where noteworthy, the reasons for chosing these particular features.

Cost estimates, based on the preliminary designs, indicated that it would be cheaper to use a rotor permanently attached to the drive and to provide some convenient means of elevating the stator. These estimates also favored the support of the suspension platform on three fixed columns, the uprights.

The stator is suspended from a cylinder, the elevator cylinder, which rides in a sleeve bearing, the elevator guide cylinder. A flange, force fitted to this sleeve, rests on the recessed portion of the suspension platform.

The suspension platform is supported between three pairs of adjustable coni-hexagonal nuts, the suspension platform aligning nuts, on the uprights. This type of nut eliminates any play between the platform and the uprights. They are also very easy to adjust. In order to reduce the labor involved in adjusting this system, the elevator bearing plate is turned true to the axis of the guide bushing and the bearing surface of the suspension platform is turned flat. The outer edge of the flange is inclined from the vertical so that tightening the plate locking screws will force the flange against the bearing surface.

The elevator cylinder has a triangular slot, parallel to the cylinder axis, running along most of its length. The elevator locking screw has a truncated conical end whose taper matches that of the slot. This cone rides in the groove and prevents the

elevator from turning. It also provides a more perfect locking mechanism than can be obtained by forcing a flat ended bolt against a smooth surface.

A hollow cylinder with a #1 Starett pin vise force fitted into its top, the chuck cylinder, rides inside the upper end of the elevator cylinder and is locked to it in the manner just described. The provision of this adjustable chuck cylinder is just an added convenience.

In practice the choice of the dimensions of the rotor and stator is a compromise. To a first approximation, the torque varies directly as the length and the cube of the diameter and inversely as the annular width. The deflection of the stator varies inversely as the fourth power of the torsion wire diameter. At low viscosities this deflection will be limited by the early onset of turbulence. This early onset is accentuated by a large annular width to diameter ratio. But the annular width is dictated by the proposed investigations of drilling muds carrying rock cuttings, and may be considered constant at 1/8 in. Then, if laminar flow is to be achieved over an appreciable range, the diameter must be large.

Assuming a protractor can be read to 0.3 deg, a deflection of at least 30 deg will be necessary in order to measure the torque to 1%.

The system is bound to be underdamped so the effects of the moment of inertia may be reduced to the rule that the stator should be a hollow cylinder with as thin a wall as possible.

The wall thickness of the inner cylinder must be about 1/8 in. if it is to be machined readily to close tolerances. This value is satisfactory for cylinder diameters from 1 to 2 in. and lengths from 2 to 6 in.

The mass of such a cylinder varies approximately as its diameter and length. The mass of the shaft and the protractor may be considered constant. The length of the cylinder must be great enough to permit a satisfactory application of the differential height technique. The permissible dead load varies as the square of the torsion wire diameter.

In theory it should be possible to graph these factors and to shose a suitable set of values from these graphs. However it was found that the use of drawn seamless steel tubing would considerably reduce the machining costs. Indeed, in view of the close tolerances to which this tubing is manufactured, machining of the inner surfaces might be eliminated except for short distances at the ends of the cylinder. Under these conditions, the problem becomes a case of random choice amongst the stock tube sizes until a satisfactory combination is found.

Preliminary calculations indicated that stainless steel tubes of 2.25 in. O.D. by 1.75 in. I.D. for the rotor, 1.5 in. O.D. by 1.25 in. I.D. for the stator, and a stator length of 4.5 in. should prove a satisfactory compromise. The reasons underlying the selection of these dimensions are outlined below.

a) Preliminary experiments were performed, with a MacMichael viscometer, to obtain a rough idea of the torsion wire constant of a #34 MacMichael torsion wire. A deflection of about 5 deg was obtained with water when: the cylinder radii were about 1 1/16 in. and 7/8 in., the depth of immersion was about 1 in., and the speed was about 30 rpm. From the Reiner and Riwlin equations (24) the deflection for the proposed at 30 rpm and 4 in. immersion in water is

$$\text{deflection} \quad \frac{h_2 R_2^2 R_1^2 (R_4^2 - R_3^2)\,\Omega_2\,(5\,\text{deg})}{h_4 R_3^2 R_4^2 (R_2^2 - R_1^2)\,\Omega_4} \qquad (5)$$

or about 100 deg at 4 in. immersion in water and at

30 rpm. where h is the depth of immersion (in), R is the radius (in.), Ω is the angular velocity (rpm), and the subscripts 1 & 2 refer to the proposed system and 3 & 4 to the MacMichael system.

b) The diameter of the #34 torsion wire is about 0.006 in. Assuming that drawn phosphor bronze wire will take 50,000 lb/in^2 safely and possibly 100,000 lb/in^2 before rupture (39) this torsion wire will carry a dead load of 1.5 lb. safely. Assuming that the additional stress in torsion may become equal to the safe load and that it acts at right angles to the tension stresses of the dead load, the safe load will be about $\sqrt{1.5}$ or 1.2 lb. This will be further reduced by the stresses set up, at the points of suspension, by the pin vises.

The density of type 304 stainless steel tube is about 490 lb/ft^3. The weight of the proposed inner cylinder is, therefore, about 0.88 lb. A quarter inch thick stainless steel plug in the base adds a further 0.1 lb. Therefore, the minimum stator weight is greater than 1 lb.

c) The system is bound to be underdamped so that additional damping is advisable. It may prove necessary to add bearings. A 3.5 in. length of shaft is necessary to support the dash pot and to provide for the future use of bearings. The diameter of this shaft is governed by the machining problem. A diameter of 0.5 in. seemed the best compromise. The shaft and the plug for the upper end of the cylinder adds 0.3 lb. if of stainless steel and 0.1 lb. if of aluminum. Since the safety factor is already negligible, the shaft is made of aluminum.

d) The dimensions of these tubes are such that a short length should be round to within 0.002 in. Therefore machining the inside of the stator is not essential.

The lower limit of this system is the viscosity of water if laminar flow can be obtained up to 30 rpm. Extreme care will be necessary to avoid breaking the torsion wire.

The base of the stator is a cone having a large apex angle. This prevents any air being entrapped at this point.

The damping device is a 7/8 in. length of brass tube forced onto an aluminum ring, having an inner collar which is drilled and tapped for three locking screws. This collar just slides along the stator shaft. It is normally locked about 1 1/4 in. above the stator cylinder. The two holes drilled in the aluminum ring prevent the damping cylinder from acting as an unstable float.

The oil trough for this cylinder is the annulus between two concentric brass cylinders. This trough is locked to a ring attached to the lower end of the elevator cylinder. The wide clearances between the damping cylinder and the walls of the oil trough are dictated by the danger of the surface tension of the damping agent pulling the system out of alignment.

The sight ports in the walls of the trough are a later addition. It was found that accidental blows on the stator splashed oil onto the collar of the damping cylinder and the inside wall of the elevator cylinder. The surface tension of this oil pulls the collar against the elevator cylinder and effectively, creates an appreciable friction. The sight ports permit inspection of the damping cylinder collar. The filling tube on the side of the oil trough is merely a convenience.

The protractor assembly, consisting of the outer portion of an ordinary plastic protractor mounted on a thin aluminum disc, lies flat on the upper rim of the stator. It is prevented from turning by a pin, in the stator shaft, which engages a slot in

the disc. This is probably the cheapest method of assembling a deflection indicator.

The rotor is made up of stainless steel cylinder force fitted to a stainless steel shaft. The heavy rotor wall simplifies boring the cylinder to close tolerances. The lip of the rotor is bevelled inwards to a sharp edge to simplify the problem of leveling the fluid in the annulus. The overflow trough prevents spilling of the sample onto the rotor flange. The 1/4 in. hole drilled through the rotor shaft terminates at a wide bore brass stopcock. This facilitates filling and flushing the outer cylinder.

The designs of the packing system, the bearings and the bearing housing, and the method of attaching the bearing housing to the rotor flange are fairly common and need no comment.

The rotor flange rests on shoulders on the three uprights and is locked to them by paired hexagonal nuts. The surface of this flange is machined flat. The water jacket, whose lower rim is turned flat, is forced against the flange by four cap screws. A little stop-cock grease prevents any leakage between the flange and the jacket. Provision is made for a packing between the overflow trough and the jacket. Experience shows that it is not essential.

The large base plate was originally designed to mount the Graham variable speed transmission. This plate is kept flat by the steel reinforcing ribs, (Originally, the plate was badly warped). The uprights are locked to this plate by opposed brass nuts. The base plate bears against the cylindrical portion of the upper nut. This method eliminates the excessive wear which may occur when the base plate is in direct contact with the

threads of the uprights.

It was hoped that the drive would be nearly vibrationless. However, it was decided to provide for the use of shock mountings if this was not the case. The long threaded portion of the uprights permits a wide range of adjustment between the drive mounting and the rotor shaft.

The rotor may be leveled by means of the locking nuts on the base plate, or by the finely threaded leveling screws which support the base plate.

The deflection indicator is attached to one of the uprights because this was the quickest method of manufacture. It would be more convenient if it were attached to the elevator cylinder.

The use of the separately mounted drive and the belt connection is dictated by the excessive vibration of the Graham variable speed transmission.

V OPERATION OF THE VISCOMETER

Alignment of the Viscometer

Experience shows the best procedure to be as follows:

a) Level the base plate by means of the four leveling screws. This level is not critical, but the thrust of the screws into the "ground" must be balanced at all times.

b) Align the rotor axis with the vertical by means of the rotor aligning nuts. Keep these nuts nearly tight during the fine adjustment. The rotor axis is vertical when the flange is level.

c) Level the recessed portion of the suspension platform. Keep the platform aligning nuts nearly tight during the fine adjustment. The elevator axis is vertical when the platform is level.

d) Hang the stator from a fine cord. Adjust the stator for coaxiality by means of the flange locking screws. The use of a feeler gauge, ground to few thousandths of an inch less than the annulus width, is the only satisfactory method. The use of the techniques involving the meniscus level in the annulus or the point of minimum torque are obviated by the centering forces of the rotating fluid - see journal bearings.

e) Chuck the torsion wire so that the bottoms of the white bands just touch the tops of the jaws of the vises. Let the damping cylinder rest on the oil trough during this operation.

f) Raise the elevator cylinder until the fine engraved line at the edge of the triangular slot corresponds to the base of the guide cylinder. Adjust the chuck cylinder until the lower rim of the stator is level with the rotor lip. This is the zero absolute depth of immersion.

g) Lower the elevator cylinder until the engraved line corresponding to the desired depth of immersion is just visible below the guide cylinder.

The instrument is now aligned and is ready for filling.

A sensitive spirit level is the best method of leveling the various components. However a friction technique was employed during this project. The procedure is:

a) Thoroughly clean the rotor and stator.

b) suspend the stator from a fine cord. Give the stator an initial deflection and allow it to oscillate.

c) move the stator against the rotor wall. Damping commences on contact.

The system is aligned when, at the onset of damping, no gap is visible between the rotor and the stator at any of the four points of the compass and at two elevations of the stator. This method is accurate to about 0.005 in. in 3 in. Since it is a trial and error method it is very time consuming. However, the instrument remains in alignment over a long period of operation.

Filling and Cleaning the Viscometer

Newtonian fluids may be poured directly into the annulus. However, great care must be exercised because the filling tube tends to create air bubbles. These air bubbles are very difficult to expel above 50 centipoises. In practice the fluids below 30 centipoises are poured directly into the annulus, but the higher viscosity fluids are either poured slowly down a rod extending into the filling tube or are pumped up through the filling tube.

The clay - water slurries must be pumped up through the filling tube. The stator should be held on axis during this operation.

The annulus is always filled until the fluid flows freely over the rotor lip.

Air pressure is used to drive the fluids into the rotor, and a partial vacuum is used to suck them back. The resevoir must contain a large excess of fluid to avoid the danger of blowing air into the rotor. Extreme care is necessary when sucking the fluids out of the rotor. It is advisable to let the last fraction drain out.

The system is cleaned by directing a jet of a suitable solvent against the rotor and stator walls and letting the fluid drain out through the filling tube. The stator must be disconnected from the torsion wire before either it or the rotor are wiped. This is necessary because the torsion wires are easily damaged.

Measurement of the Rotor Speed.

A fair tension must be applied to the drive belt to prevent it from slipping. A friction drag must be placed on the control handle to prevent it from creeping.

Up to about 250 rpm the number of revolutions may be counted by touch and timed with a stop watch. To this end a long stud is screwed into the drive pulley and a strip of thin brass is attached to one upright so that it touches the stud. A sharp tap is felt every time the stud hits the strip.

Continued use of the instrument showed that the dial setting of the transmission could be used to determine the speed within one percent. The calibration curves are shown on Figure #1.

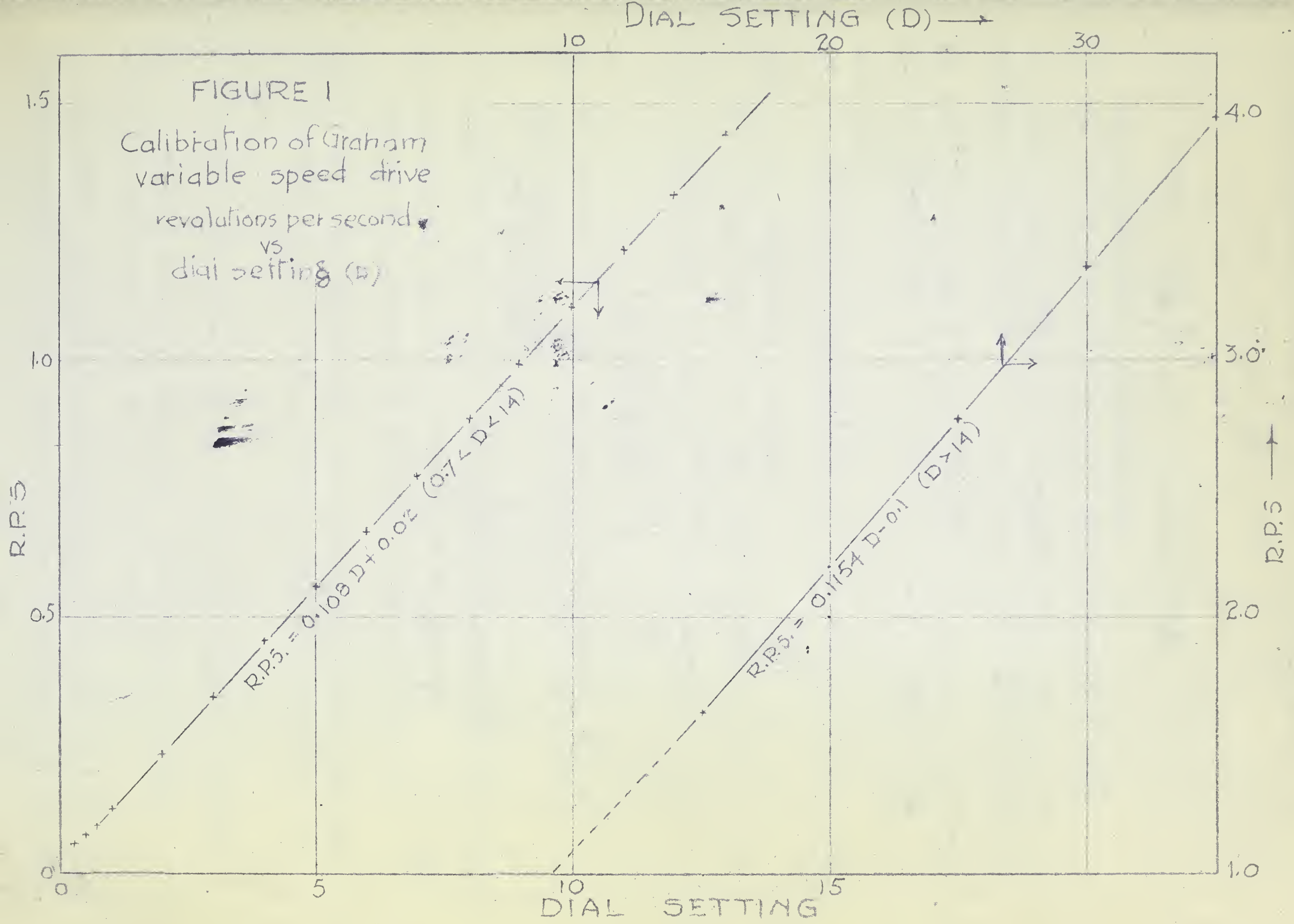

FIGURE I

Calibration of Graham variable speed drive revolutions per second vs dial setting (D)

VI EXPERIMENTAL DATA WITH THE VISCOMETER

BEHAVIOR WITH NEWTONIAN FLUIDS

Calibration of the Torsion Wires.

The equations of Couette for a Newtonian fluid between rotating concentric cylinders are assumed to be correct. Therefore the torque, T (lb force ft) is related to the viscosity, μ (cp), the angular velocity, ω (rps), the effective depth of immersion, h (in, and the radii of the cylinders, R_2 and R_1 (in) by the equation

$$T = \frac{4\pi h \mu \omega R_2^2 R_1^2 (c)}{R_2^2 - R_1^2} \qquad (6)$$

where   is a dimensional constant.

For a given torsion wire, the torque varies directly as the angle of deflection, θ (deg) or $T = K\theta$ (33), therefore

$$K = \left(\frac{h\mu\omega}{\theta}\right)\left(\frac{4\pi h R_2^2 R_1^2 (c)}{R_2^2 - R_1^2}\right) \qquad (7)$$

For convenience, let the torsion wire constant, K', be

$\frac{h\mu\omega}{\theta}$ $\frac{\text{(in)(cp)(rps)}}{\text{(deg deflection)}}$

Since the radii of the two cylinders are 0.882 in. and 0.744 in. (Appendix G) then $T = 1.83 \times 10^{-6} K'\theta$ lb force ft (8)

The determination of the height equivalent to the end effect, Δh, (Appendix D) may be combined with the calibration of the torsion wires. This combined operation is performed as follows:

a) Plot the curves of deflection against angular velocity for the several depths of immersion. For laminar flow these curves are linear and pass through the origin.

b) Chose some convenient arbitrary velocity and plot the corresponding deflections, from the above curves, against the

absolute depths of immersion. These curves are linear and intercept, at zero degrees deflection, the depth of immersion axis at a negative value, Δh. This is the height equivalent to the end effect.

c) From all the available data, find the mean height equivalent to the end effect, Δh_m. If these data are weighted according to the number of points on the deflection - depth of immersion curves, then

$$\Delta h_m = \frac{\Sigma \,\text{intercepts} \times \text{weights}}{\Sigma \,\text{weights}} \qquad (9)$$

d) Find, at some convenient arbitrary angular velocity, the values of the products $\frac{(h+\Delta h_m)\nu\Omega}{\theta}$ from the curves plotted for part (a) above, for every depth of immersion and viscosity used with a given torsion wire. Then the mean torsion wire constant is given by the equation

$$K'_m = \frac{1}{n}\sum_1^n \frac{(h+\Delta h_m)\nu\Omega}{\theta} \qquad (10)$$

where n is the number of deflection - speed curves involved.

Figures #2 to #8 inclusive show plots of deflection against speed for the various depths of immersion, viscosities, and torsion wires. The solid lines represent valid data and the dashed lines represent data whose interpretation is in doubt. The data are found in Appendix 11, tables 3 to 7 inclusive.

Figure #9 shows plots of deflection, at 1 rps, against the absolute depth of immersion. The solid lines represent consistent data and the brokenlines represent excessive scattering of the data. The intercepts on the depth of immersion axis are listed against their respective curves. The mean height equivalent to the end effect is 0.19 in.

Table #8, Appendix H, lists the values of the torsion wire constant, K', for each deflection - speed curve and the mean value of for each viscosity.

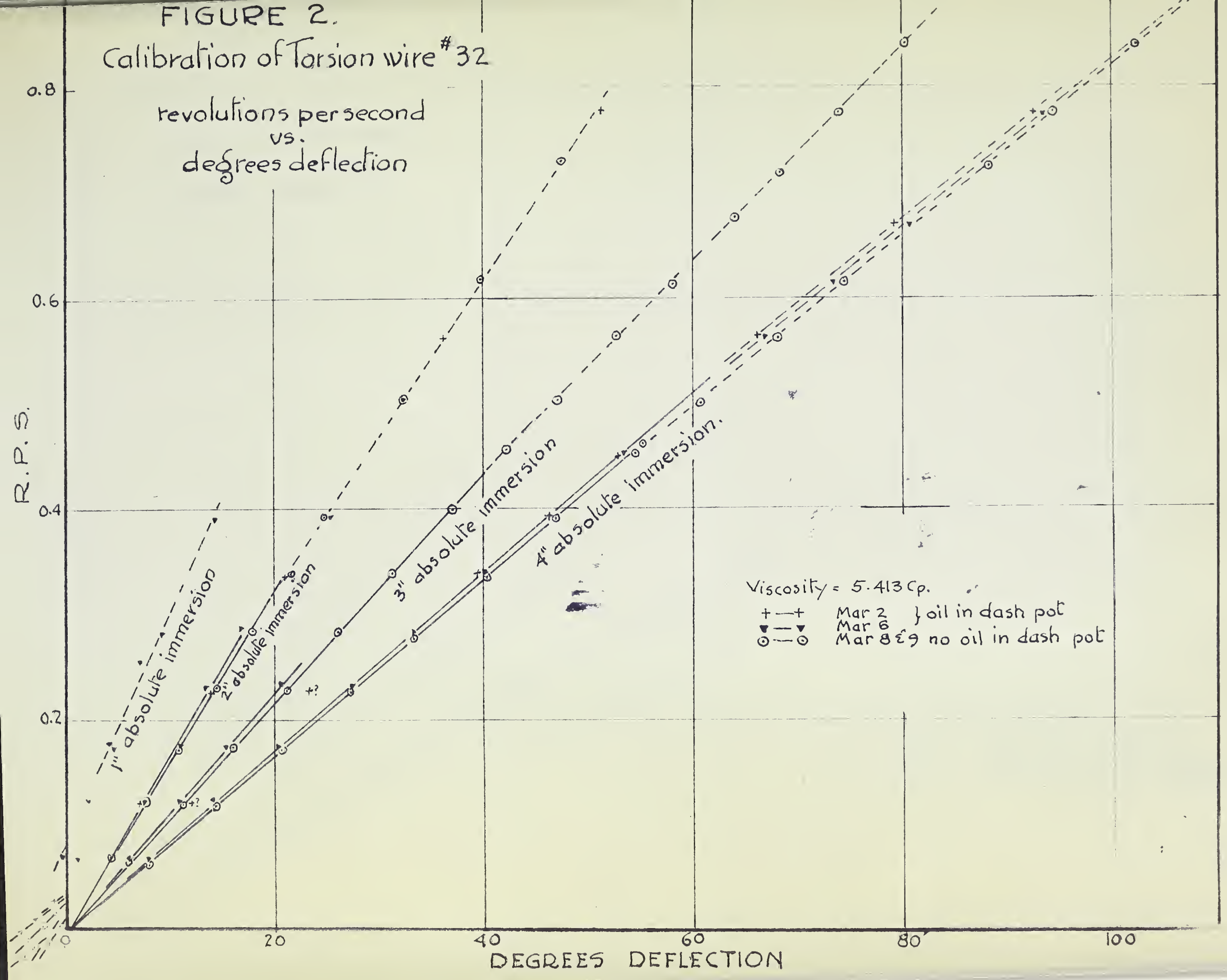

FIGURE 2.

Calibration of Torsion wire #32

revolutions per second
vs.
degrees deflection

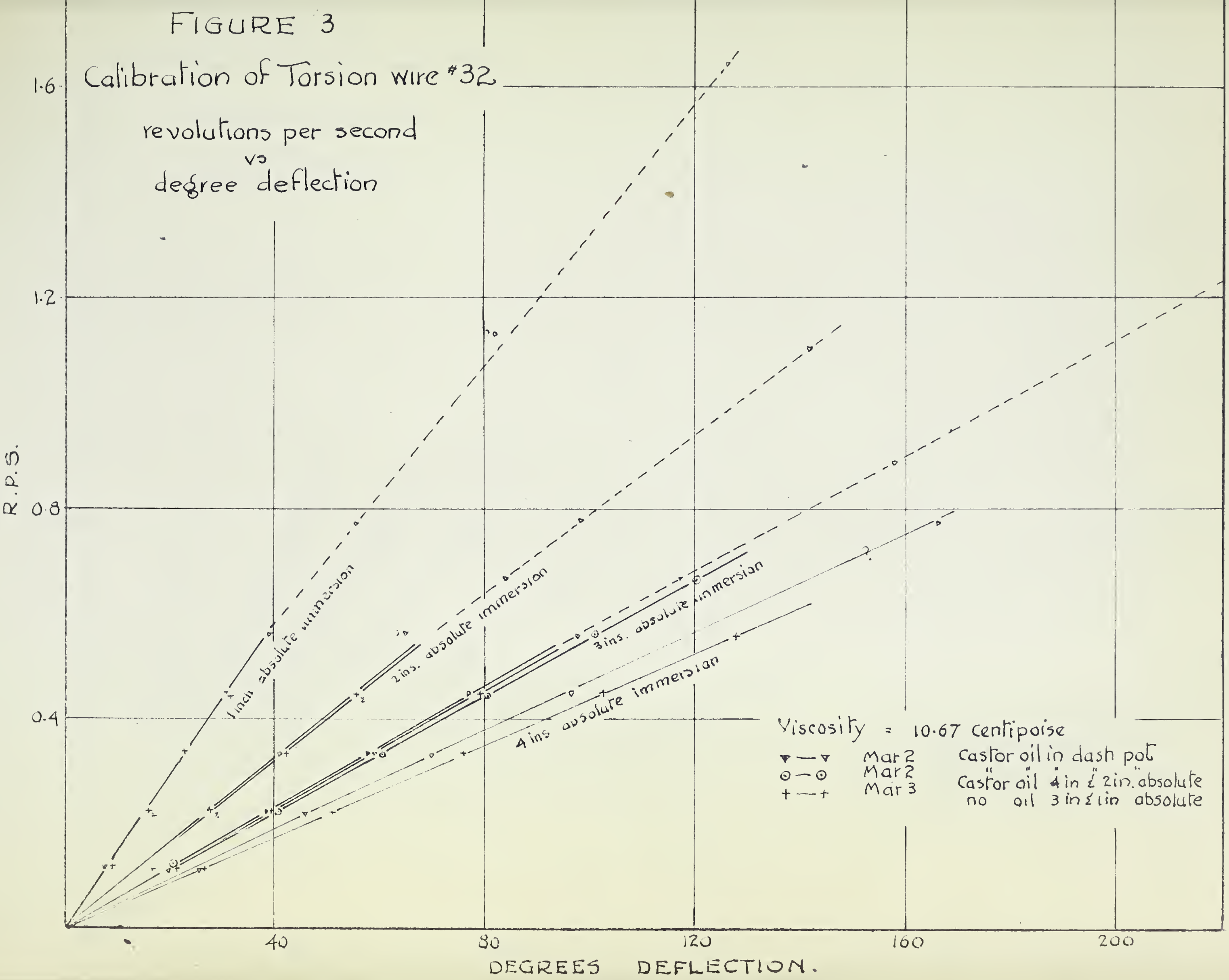

FIGURE 3

Calibration of Torsion wire #32

revolutions per second vs degree deflection

FIGURE 4.

Calibration of Torsion wire #30

revolutions per second vs. degrees deflection

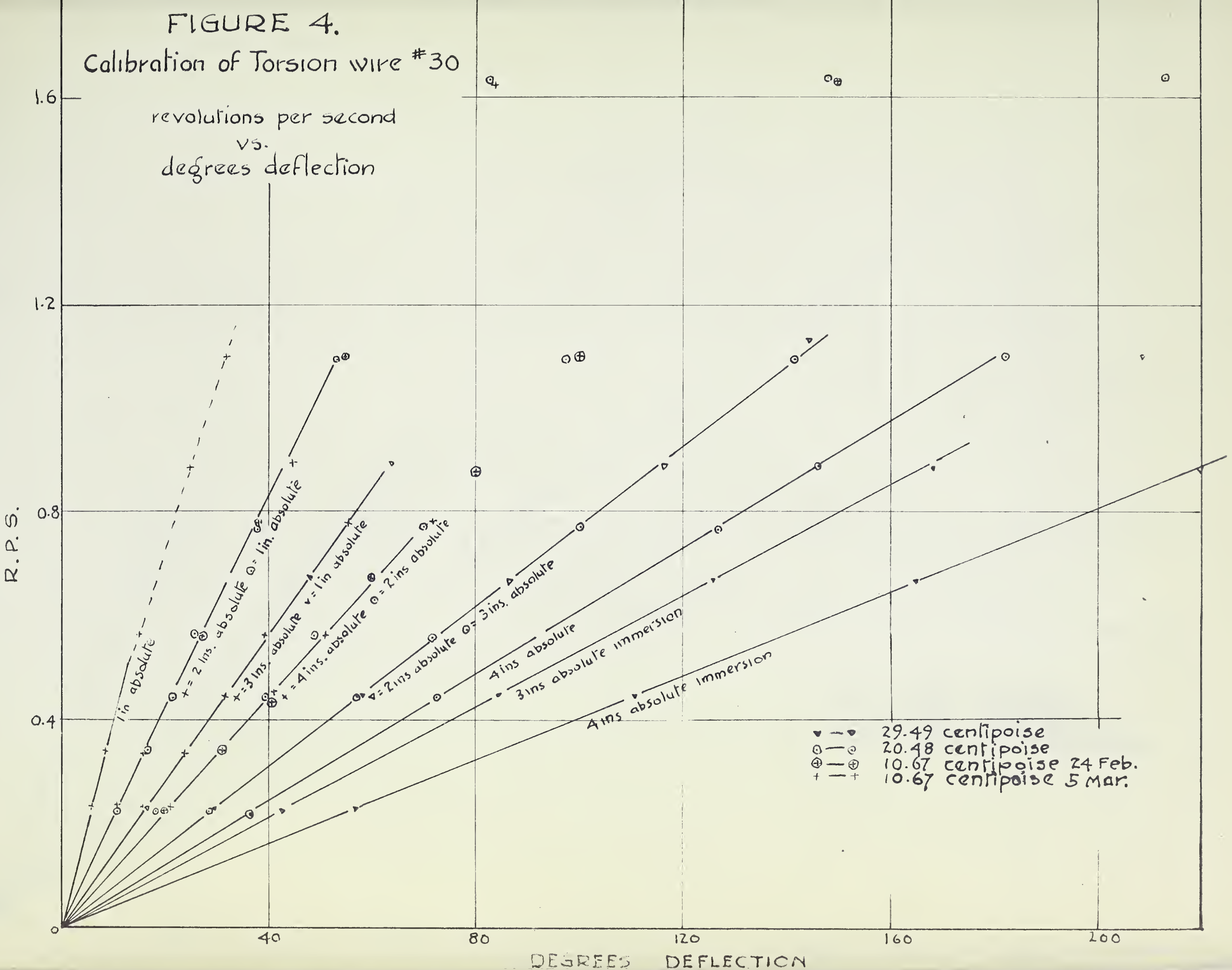

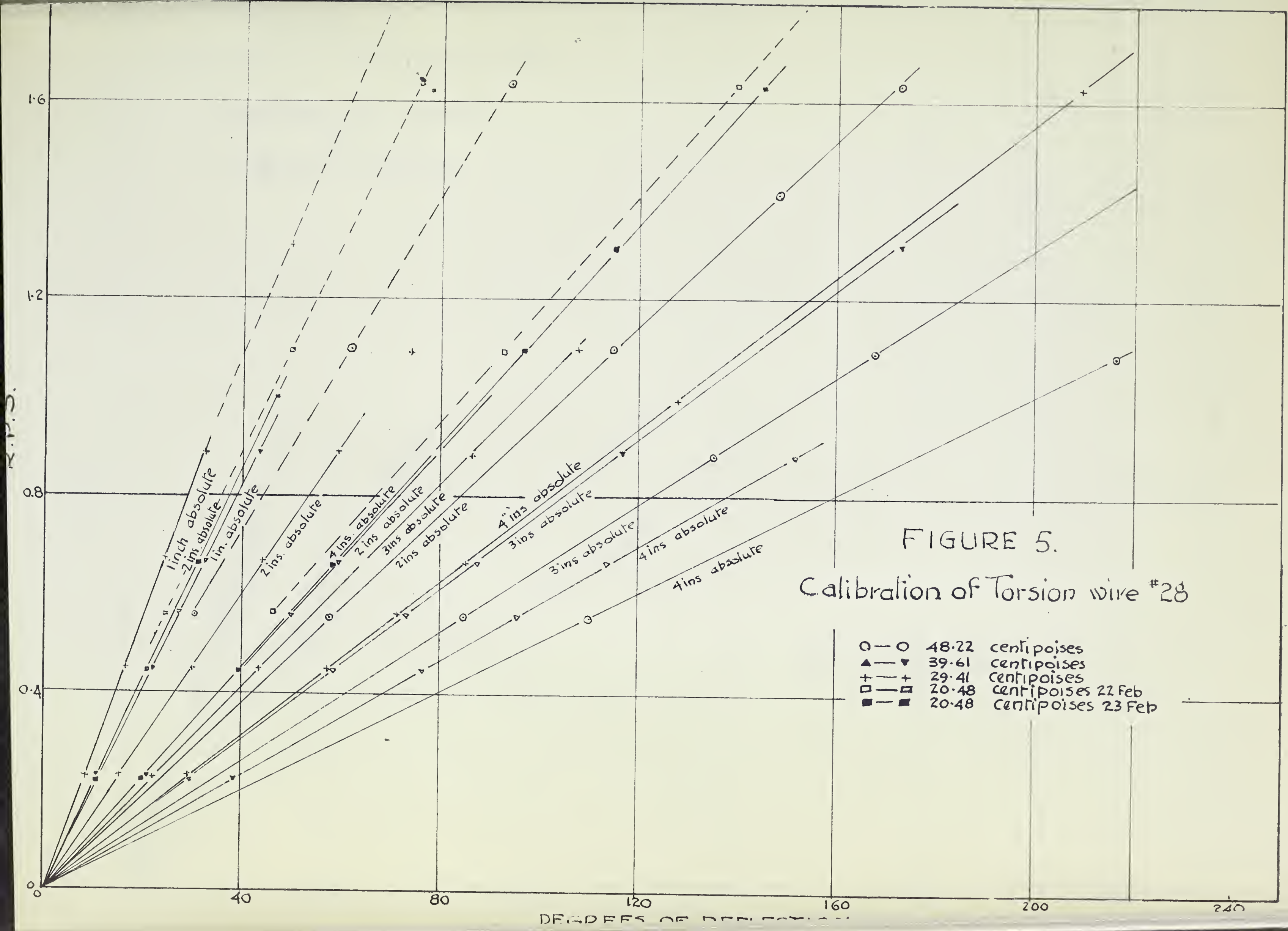

FIGURE 5.

Calibration of Torsion wire #28

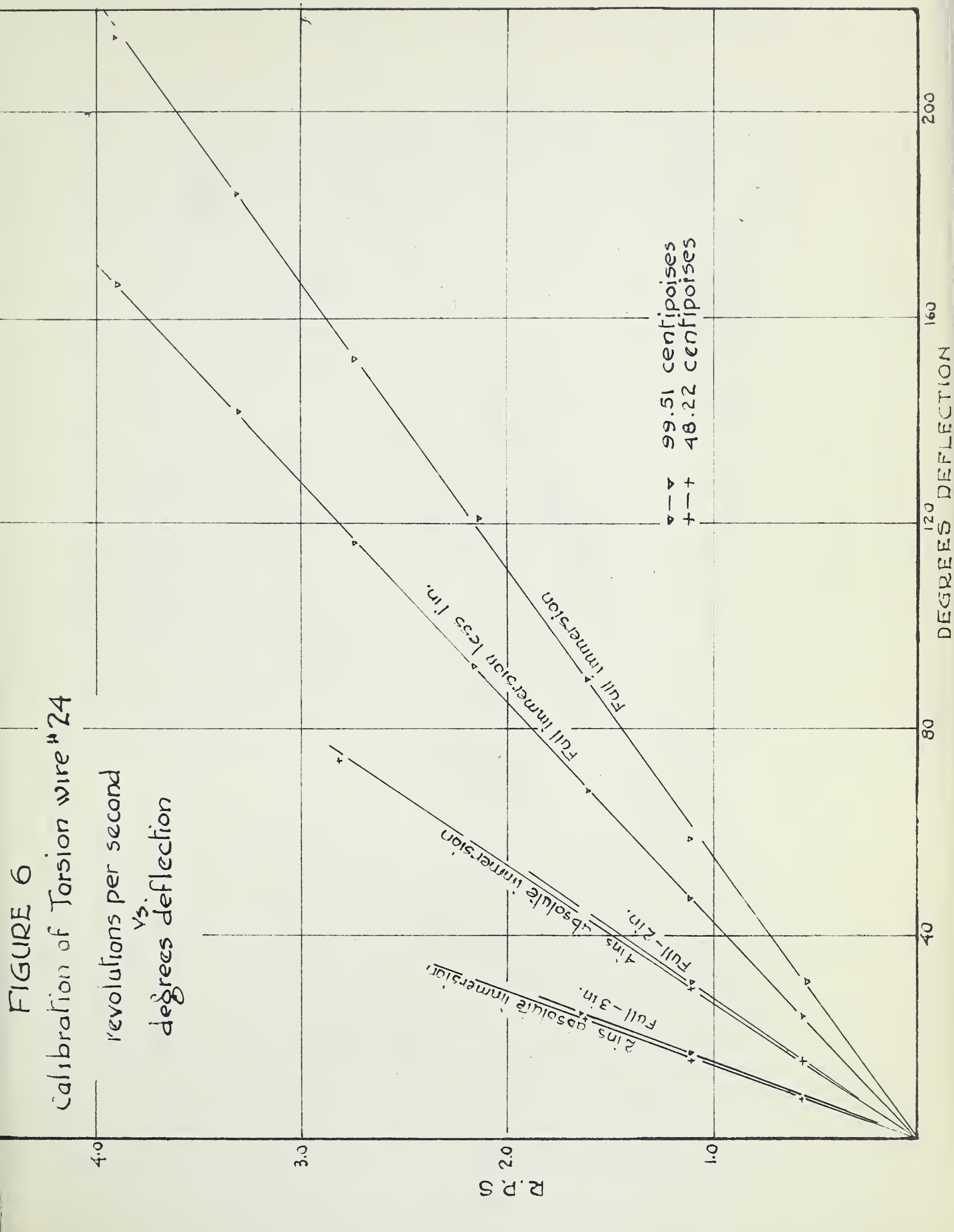

FIGURE 6

Calibration of Torsion wire #24

revolutions per second

vs.

degrees deflection

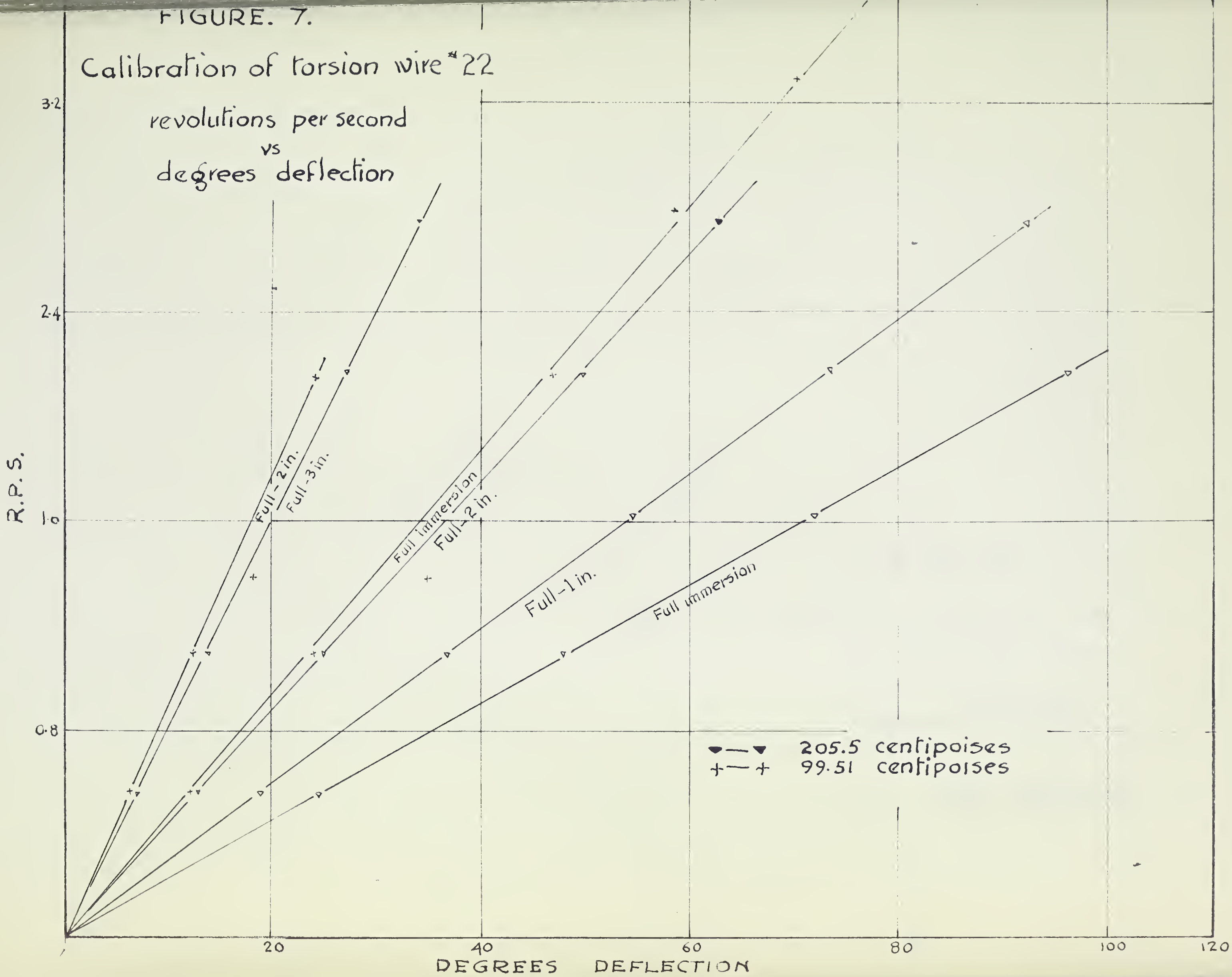

FIGURE. 7.

Calibration of torsion wire #22

revolutions per second
vs
degrees deflection

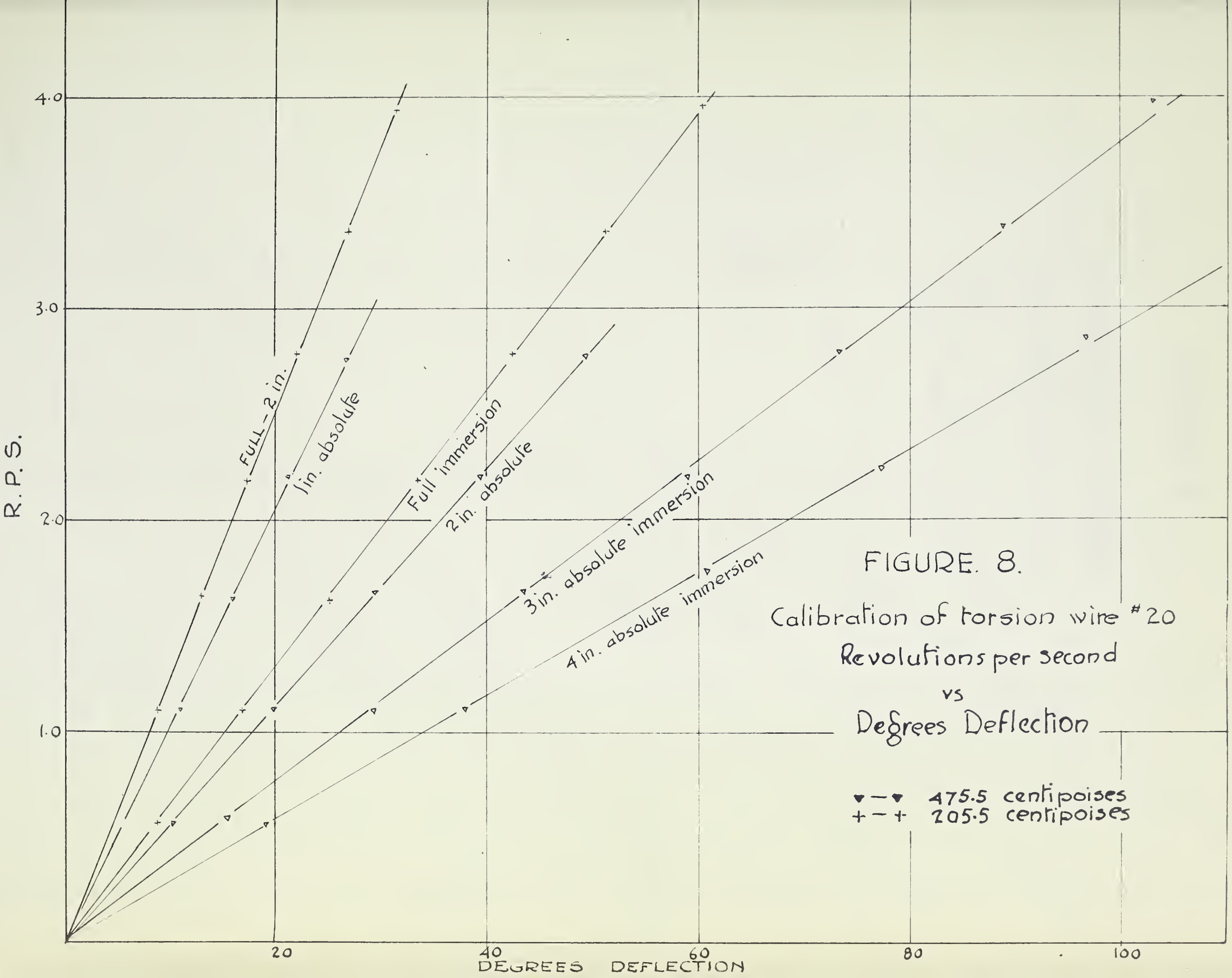

FIGURE. 8.

Calibration of torsion wire #20
Revolutions per second
vs
Degrees Deflection

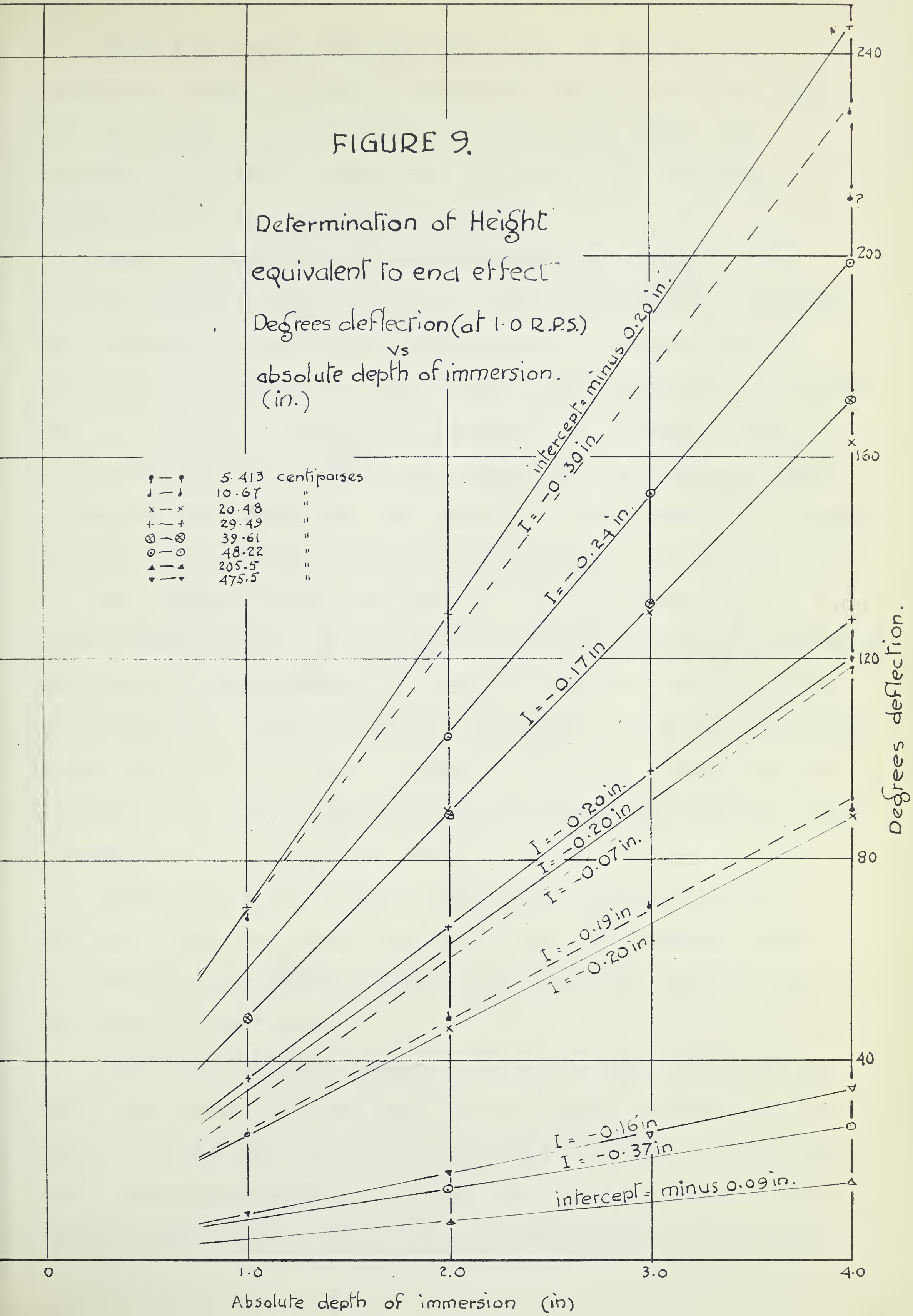

FIGURE 9.

Determination of Height equivalent to end effect

Degrees deflection (at 1·0 R.P.S.) vs absolute depth of immersion. (in.)

These above mentioned data show that, in general, the deflection - speed curves are linear and pass through the origin, the deflection - depth of immersion curves are linear and intersect at a common point, and the torsion wire constant depends only on the torsion wire itself.

Where the absolute depth of immersion is uncertain, the relative depth of immersion may be used to determine the torsion wire constant. If the height equivalent to the end effect is constant, the reciprocal of the slope of the deflection - relative depth of immersion curve is the torsion wire constant. This is illustrated on Figure #10 for the cases when the absolute depth of imersion was uncertain. The values of the torsion wire constant obtained by this method are given in Table #9, Appendix H.

The estimated error per point of the deflection - speed curves varies between 3% and 8% as the depth of immersion decreases. This yields a maximum error of about 3% per point on the deflection - depth of immersion curves. Therefore the height equivalent to the end effect could be in error by 3% of full immersion for 2 points and by 2% for 4 points on the curve. The basis for these estimated errors are outlined below.

a) Markers of the torsion wires permit assembly within 0.04 in. in 10.5 in, or within about 0.4%. The stretch under full load of the lightest torsion wire available, #34, is less than 0.1% of full length.

b) The calibrating oils are added until they flow over the lip of the rotor. The maximum meniscus height is about 0.15 in. above the rotor lip. Therefore, assuming a maximum variation of 50% in the meniscus height and that the effective heighth under shear of this fluid is 50% of the meniscus height, the maximum

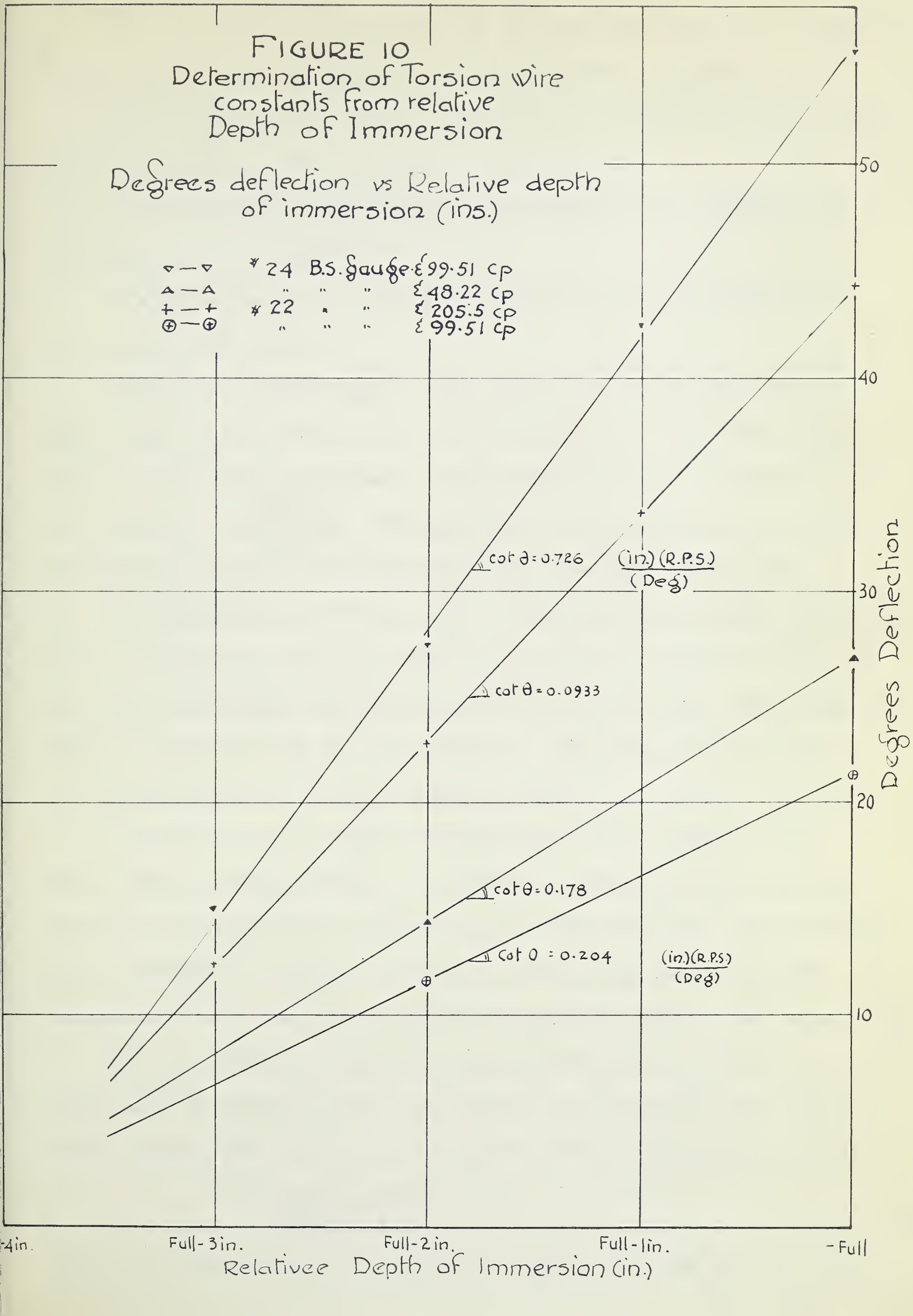

FIGURE 10
Determination of Torsion Wire constants from relative Depth of Immersion

Degrees deflection vs Relative depth of immersion (ins.)

error from this variation will be about 0.04 in.

c) The initial adjustment of the relative vertical locations of the rotor and the stator is reproducible within 0.04 in.

d) The number of revolutions are so chosen that the timing is reproducible within 1%.

e) The overall deflection may be read to 0.5 degrees and estimated to 0.2 degrees.

f) The effects of errors in adjusting the cylinders for coaxiality are known.

Therefore, assuming all the errors occur in the worst direction, the maximum variation per point on the deflection - speed curves will be between 3% and 8% per point, depending on the depth of immersion. The expected error per point on the deflection - depth of immersion curves is then about 3%.

An examination of Figure #9 shows that the maximum deviation of the effective depth of immersion from the absolute depth of immersion is 4% and the average deviation is 1.5%. The mean height equivalent to the end effect, $\Delta h_m = 0{\cdot}19$ in. is therefore within the limits of experimental error.

A study of Tables #8 and #9, Appendix 11, shows that, for a given torsion wire, the maximum deviation from the mean torsion wire constant is less than 4% and that the mean torsion wire constant from each calibration fluid agrees within 2%. The excessive deviation of the 48.22 centipoise oil is the exception,

If the chemical compositions and structures of the torsion wires are identical, then the torque is related to the torsion wire diameter, D , and the deflection, θ by the formula, (33).

$$T = \left(\frac{2\pi\theta}{360L}\right) G \left(\frac{\pi D^4}{32}\right) \tag{11}$$

where G is the modulus of rigidity and L is the torsion wire

length.

If the analysis, at the beginning of this section, is correct, the torsion wire constant is related to the torque by the formula

$$T = 1.83 \times 10^{-6} K' \theta \qquad \text{(lb force ft)}$$

Therefore $\log K' = 4 \log D + \text{constant}$ (12)

and a plot of the logarithm of the torsion wire diameter, D, against the logarithm of the torsion wire constant, K', will be a straight line of slope 0.25.

This plot is shown on Figure #II. The observed slope is 0.247, as compared to the theoretical value of 0.250. In other words, the theoretical analysis of the flow of Newtonian fluids between rotating concentric cylinders is consistent with the experimental data. The small scattering of the data around the best fit straight line indicates that the experimental data is at least self consistent.

The Behaviour of Newtonian fluids Between Rotating Concentric Cylinders.

The readers' attention is redirected to Figures #2 to #5 inclusive showing plots of deflection against speed for the 5, 10 and 20 centipoises oils. These curves exhibit two linear regions, the low speed region, solid lines, which pass through the origin; and the higher speed region, broken lines, which extrapolate to a positive intercept on the speed axis. The region of discontinuity on these curves is not a function of the torsion wire, but it appears to be a complex function of the viscosity, speed and depth of immersion. In the light of Taylor's work (31). The explanation may lie in the development of a stable form of turbulence. Whatever the explanation, it is fortunate that these curves are linear since this defines the region of

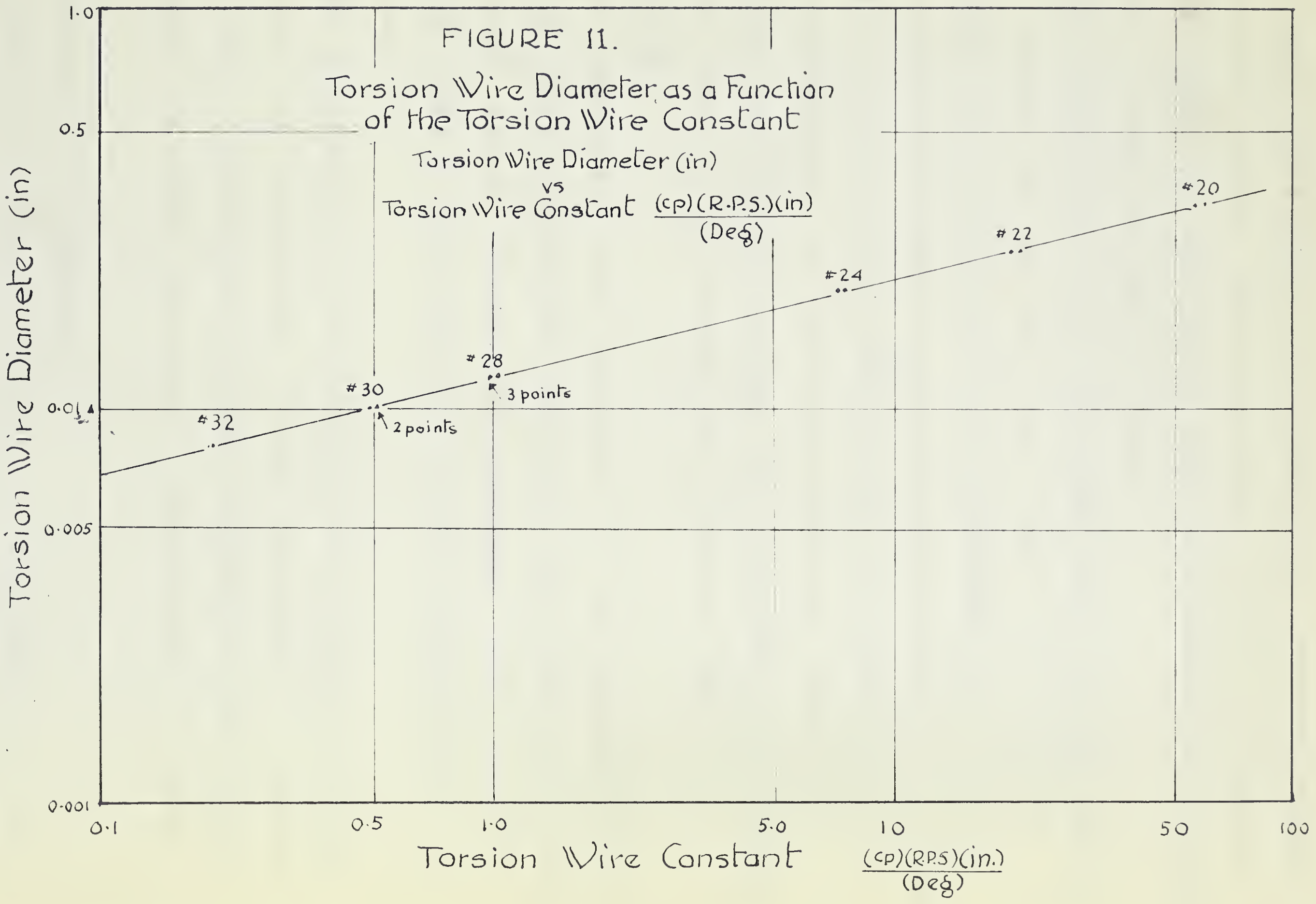

FIGURE 11.

Torsion Wire Diameter as a Function of the Torsion Wire Constant

Torsion Wire Diameter (in) vs Torsion Wire Constant $\frac{(cp)(R.P.S.)(in)}{(Deg)}$

discontinuity fairly closely.

If the above explanation is correct, more than one linear region should exist before the curved region indicating random turbulence is reached. This aspect has not been investigated.

The reasons for the earlier onset of turbulence with decreasing depth of immersion are not known.

The maximum speed of the instrument, about 240 rpm, was not always reached. In some cases this is due to the danger of overranging the torsion wires, but in many cases, it is due to the unexpected development of an oscillatory motion of the stator. The onset of this motion is earlier with decreasing depth of immersion, but it is too erratic to permit any satisfactory conclusions regarding its causes. The conditions, under which this oscillatory motion occured, are listed in Table #18, Appendix H.

The combination of the instability of the inner cylinder and the early onset of turbulence seriously limits the range of the instrument. Diagram #2 shows the approximate safe region of operation, that is, the region of laminar flow and stable operation.

The impossibility of straightening the torsion wires may accentuate this instability. It might be alleviated somewhat by the use of irrotational universal couplings on the chucks. This system will allow the stator to hang true at all times.

Damping the Oscillations.

Without the dash pot the system is underdamped up to at least 5 poises. It is badly underdamped below 50 centipoises. The dash pot improves the situation considerably. However, experience shows that not all fluids are suitable damping agents.

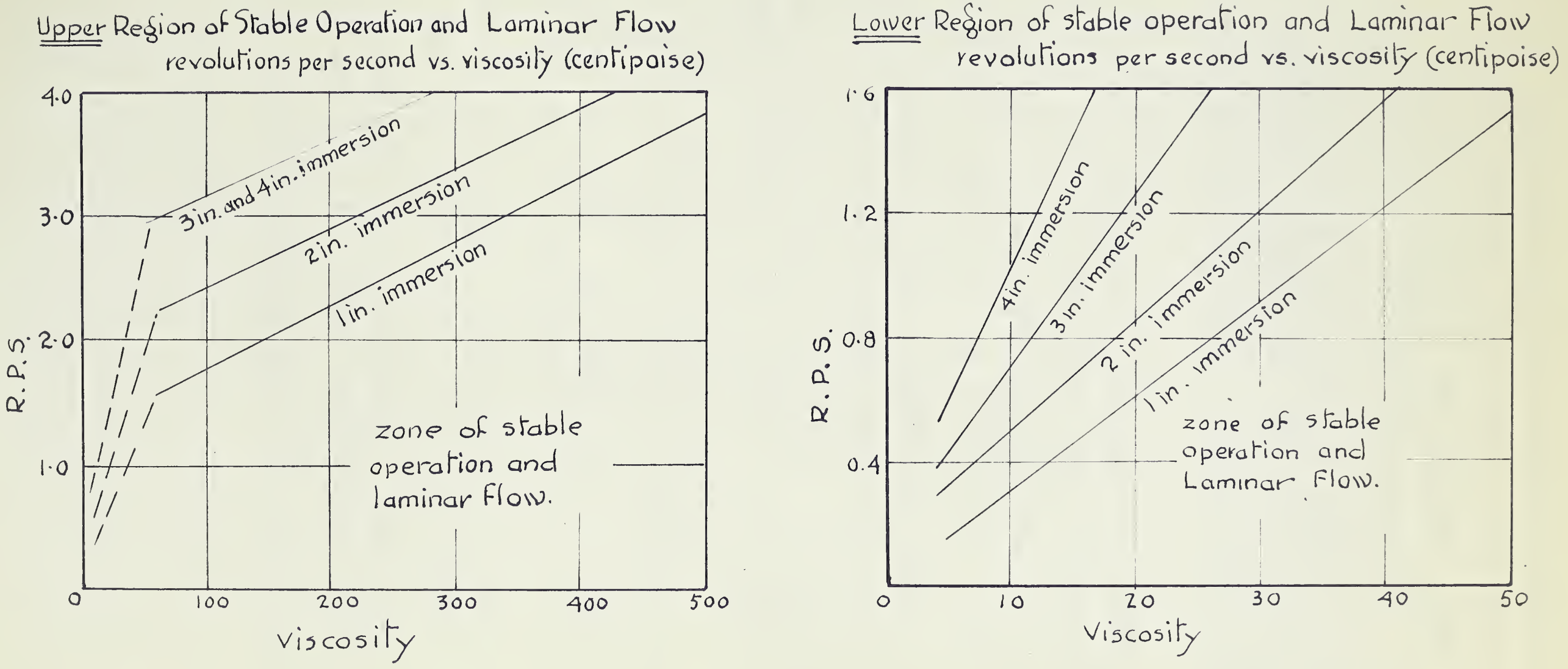

Upper Region of Stable Operation and Laminar Flow revolutions per second vs. viscosity (centipaise)

Lower Region of stable operation and Laminar Flow revolutions per second vs. viscosity (centipoise)

DIAGRAM 3. REGIONS OF "SAFE" OPERATION OF NEW VISCOMETER

For both castor oil and the 2 poises calibrating oil, a definite rigidity develops after about a half hour "rest period" that is, no violent agitation. With freshly stirred oil, the stator always returns to its original deflection. After about a half hour "rest period" the stator no longer returns to its original deflection. Castor oil, after about a four hour "rest period" caused an error of about 4 degrees with a #32 torsion wire.

The observed discrepancies between the deflection - speed curves for the 5 and 10 centipoises oils, Figures #2 to #4, when the dash pot was used, are probably due to this rigidity.

With mercury under oil, the breaking of a film on the mercury surface can actually be seen. Gurney (13) reports the development of a rigid surface on water after about four hours rest. He called this property "surface rigidity". In the absence of a better explanation about what happens in the dash pot, the rigidity of the oil will be called "surface rigidity".

This surface rigidity seriously complicates the measurement of low viscosity fluids. The drive belt is always slipping slightly. This slipping is not constant and causes a continuous oscillation of the stator, which may be as large as 3 degrees when the dash pot is not used. It is very difficult to estimate the deflection under these conditions. Unfortunately, the large vibrations set up by the Graham transmission and the 45 degree bevel gears prohibit mounting this drive of the base plate.

BEHAVIOR WITH CLAY-WATER SLURRIES

Measurement of the Rheological Properties of Clay - Water Slurries.

In general these slurries approach fairly closely the ideal case of the Bingham plastic. However, their rheology is complicated by the lack of a real yield value, the existence of a mild degree of thixiotrophy, and the appreciable settling rates at low concentrations.

Determination of the Torque per Inch of Immersion.

It is assumed that the height equivalent to the end effect is independent of the type of fluid (II). This is not the case for a Bingham plastic at the onset of motion. At the onset of motion, the relative end effect in this viscometer is the torque on the base, $\approx \frac{2\pi R_1^3}{3} f$, divided by the torque on the stator wall, $\pi R_1^2 h f$, which is $\frac{2}{3} \frac{R_1}{h}$. The relative end effect is therefore about 10% at full immersion compared to about 4% for Newtonian fluids. However the torque on a given stator increases with decreasing annular width, providing all the fluid is in laminar flow. The annulus width in the viscometer is very much smaller than the clearance between the bases, the relative end effect may be expected to decrease rapidly with increasing rotor speeds, possibly to the value for Newtonian fluids.

No correction for settling was made for the 29%, 25%, and 22% solids slurries. A correction for settling was applied to the 21%, 18% and 15% slurries. The effects of settling at constant shear on the torque are shown on Figure #12. These data are listed in Table #12, Appendix G. The slopes of the "linear" portions of these plots of percent change in torque against time are

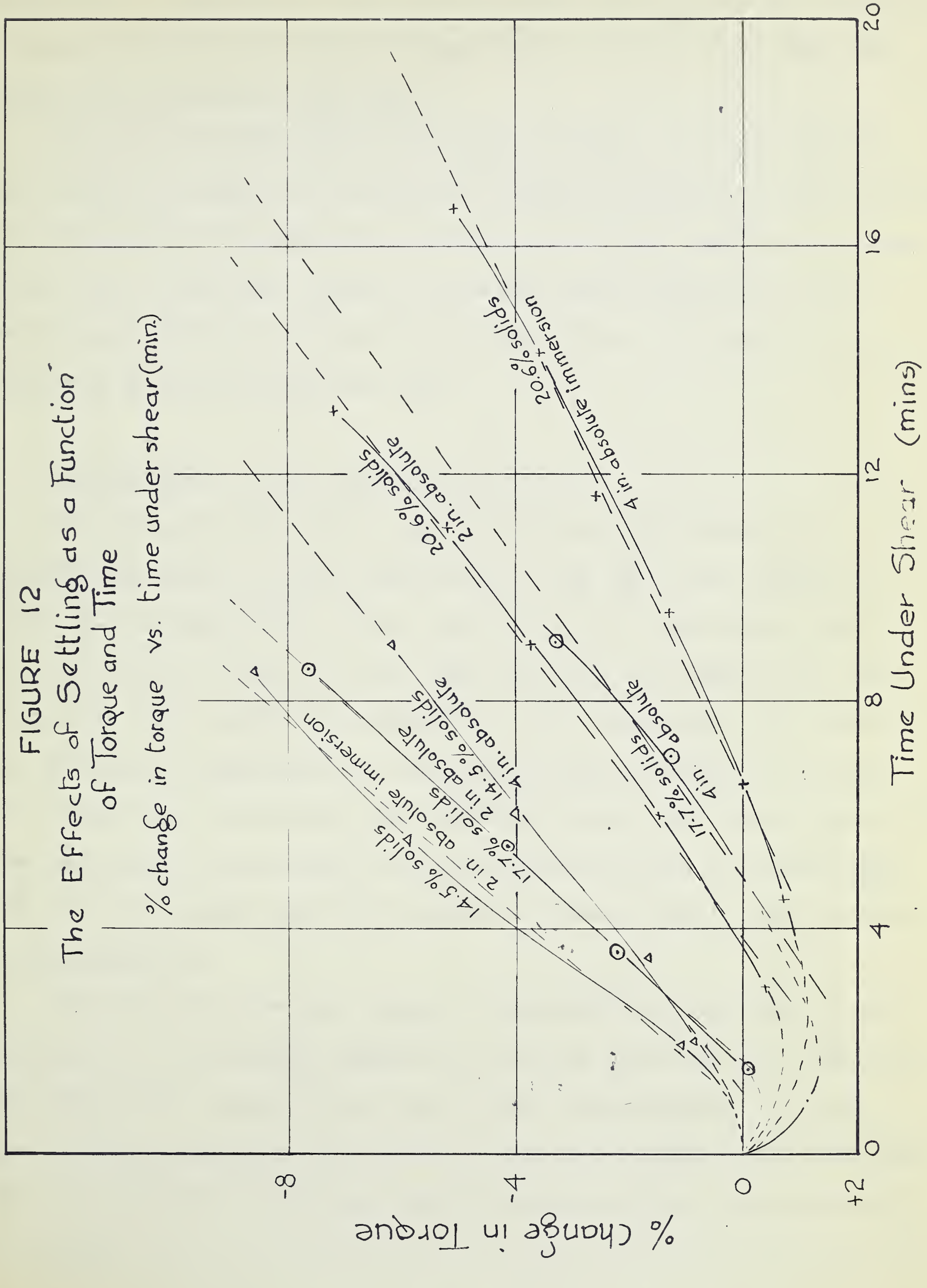

FIGURE 12

The Effects of Settling as a Function of Torque and Time

% change in torque vs. time under shear (min.)

assumed to be independent of all variables but the depth of immersion. These slopes are assumed to vary linearly with immersion. Therefore, the correction for settling is the observed torque multiplied by the settling factor multiplied by the time from the beginning of the run.

It is noteworthy that these clay - water slurries exhibit an initial increase in stress with time, as opposed to the majority of thixiotropic fluids which exhibit an initial decrease in stress with time at constant shear. The above approximation for the settling correction does not take into effect this initial build-up of the stress with time.

Measurement of the Consistency Curve

The data for the clay - water slurries were taken at increasing rates of shear from about 1 rpm up to the limit of stability of the stator, and, immediately, at decreasing rates of shear down to about 1 rpm. The data for the upcurve and the downcurve are separately reduced to 1 in. immersion. The mean of the different immersions is calculated and converted to torque (lb force ft),a correction for settling being made where applicable. The resultant torque speed curves are illustrated on Figure #13. The data for these plots are listed in Tables #II to #16 inclusive in Appendix H.

The data for the two highest concentration slurries are too scattered to be readily separated into the upcurves and downcurves The hysteresis loops for the four lower concentration slurries are readily apparent. The points above the broken lines represent the mean observed torque per inch immersion at the various rates of shear.

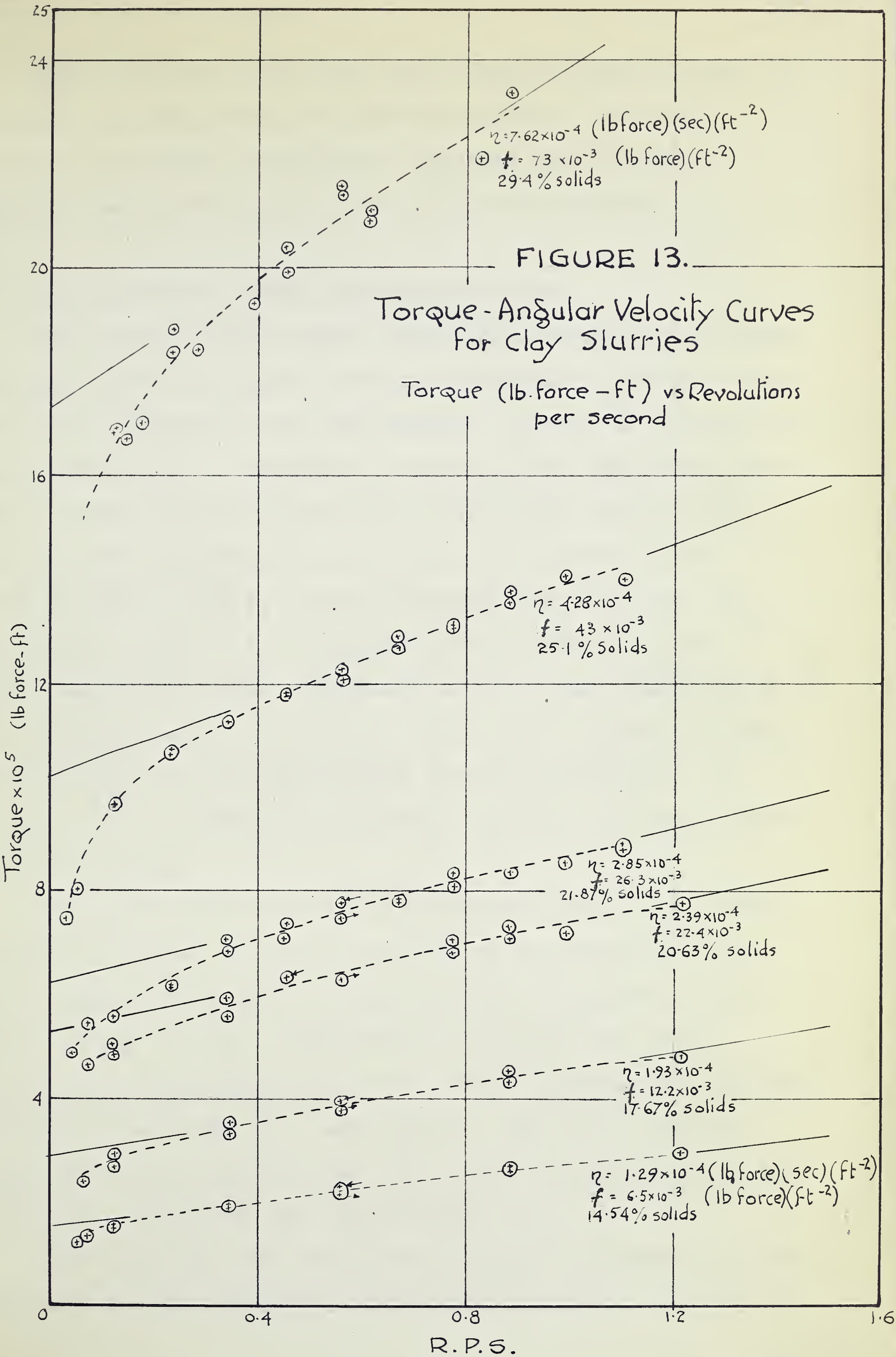

FIGURE 13.

Torque - Angular Velocity Curves for Clay Slurries

Torque (lb.force – ft) vs Revolutions per second

These hysteresis loops may be due only to settling and, or, to errors in interpreting the settling curves, Figure #12, However, the changes in torque at constant rate of shear indicate that these slurries are mildly thixiotropic.

Interpretation of the Consistency Curves.

The torque - speed curves, Figure #13, indicate that these slurries behave in a manner similar to Bingham plastics. While they do not exhibit a real yield value, the rate of increase of torque with speed is tremendous over the first ten percent, or less, of the non-linear portions of the torque speed curves. For the lower concentration slurries, the majority of the curve is nearly linear. As the concentration increases the fractional length of the "linear" portion decreases to an almost negligible value. This may be due to the dimensions of the instrument and, or, the fluid properties. Since the lower concentration slurries approximate Bingham plastics, it is assumed that the higher concentration slurries also approximate Bingham plastics.

Extrapolation of the best fit straight lines, through the "linear" portions, to the torque axis yield intercepts which differ greatly from those calculated from the apparent yield values of the fluids. Consequently, the trial and error technique for the evaluation of the yield value and the mobility, outlined in Appendix F , was applied. The solid lines in Figure #13 are proportional to those yield values and mobilities which most closely fit the experimental data.

This technique was particularly helpful in evaluating these constants for the 25% and the 29% solids slurries. Indeed, it

may be the only satisfactory method of reducing these forms of curves to a yield value and a mobility.

Substitution of the dimensions of the instrument into the Reiner and Riwlin equations (Appendix D) shows that the intercept on the torque axis, T' is related to the yield value, f , by the equation $$f = 422\,T' \text{ lb force ft}^{-2} \tag{13}$$ and that the slope of the straight line $\frac{\Delta T}{\Delta RPS}$, is related to the coefficient of rigidity, η , by the equation
$$\eta = 11.4\,\frac{\Delta T}{\Delta RPS} \text{ lb force sec ft}^{-2} \tag{14}$$
The values of these constants are listed opposite their respective torque - speed curves, Figure #13.

Smoothing the Data

In view of the difficulties in interpreting the data, it is advisable to check the consistency of the interpretations placed on the data by smoothing the yield values and mobilities against the solids concentrations. Now, the measured variables are torque and speed. Therefore, if the value of one of the constants is changed, the value of the other constant must be changed by that amount which makes the new pair of values consistent with the torque speed data.

The two most practical methods of smoothing the data were found to be: plotting the constants on log-log paper as functions of the percent solids, and plotting the constants on semi-log paper as exponential functions of the percent solids.

Figure #14 shows plots, on log-log paper, of the yield values and the mobilities against percent solids. The plot of yield value against percent solids is an almost perfect straight line, the data scattering only slightly around it. The mobilities are

rather widely scattered around their best fit curve. The yield values were adjusted to the straight line and the mobilities were re-evaluated. The new values of the mobilities scatter slightly around their best fit curve. These constants are replotted, Figure #15, on semi-log paper as functions of percent solids. The solid lines illustrate the smoothed values over the range investigated and the broken lines illustrate the extrapolated values. The plotted points are the original interpretations.

Figure #16 shows plots of the yield values and the mobilities as exponential functions of the percent solids. Theoretically, these curves would be linear if the properties of the slurries were exponential functions of the percent solids. The yield value should be zero and the mobility should be the viscosity of water at zero percent solids. However, the data from "S" shaped curves around the best fit straight lines. The data were smoothed to these curves in a manner which gives, over the concentration range investigated, equal areas above and below the best fit straight lines. Adjustment of either the yield value or the mobility for the change in their opposite number does not reduce the scattering. Therefore, these smoothed curves are shown "as is".

The log-log method of smoothing appears to produce the more consistent results. However it does not account for the properties of the slurries at zero percent solids.

The original data on the 29% solids slurry gave two values, 29.4% and 28.6% solids. Both methods of smoothing indicate that 29.4% is the correct concentration.

Regardless of the method of smoothing, the inflections of the smoothed data indicate that the slurries may no longer behave as Bingham plastics below about 5% or 10% solids. Green

FIGURE 14

Yield Value and Mobility as a Function of % Solids

% solids (wet basis) vs. yield value, f, (lb force ft^{-2}) and (mobility)$^{-1}$, η, (lb force ft^{-2} sec)

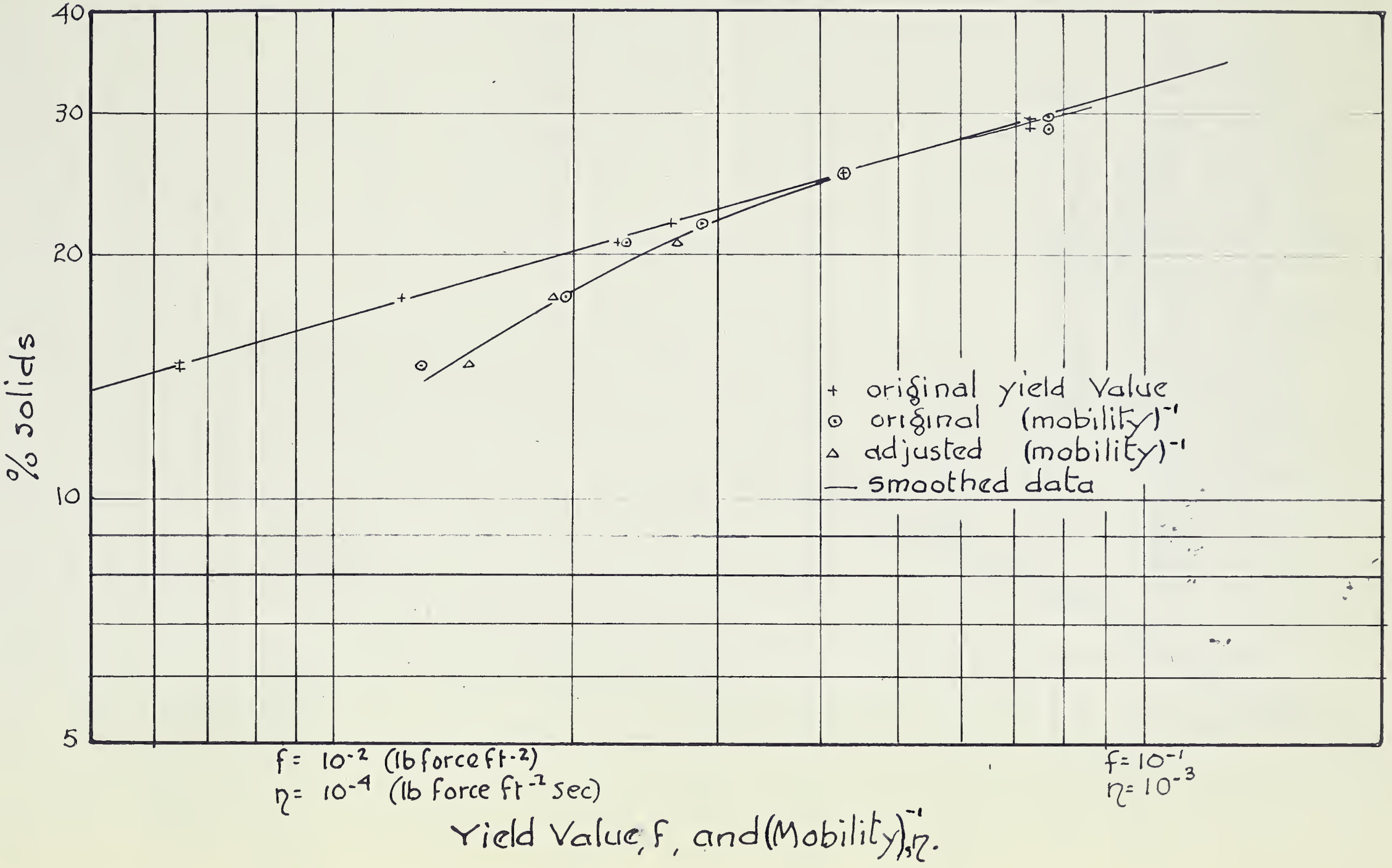

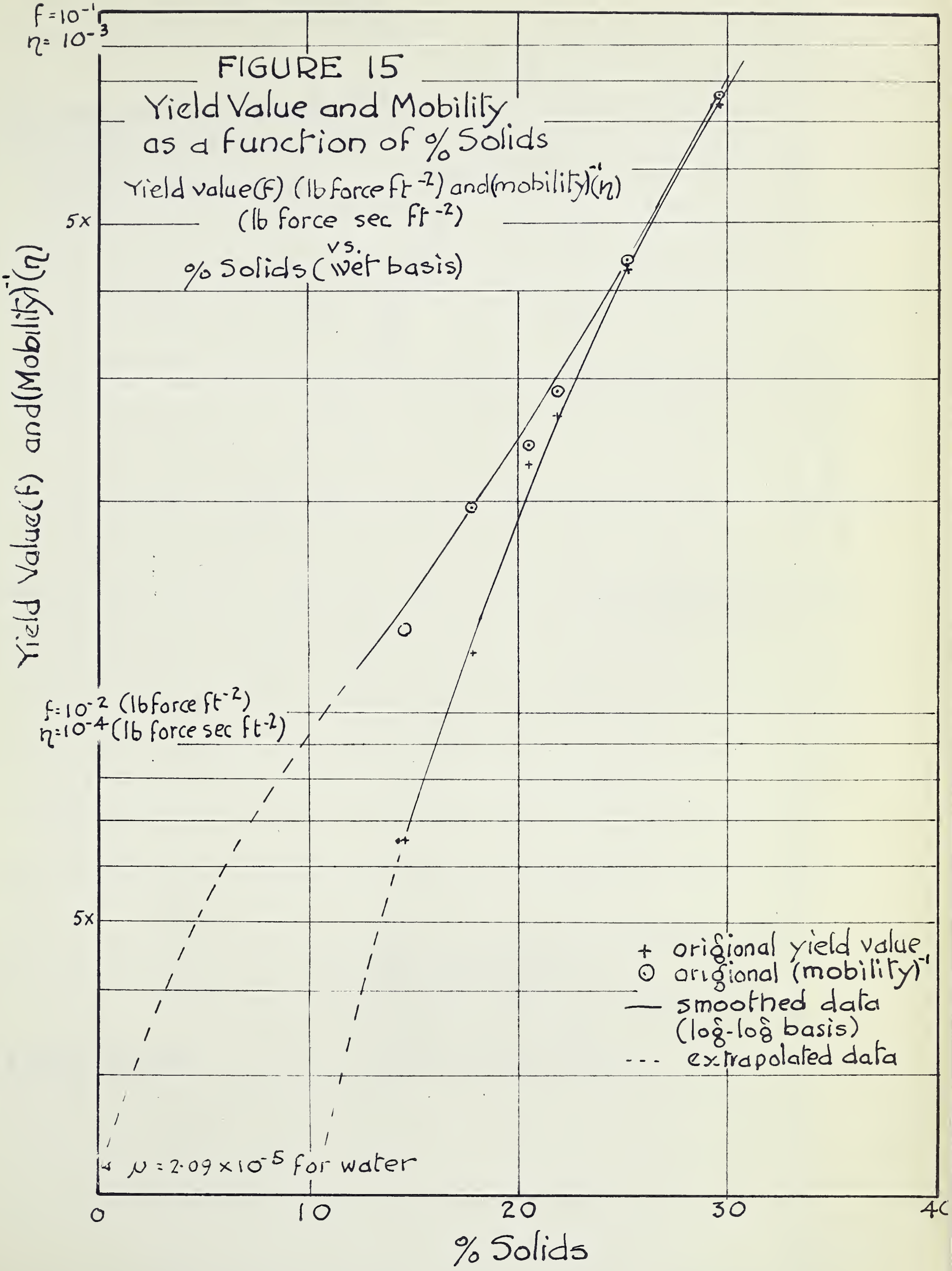

FIGURE 15

Yield Value and Mobility as a function of % Solids

Yield value (f) (lb force ft^{-2}) and (mobility)$^{-1}$ (η) (lb force sec ft^{-2}) vs. % Solids (wet basis)

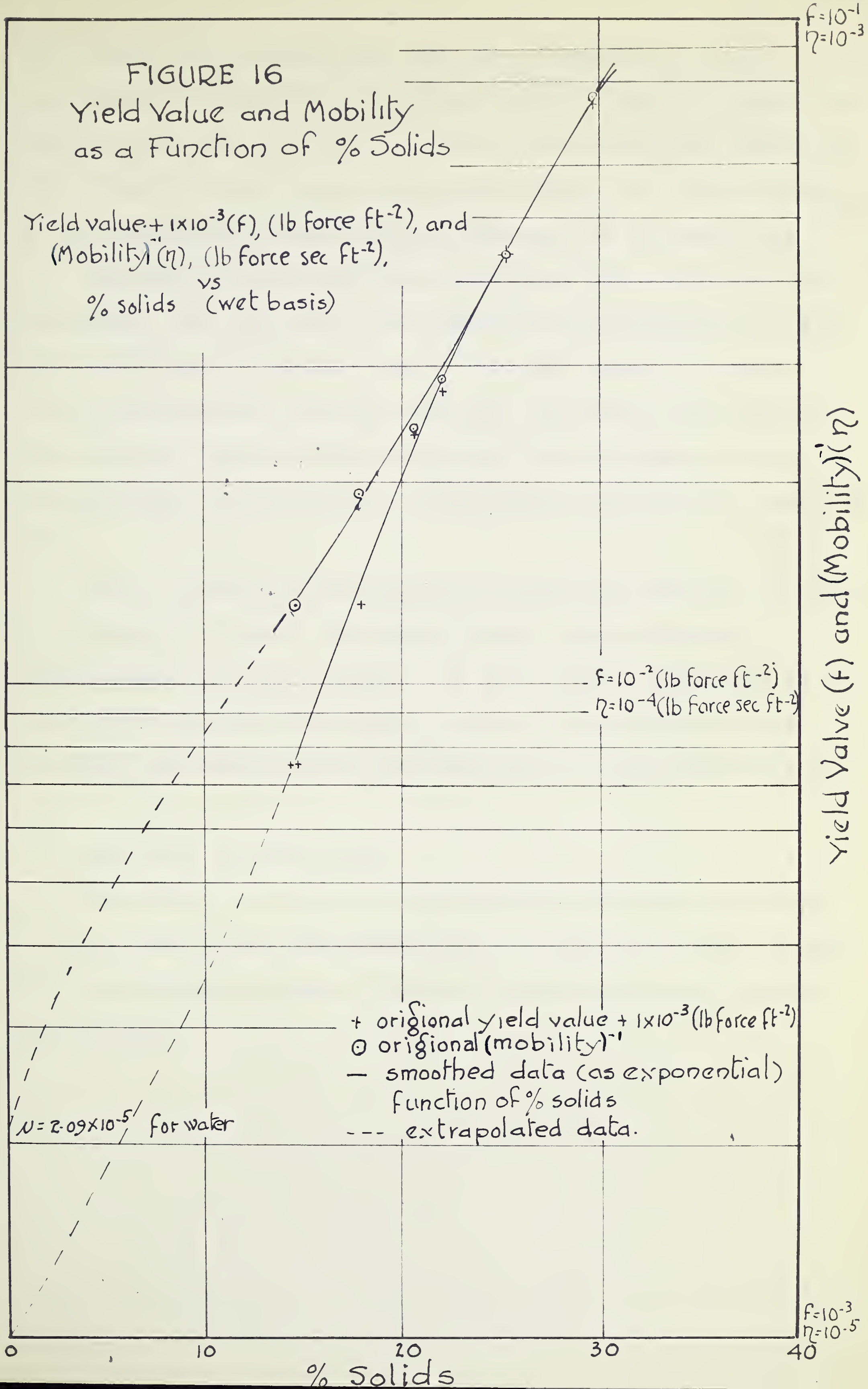

FIGURE 16
Yield Value and Mobility as a Function of % Solids

(II) states that suspensions must have "structure" and be "continuous" throughout the carrier fluid in order to behave as Bingham plastics. That the effects of the structural forces of the suspensions may become negligible before the other effects of the suspension on the carrier fluid do, is not unlikely.

Extrapolation of the data below about 10% solids may be dangerous. The interpretations placed on the data for the 25% and the 29% solids slurries is , from the nature of their torque-speed curves, open to question. As well, the values of the constants increase "exponentially" with percent solids. Consequently, extrapolation to much above 35% solids is questionable.

These comments do not apply to conditions where it is vital to extrapolate limited data over a wide range, and when it becomes "any port in a storm". In these cases, smoothing as an exponential function of percent solids is the easier method and does take into account the properties of the carrier fluid.

Stability of the Stator

The stator is very much more unstable with the clay-water slurries than it is with Newtonians of comparable "viscosities". This instability appears to increase with increasing apparent yield value.

VII EXPERIMENTAL DATA FROM THE STORMER VISCOMETER.

BEHAVIOR WITH NEWTONIAN FLUIDS

Calibration of the Stormer Viscometer

The fluid boundaries, for the Stormer viscometer used in this investigation, consist of a rotating hollow cylinder with a perforated up er plate, and a fixed outer cylinder with baffles projecting inwards from the sides and with a central baffle projecting upwards from the base. In addition, it has a thermometer well attached to the upper portion of oneof the side baffles. It is normally filled until the fluid is about 1/16 in. above the rotor surface. Such complex flow boundaries as these are not yet amenable to mathematical analysis, even for Newtonians.

The operating technique

a) Measure the load which just keeps the rotor turning in air.

b) Allow a start-up period of 25 revolutions.

c) Measure the time for the next 100 revolutions. This measurement is duplicated for Newtonian fluids.

The temperature was held constant at 70 ± 0.2 deg F during all measurements with this instrument.

Plots of gross load against speed, for each of the standard Newtonian oils used, are illustrated on Figure #17. These data are listed in Table #19, Appendix I. The curves are linear for the higher viscosity oils and are therefore assumed to be linear for the lower viscosity oils as the speed approaches zero. The solid lines indicate laminar flow, either observed or estimated, and the broken lines indicate turbulent flow.

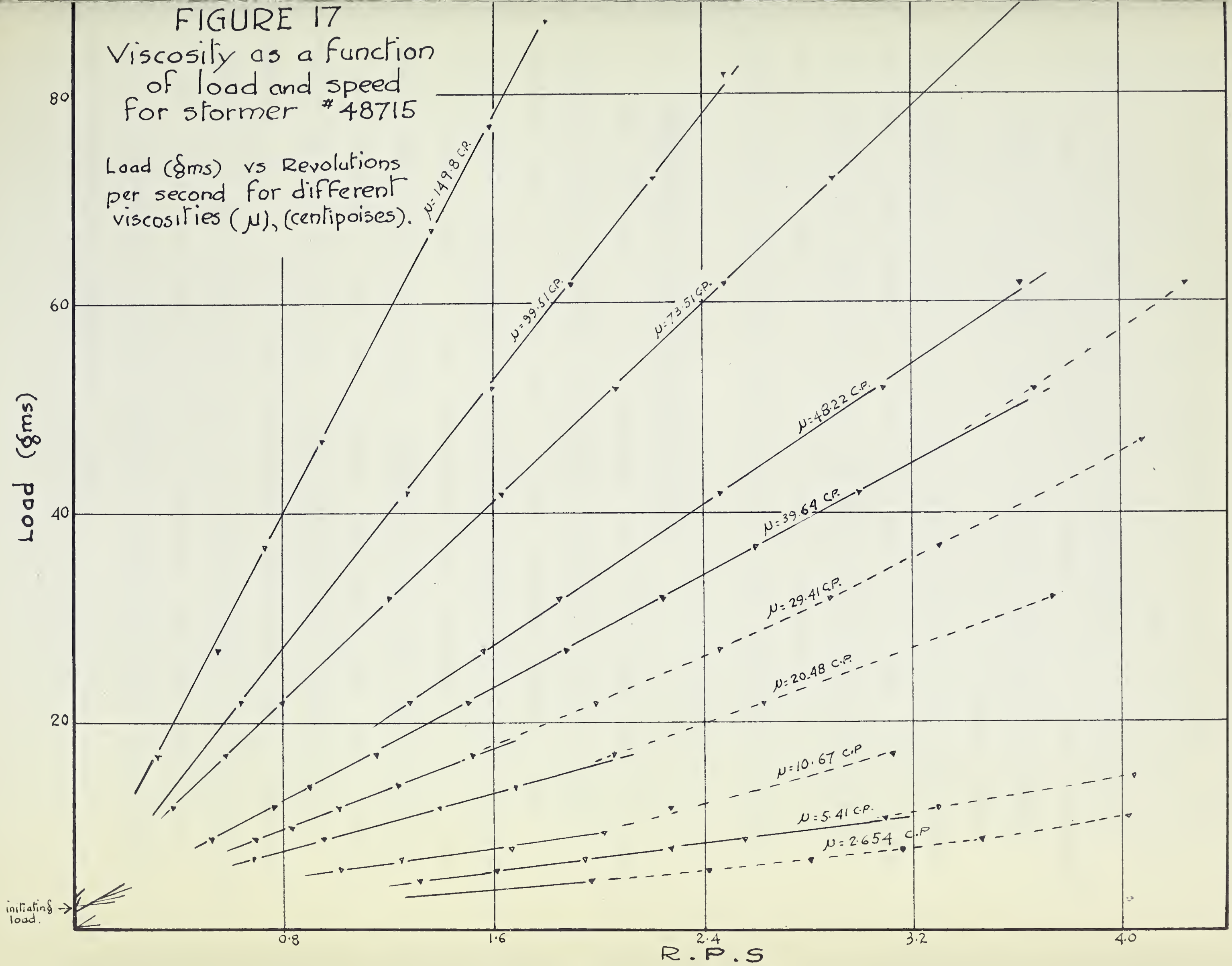

FIGURE 17
Viscosity as a function of load and speed for stormer #48715

Load (gms) vs Revolutions per second for different viscosities (μ), (centipoises).

In the light of the analysis of this instrument, Appendix G, it is noteworthy that the intercepts of the majority of these curves coincide with the experimental initiating load. It is doubtful whether this intercept is due to any undetected change in the flow pattern since it is in the opposite direction to that expected if the flow pattern changed as the speed decreased.

Figure #18 shows a plot of viscosity against the slopes of the load - speed curves, as the velocity approaches zero. The remarkable linearity of this curve indicates that the flow pattern is independent of viscosity at low speeds. This tends to confirm the analysis of the Stormer viscometer outlined in Appendix G. There is little difference between the results based on the initiating load concept or the intercept concept.

Magnitude of the Friction Forces.

The friction in the instrument was determined from the data obtained from balancing the torque transmitted to the rotor against the torque from equal opposed weights acting on the rotor shaft, via threads passing over almost frictionless pulleys. The friction factor is the torque applied directly to the rotor shaft divided by the torque, transmitted via the gear train to the rotor shaft, from that applied load which just keeps falling minus the initiating load. This friction was determined for loads of about 30, 60 and 110 grams. From these data, Table #20 Appendix 1, the mean value of the friction factor is approximately 0.93. This low friction factor indicates that the calibration curves represent a fairly accurate picture of the viscous torque on the rotor as a function of speed.

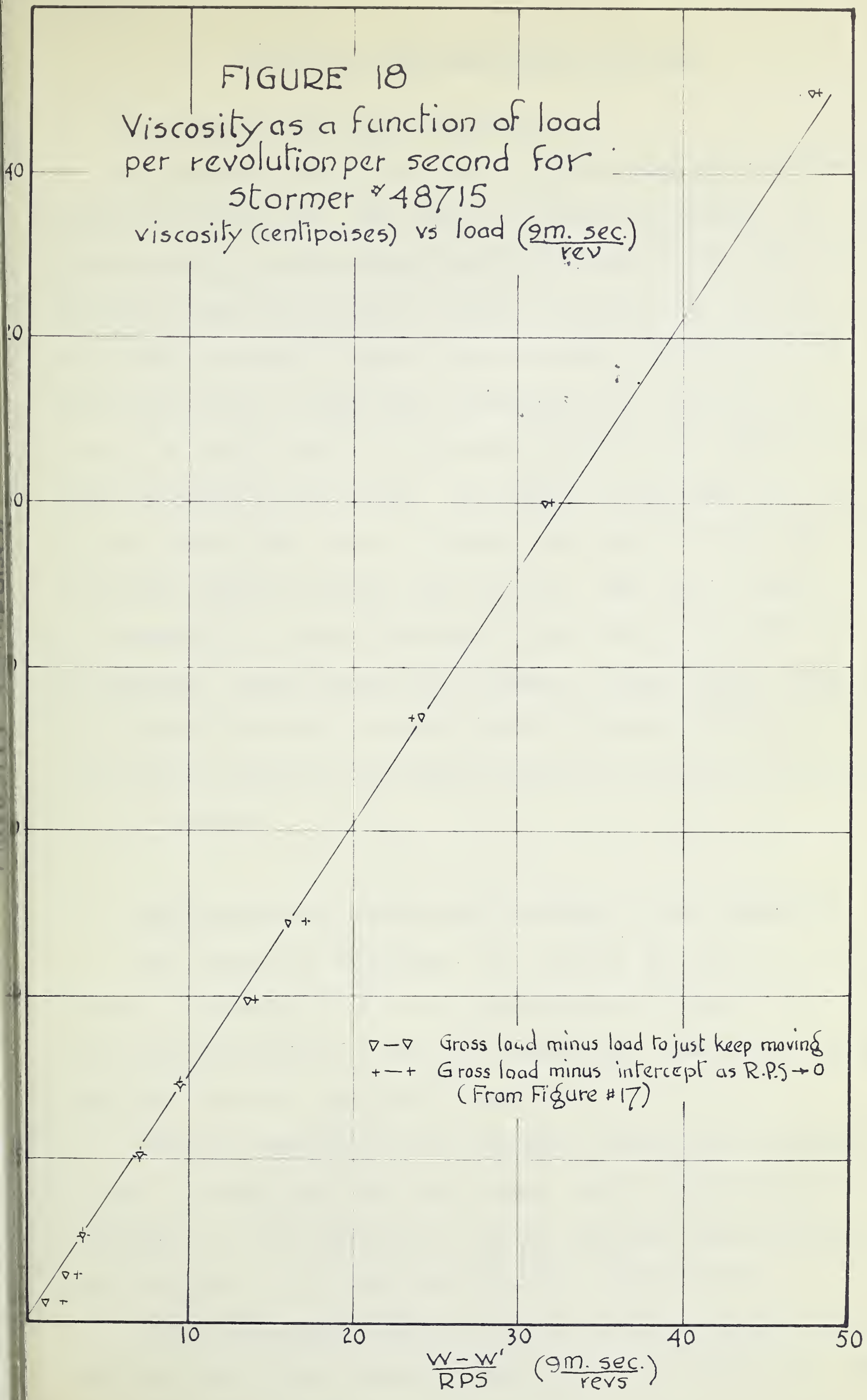

FIGURE 18

Viscosity as a function of load per revolution per second for Stormer #48715

viscosity (centipoises) vs load $\left(\frac{\text{gm. sec.}}{\text{rev}}\right)$

BEHAVIOR WITH CLAY-WATER SLURRIES

The Form of the Flow Boundaries.

In general, the yield value of these slurries creates its own flow boundaries. The shapes of these boundaries are obtained, unfortunately for the outer portion of the system only, by pouring a very fine line of india ink across the annulus. From relatively low up to fairly high speeds, these boundaries remained nearly cylindrical extending out, depending on the speed, to about twice the clearance between the baffles and the outer surface of the rotor. At higher speeds the flow boundary bulged towards the outer cylinder wall, and at very high speeds vortices appeared beside the baffles. The load - speed curves are remarkably linear throughout these changes in the flow boundaries. These curves are shown on Figure #19. These curves are similar to those expected from a Bingham plastic in a concentric cylinder rotational viscometer having a relatively narrow annulus.

The Consistency Curves of the Clay - Water Slurries

The operating techniques are similar to those for Newtonian fluids. However, in view of the rate of settling of the slurries, the speed determination is not duplicated. The load - speed data are taken as rapidly as possibly.

From the analysis of the Stormer viscometer in Appendix G, it may be shown that the net torque on the rotor corrected for friction, T, is related to the net applied load, $W-W_0$(gm), by the equation $T = 8.85 \times 10^{-6} (W - W_0)$ lb force ft

Figure #20 shows plots of the net torque against speed for the identical clay slurries used in the new viscometer. These

FIGURE 19

Correlation of Flow Boundaries with Torque -speed data for clay-water slurries.
Load (gm.) vs. Revolutions per second

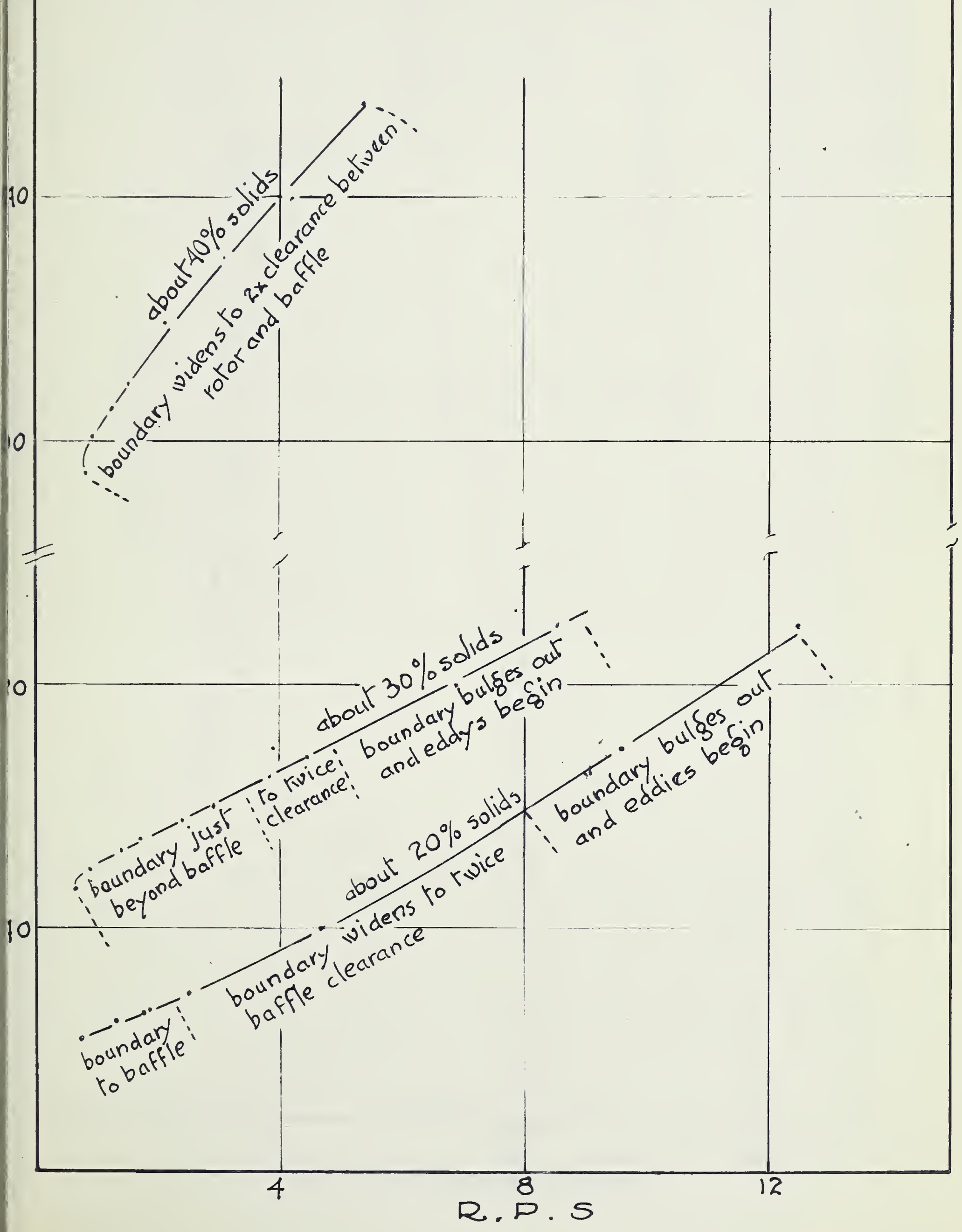

FIGURE 20

Torque - Speed curves for clay-water Slurries
obtained with stormer #48715

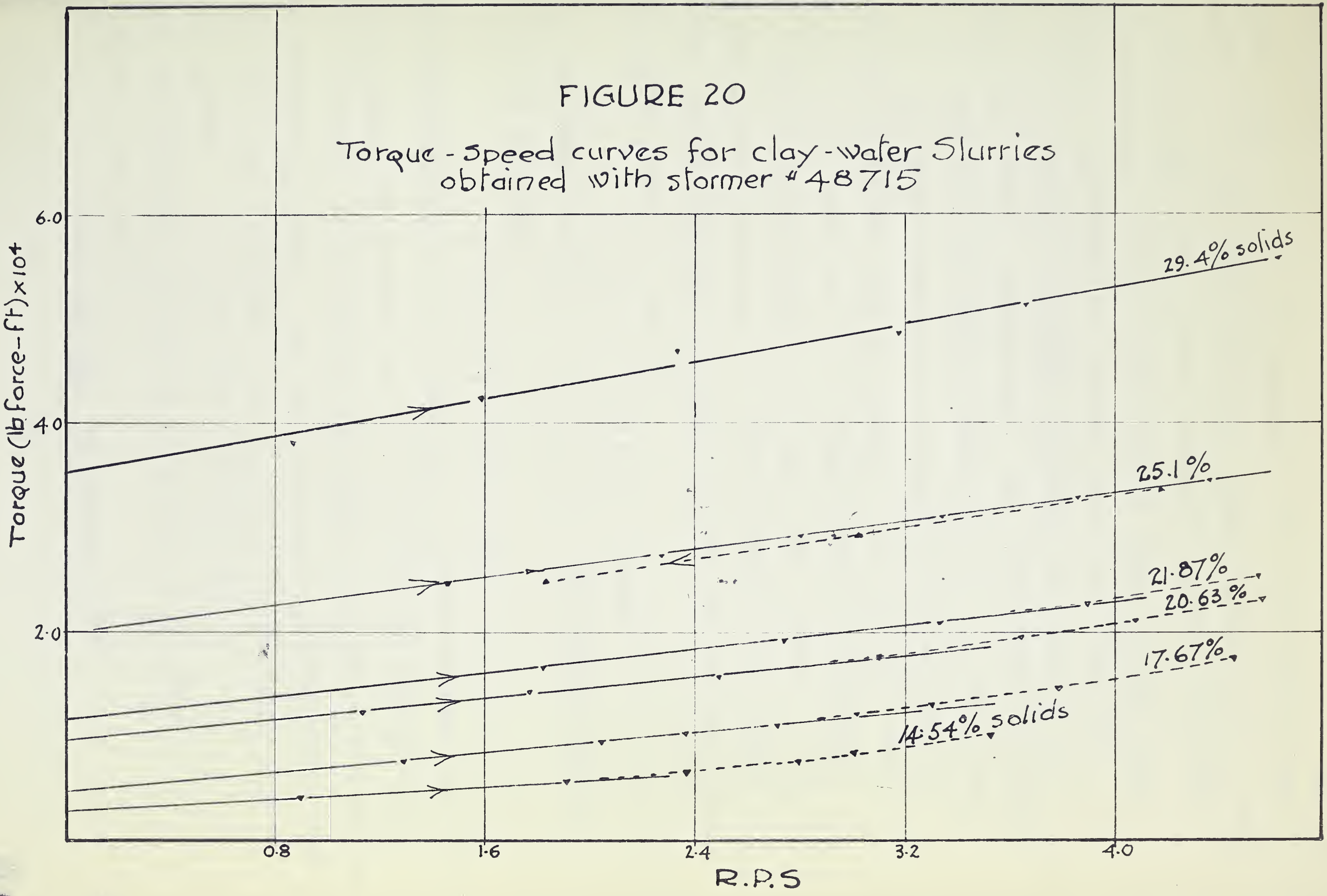

data are listed in Table #21 Appendix I. The solid lines are the tangents to the low speed end of the "linear portions of the curves.

In the light of the apparent similarity between the Stormer and a concentric cylinder system having a narrow annulus, these data will be interpreted on the basis that the baffles limit the flow to concentric cylinders. Therefore the slopes of the tangents are directly proportional to the coefficients of rigidity and the intercepts are directly proportional to the yield values.

If the system is assumed to be equivalent to two pairs of concentric cylinders, then the torque, T, is the sum of the torques on the inner and outer systems, T_i and T_o respectively. The torque on either system is the sum of the intercept of the tangent on the torque axis, T', and the product of the slope, $\tan\theta$, of this line and the angular velocity, Ω, of the system. This may be written in the form,

$$T = T_o' + T_i' + \Omega(\tan\theta_o + \tan\theta_i)$$

From the Reiner and Riwlin equations (24), this equation may be written in the form,

$$T = (C_1 + C_2)f + \Omega(C_3 + C_4)\eta$$

where the constants C_1, C_2, C_3 and C_4 are dependent only on the dimensions of the cylinders and the assumed height equivalent to the end effect. If the relative end effect is assumed equivalent to an incremental length of cylinder equal to the annulus width, then the yield value is related to the intercept on the torque axis by the equation $f = 2.79 \times 10^2\, T'$ lb force ft^{-2}

and the coefficient of rigidity is related to the slope of the tangent by the equation

$$\eta = 3.88 \frac{\Delta T}{\Delta RPS} \text{ lb force sec ft}^{-2}$$

where the torque is T (lb force ft)

Also, it may be shown from the equations of Reiner and Riwlin (24) that, in a concentric cylinder viscometer, the coefficient of rigidity bears exactly the same relationship to the slope of the tangent as the viscosity bears to the slope of the calibration curve. Therefore, from the calibration curves of the Stormer,

$$\eta = 7.33 \frac{\Delta T}{\Delta RPS} \text{ lbforce sec ft}^{-2}$$

However, in the Stormer viscometer the flow boundaries of a Newtonian fluid are different from those of a Bingham plastic.

Since the values of the mobilities obtained by either method are directly proportional to each other, and since the latter method of interpretation yields values closer to those obtained with the new viscometer, it will be used to determine the mobilities.

Smoothing the Data

Since it is difficult to determine the tangents to the curves, the dat a is smoothed in order to check the consistency of the interpretations. The yield values and the mobilities are smoothed by the methods previously outlined for the new viscometer.

The plots of the yield values against the percent solids on log-log paper, Figure #21, form an almost perfect straight line. Initially, the 18% solids slurry showed a fair discrepancy but a re-examination of the origional data led to an interpretation which is more consistent with the interpretations placed on the data for the other slurries and which gives a yield value almost exactly on the straight line. The yield values are smoothed to

FIGURE 21

Stormer yield value and mobility as a function of % solids

% solids (wet basis) vs yield value, f, (lb force ft^{-2}) and (mobility)$^{-1}$ η, (lb. force ft^{-2} sec.)

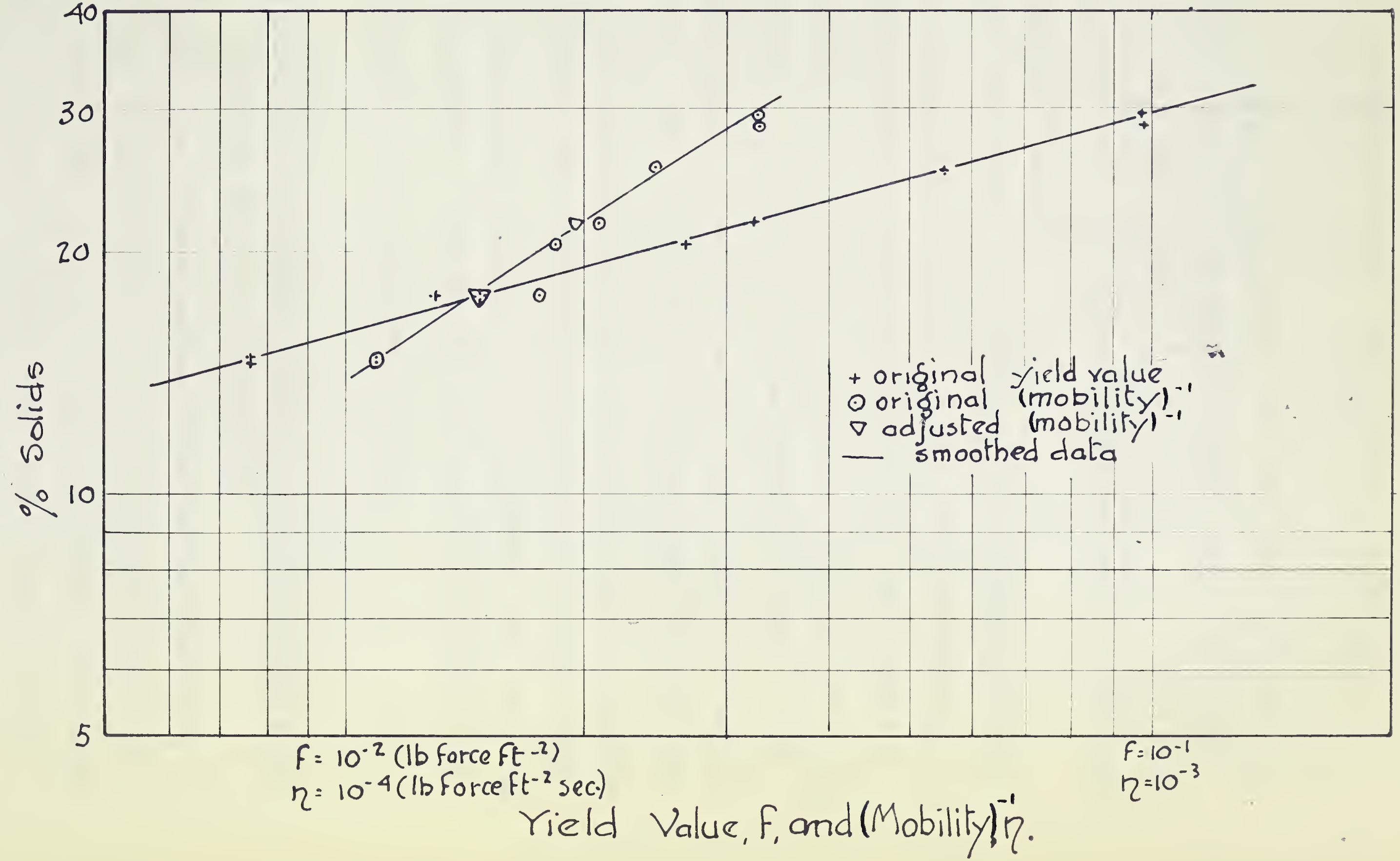

their best fit straight line. The new mobilities scatter slightly around a flat curve, slightly displaced from their original best fit straight line. This curve is shown on Figure #21.

The smoothed values of constants are replotted on semi-log paper, Figure #22. The plotted points are the original data - the new value for the 18% solids slurry is used. The solid line represents data over the range investigated and the broken lines represent extrapolated values.

Plotting the mobilities as an exponential function of the percent solids, Figure #23, produces a negligible scattering around the theoretically required straight line. The yield values are adjusted to the smoothed values of the mobilities and plotted as exponential functions of the percent solids. They scatter slightly about a flat "S" shaped curve around the best fit straight line. The solid lines on Figure #23 represent the smoothed values of the constants and the broken lines represent extrapolated values. The plotted points are the original data.

The above smoothing processes, in conjunction with the data from the new viscometer, confirm the selection of 29.4% as the correct concentration of the heaviest slurry.

Comparison of the Consistency Curves of the New Viscometer and the Stormer Viscometer.

In both cases, the log-log method of smoothing the data appears to produce results which are more consistent with the original data. Since this method of smoothing makes no assumptions regarding the relationships between the percent solids and the fluid properties, and since the particular clay slurries used in each instrument are identical, the smoothed values of

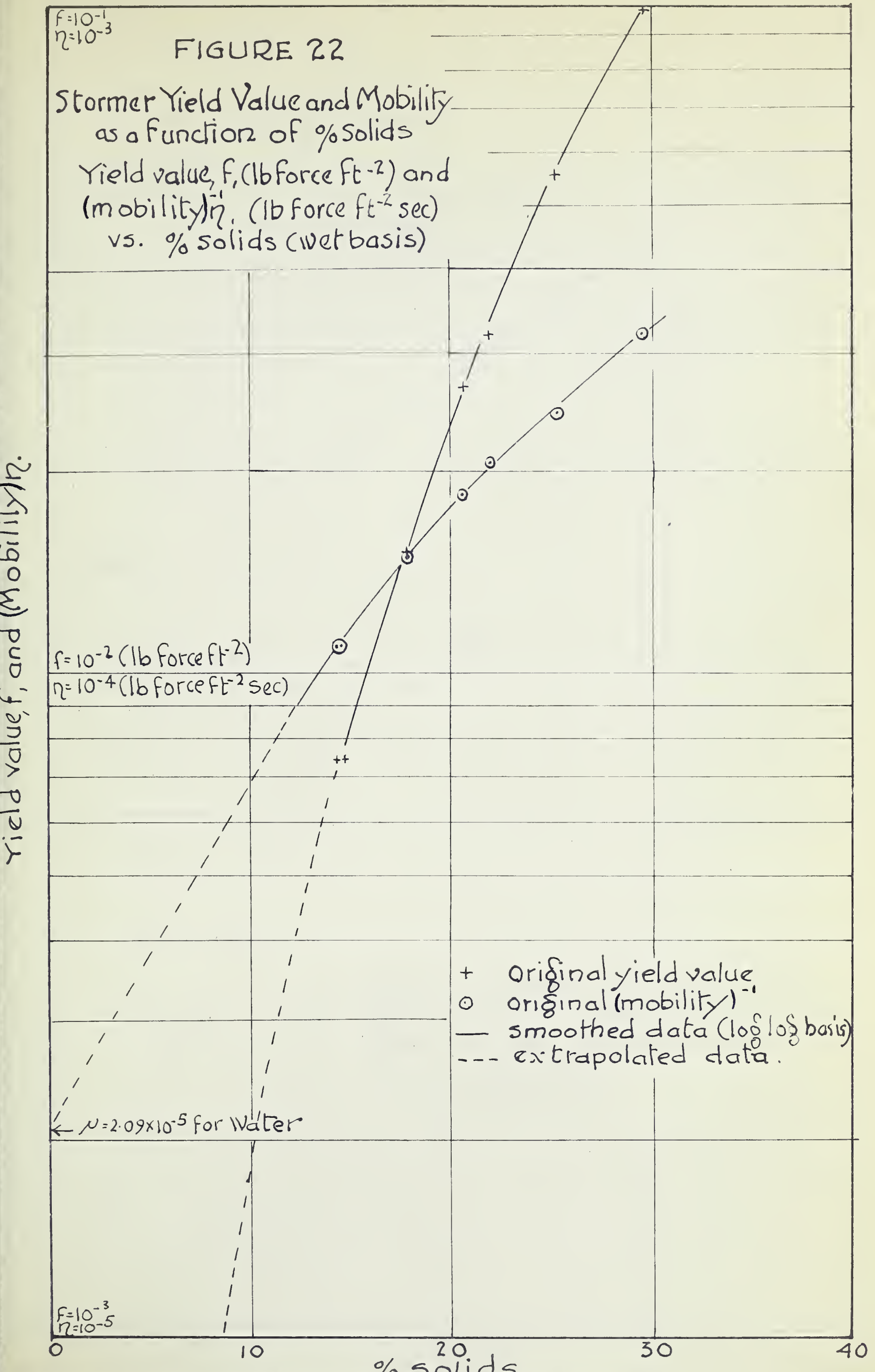

FIGURE 22

Stormer Yield Value and Mobility as a Function of % Solids

Yield value, f, (lb force ft^{-2}) and (mobility)$^{-1}$ η, (lb force ft^{-2} sec) vs. % solids (wet basis)

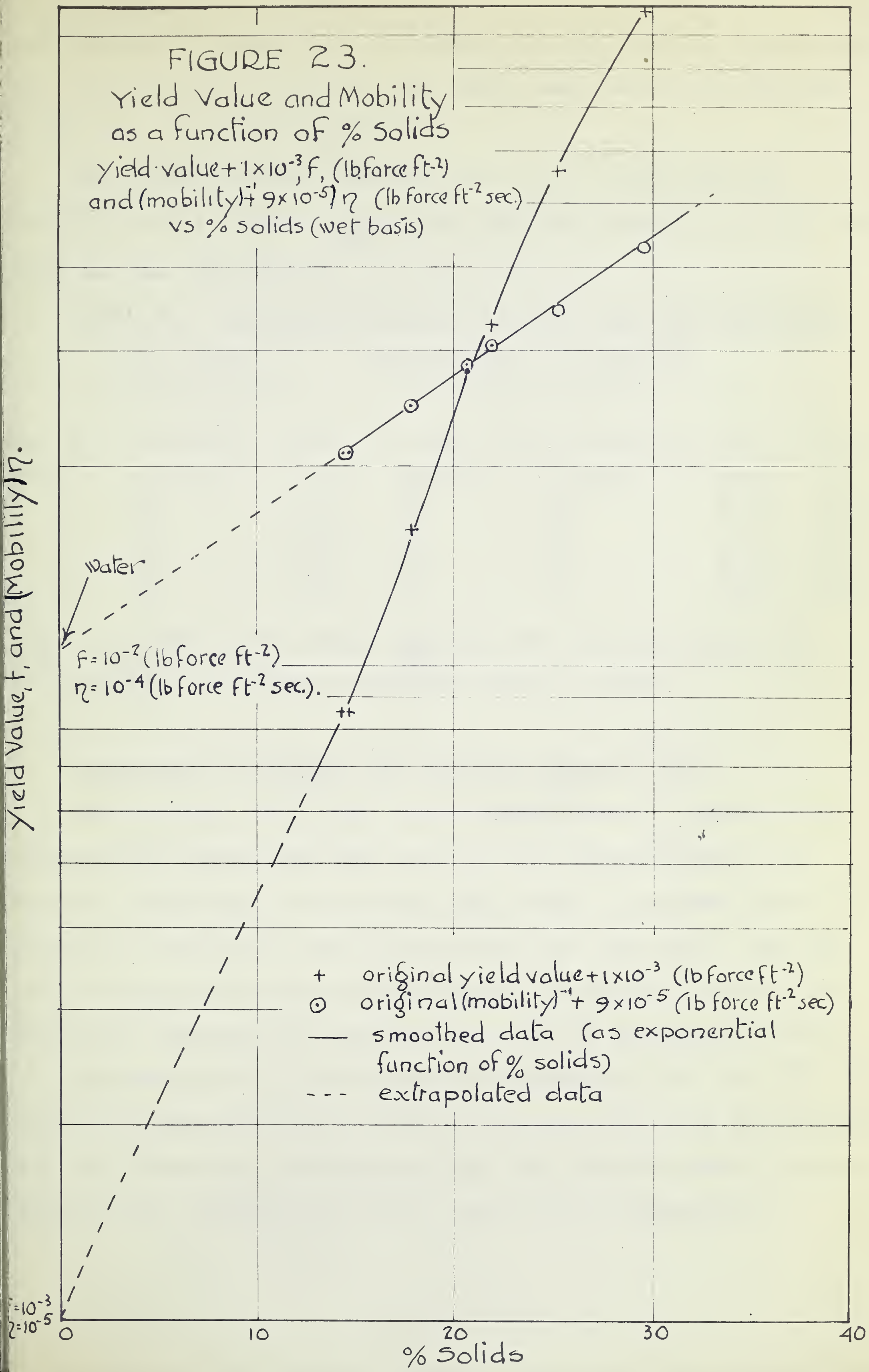

FIGURE 23.

Yield Value and Mobility as a function of % Solids

yield value + 1×10^{-3}, f, (lb force ft^{-2}) and (mobility)$^{-1}$ + 9×10^{-5}, η (lb force ft^{-2} sec.) vs % solids (wet basis)

the constants obtained by this method are used for the comparisons. The coefficients of rigidity are those based on the calibration curves for the Newtonian fluids.

The following table compares the yield values and the coefficients of rigidity, from the smoothing process outlined above, from the two instruments.

TABLE #1 CONSISTENCY CURVES OF STORMER AND NEW VISCOMETER

YIELD VALUES (lb force ft^{-2})			COEFFICIENTS OF RIGIDITY (lb force sec ft^{-2})			
ER	NEW VISCOMETER	RATIO	STORMER	NEW VISCOMETER	RATIO	%SOLIDS
x10^{-3}	6.3x10^{-3}	1.16	11x10^{-5}	14x10^{-5}	0.79	14.5
	12	1.25	15	19	0.79	17.67
	22	1.23	19	26	0.73	20.6
	26.5	1.27	20	29	0.69	21.9
	42	1.33	25	42	0.60	25.1
	73	1.34	33	77	0.43	29.4

The variations in the ratios indicate that neither method of interpreting the Stormer viscometer data is valid.

Comparison of Present and Previous Stormer Data

Re-examination of the calibration curves of the old model Stormer (12) shows that the plots of load against speed, for constant viscosity, pass through the origin. It appears that the concept of initiating load is not valid for this case. This may result from the use of a sleeve bearing on the main gear of the old model, whereas ball bearings are used in the present model.

Mathematically, the data may be written in the form $\frac{W}{n} = K_x \mu_x$, where W is the load, μ_x is a given viscosity, and K_x is the constant for that viscosity. Rearrangement of this equation into a torque form results in $C_1 \mu_x (n) = C_2 W \phi$ where C_1 is a dimensional

constant which converts the product $\mu \times n$ to the viscous torque on the rotor, and where c_2 is a constant, obtained from the dimensions of the gear train, which converts the applied load to the gross torque on the rotor, and where ϕ is a correction factor defined so that the equation is an identity.

By construction, the fluid boundaries of the old and the new Stormer are identical. Therefore the constant c_1 is the same for both instruments. Assume that the correction factor, which should be due only to friction, is unity for the present instrument. Then the only difference between the torques applied to the rotors of the two viscometers, for a given value of the product $\mu \times n$, should be the friction in the old model Stormer.

Plots of the viscosity against gross torque per revolution per second, for the old Stormer, and net torque per revolution per second, for the new Stormer, are shown on Figure #24. The correction factor, at various rates of shear, is shown as a function of the gross torque on the old model Stormer, on the same Figure.

These plots show that the viscous torque on the old model Stormer is almost completely masked by friction in the low viscosity region. Unfortunately, the calibration data in the high viscosity region is rather limited and may not be very reliable.

Attempts to re-evaluate the previous data, from the old model Stormer, for the clay - water slurries, using this correction factor, produced unreasonable results.

Figure #25 compares the consistency curves of the clay - water slurries obtained with the new viscometer, the present Stormer viscometer and the reported values with the old model

FIGURE #24

MAGNITUDE OF FRICTION IN OLD STORMER

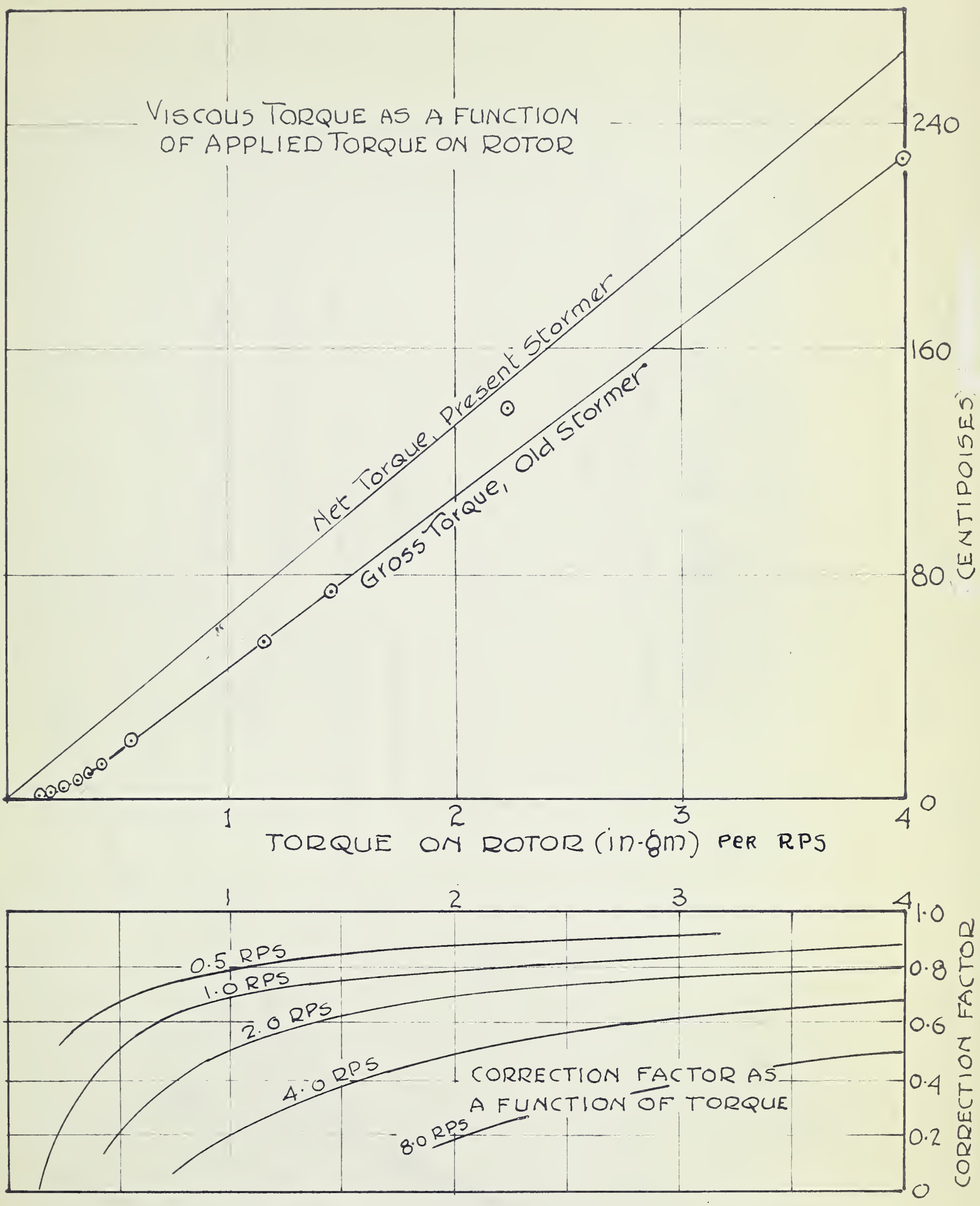

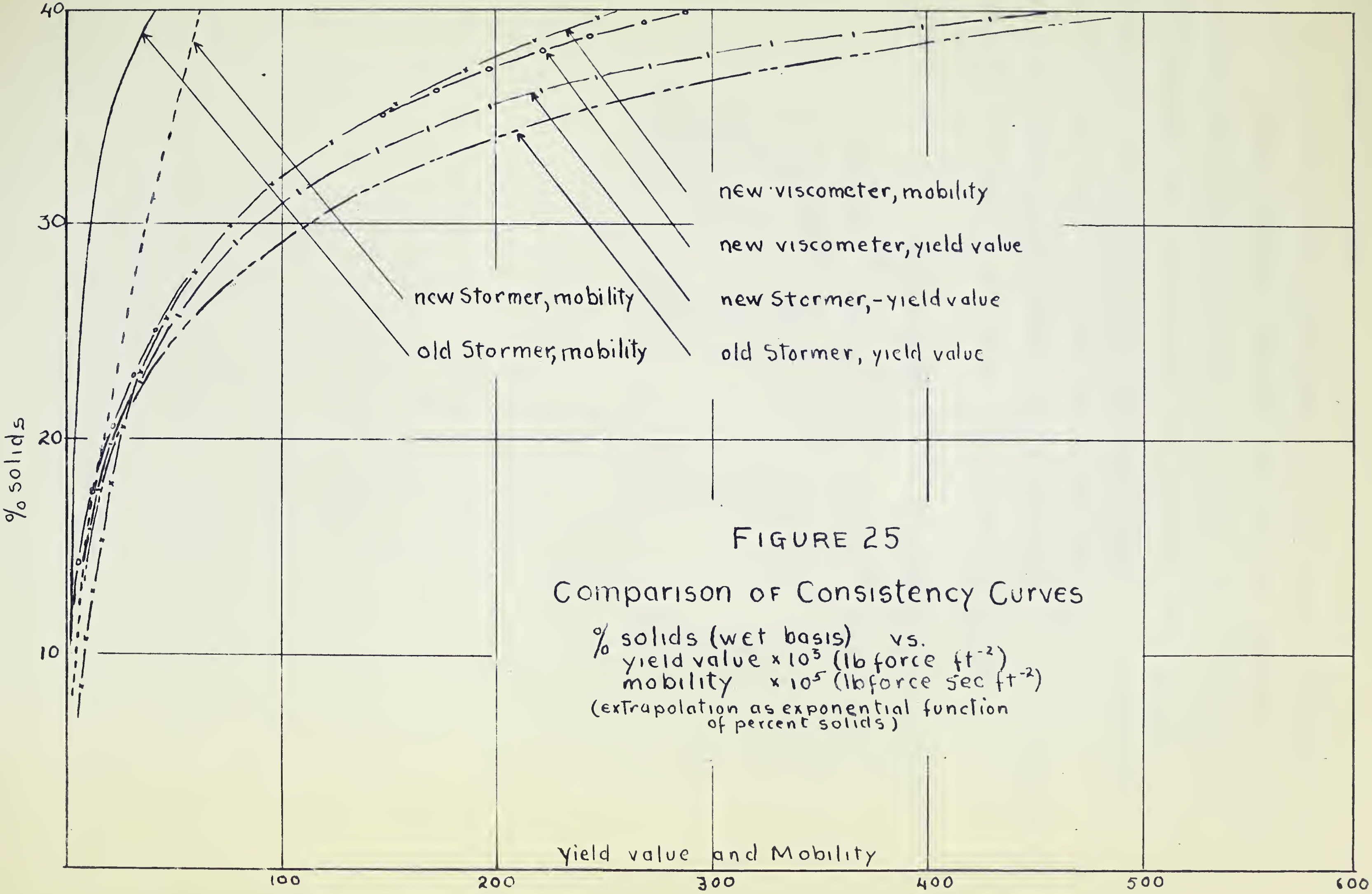

FIGURE 25

Comparison of Consistency Curves

% solids (wet basis) vs.
yield value × 10^3 (lb force ft^{-2})
mobility × 10^5 (lbforce sec ft^{-2})
(extrapolation as exponential function of percent solids)

Stormer viscometer (10).

The following table correlates the rheological properties of the clay - water slurries, obtained with the new viscometer, with the percent solids concentration (wet basis). The values of the yield values and the coefficients of rigidity obtained from smoothing on log-log paper and from smoothing as an exponential function of the percent solids are listed. The extrapolated values are shown in parentheses. The reliability of the extrapolated values above 35% solids and below 10% solids is doubtful.

% SOLIDS	YIELD VALUE (lb force ft^{-2})		COEFFICIENT OF RIGIDITY (lb force sec ft^{-2})	
	log-log	exponential	log-log	exponential
5	(0.15)x10^{-3}	(0.85)x10^{-3}	(5.3)x10^{-5}	(4.7)x10^{-5}
10	(1.8)	(2.6)	(9.1)	(8.4)
15	7.0	7.4	14.7	14.0
20	19.0	20.0	24.5	24.0
25	42	43	43	44
30	79	77	81	80
35	(135)	(144)	(160)	(145)
40	(200)	(310)	(340)	(270)

CONCLUSIONS

A concentric cylinder rotational viscometer for use with non-Newtonian fluids in the "viscosity" range between 1 and 10^4 centipoises has been designed and constructed. Its operating characteristics with Newtonian fluids and Bingham plastics confirm the theories concerning this type of instrument.

Unfortunately, this instrument possesses some serious limitations. The most serious limitation is the low rate of shear range resulting from the early onset of turbulence with low viscosity fluids and the instability of the inner cylinder, particularly with plastic fluids having an appreciable yield value. The early onset of turbulence prevents the satisfactory measurement of the rheological properties of fluids below about 10 centipoises. The instability of the inner cylinder is not serious with Newtonian fluids, but with Bingham plastics the upper range is a fluid having a yield value of about 5×10^2 lb force ft^{-2} and a coefficient of rigidity of about 5×10^{-4} lb force sec ft^{-2}.

The inner cylinder is badly underdamped with fluids below about 50 centipoises. The dash pot greatly improves the damping, but both of the fluids used as damping agents developed an unexplained rigidity. The danger of appreciable errors, with fluids below 20 centipoises, from this effect prevents its application with low viscosity suspensions. When these suspensions settle readily, as do those used in this investigation, this is a serious disadvantage.

The consistency curves of a series of clay - water suspensions have been carefully determined. The reported rheological properties are believed to be accurate within the limitations imposed by the instrument

The consistency curves of these suspensions from the new viscometer are compared with those from a standard Stormer viscometer. The previously used and presently proposed methods of interpreting the Stormer data have proven incorrect. This confirms the original concern over the validity of the interpretations normally placed on such Stormer data.

The consistency curves obtained with the present Stormer viscometer are compared with those reported for an old model Stormer (10). The analysis of these data discloses the presence of important but unknown friction forces in the old model Stormer viscometer.

RECOMMENDATIONS

If a reduction in the annulus width does not reduce the present range of stable operation, the insertion of a sleeve into the outer cylinder will increase the useful range of the instrument. An annulus width of about 1/16 in. should permit satisfactory determinations of the consistency curves of fluids having viscosities as low as about 5 centipoises. A considerable increase of the "linear" portion of the torque - speed curves of fluids approximating Bingham plastics will also accompany this change in dimensions. The accompanying shortening of the region of high curvature will permit a more reliable interpretation of the torque - speed curves.

If at all practical, bearings should be provided for the stator. One bearing, which may solve the problems of the stator instability and of the extremely low friction demanded by low viscosity fluids, is a magnetic bearing. Permanent magnets in the form of cylindrical shells could be placed on the stator shaft and the elevator cylinder, the like poles opposing each other. If the clearances are small, such a system should be sufficiently rigid for most purposes. The magnetic bearing has the enormous advantage of being unaffected by dirt and relatively unaffected by shock.

BIBLIOGRAPHY

1. Ambrose H., and Loomis A., Physics 4 265 (1933)
2. A.S.T.M. Standards on Petroleum Products and Lubricants
3. Babbitt H.E., and Caldwell D.H., Trans. Am. Inst. Ch. Engrs. 37 237 (1941)
4. Beck R., Nuss W., and Dunn T., A.P.I. Drilling and Production Practice p. 9 (1947)
5. Bingham E.C., "Fluidity and Plasticity" (McGraw Hill (1922)
6. Brantly J., Rotary Drilling Handbook (Palmer Pulbications)
7. Buckingham E., Proc. Am. Soc. Testing Materials 21 1154(1921)
8. Cardwell W.T., A.P.I. Drilling and Production Practice 104 (1941)
9. Garrison and Ten Brink, Trans. Am. Inst. Mining and Met. Engr. 136 175 (1940)
10. Govier G., and Winning M., Unpublished Work
11. Green H., "Industrial Rheology and Reheological Structures" (Wiley)
12. Green H., and Halsam, Ind. Engr. Chem. 17 726 (1935)
13. Gurney C.F., Phys. Rev. 26 98 (1908)
14. Hatschek E., "The Viscosity of Liquids" (G. Bell and Sons, London)
15. Lindsley C., and Fischer E. J. App. Phys. 18 988 (1946)
16. Mallock E., Phil. Trans. A(1896) p. 41
17. Mechanical Properties of Fluids, The, (Blackie and Sons, (London)
18. Melrose and Lilienthal, J. Petroleum Tech. 159 (1951)
19. Mooney and Ewart, Physics 5 350 (1934)
20. Nissan A., Clark L., Nash C., J. Sci. Inst. 17 33 (1940)
21. Pichot M., J. Rheol. 5 200 (1934)

22. Pigott R. J., A.P.I. Drilling and Production Practice 91 (1941)

23. Poorman Applied Mechanics (McGraw Hill)

24. Reiner M. and Riwlin, J. Rheal, 1 5 (1929)

25. Richardson E. G., J. Agric. Sci. 23 176 (1933)

26. Roller P., and Stoddard C., J. Phys. Chem. 48 410 (1944)

27. Schofield K., Physics 4 122 (1930)

28. Schofield and Scott - Blair J. Phys. Chem. 34 248 (1930)

29. Scott - Blair G., and Crowther E., J. Phys. Chem. 33 (1939)

30. Stow F., Horowitz K., and Elliot J., J. Colloid. Sci.
4 321 (1949)

31. Taylor G.I., Phil. Trans. A 223 289 (1923)

32. Taylor Fielding and Mooney, Rubber Age 61 567 (1949)

33. Timeshenko and MacCollough, "Elements of Strengths of
Materials" (Van Nostrand Co. Inc.)

34. Traxler, Rhomberg and Schweyer, Ind. Eng.Chem. 14 340 (1942)

35. Ubbelohde L., Ind. Engr. Chem. An. Ed. 9 85 (1937)

36. Van Murat A., and Edsall, J., J. Biol. Chem. 89 315 (1930)

37. Weltman R.N., Ind. Engr. Chem. An. Ed. 15 424 (1943)

38. Weltman R.N., J. App. Physics 18 933 (1947)

39. White "Engineering Materials" (McGraw Hill)

40. Wilhelm R., and Wroughton D., Ind. Eng. Chem. 31 (4) 482(1939)

41 Bulletin published by Brookfield Engr. Laboratories Inc.,
Stoughton, Mass.

42. Bulletin published by Fischer Scientific Co., Pittsburg, Penn.

43. Bulletin published by A.H. Thomas Co., Philadelphia, Pa.

APPENDIX A

A MATHEMATICAL ANALYSIS OF THE LAMINAR FLOW OF A FLUID, WHOSE VELOCITY GRADIENT IS A UNIQUE FUNCTION OF THE SHEARING STRESS, IN A STRAIGHT CIRCULAR TUBE.

The following analysis is adapted from articles by Schofield and Scott-Blair (28) and by Schofield (27).

Assume that:

a) the velocity gradient is a unique function of the shearing stress

b) equilibrium conditions exist throughout the tube

c) kinetic energy and entrance effects are negligable

d) the flow is laminar throughout.

Let the pressure gradient be p units of force per unit area per unit length of tube. Let the viscous shearing stress per unit area be s at a distance r from the axis of a tube of radius R .

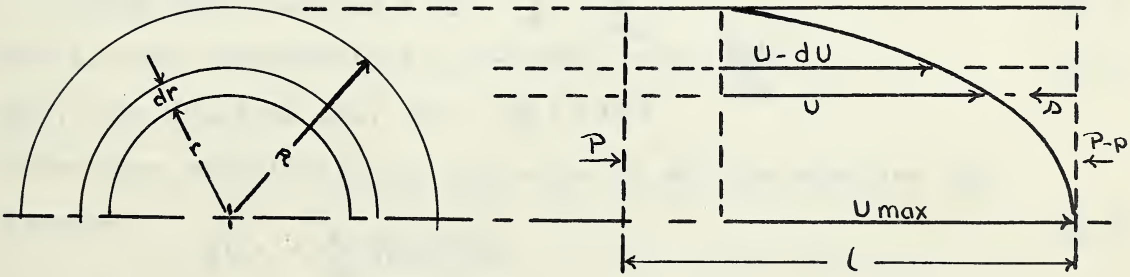

SKETCH #5. LAMINAR FLOW IN A CIRCULAR TUBE.

Consider the cylinder of radius r and length l as shown in Sketch #5. The driving force is the pressure gradient, p , times

the length of the cylinder, l , times the cross-sectional area of the cylinder, πr^2 , The opposing force is due solely to viscous shear acting over the cylindrical fluid boundary at r , i.e. the shear stress per unit area, s , times the area over which it acts, $2\pi r l$. These forces must be equal at equilibrium, therefore $p \times l \times \pi r^2 = s \times 2\pi r l$ from which the (A 1)

shear stress at radius r is $s = \frac{pr}{2}$ (A 2)

and the shear stress at the wall is $s_w = \frac{pR}{2}$ (A 3)

By definition, the consistency curve of a fluid is the plot of the shearing stress per unit area against the resulting velocity gradient, $\frac{du}{dh}$, when the fluid is confined between two infinite parallel planes. Now if the ratio of the width of an annulus, dr , between two coaxial, cylindrical shells of radii r and $r+dr$, to the radius of either shell approaches zero, the corresponding elementary areas on these shells will approach the case of infinite parallel planes. Therefore the velocity gradient, $\frac{du}{dr}$, between the cylinders is equivalent to the velocity gradient between infinite parallel planes. When this gradient is a unique function of the shearing stress

$$\frac{du}{dr} = \frac{du}{dh} = -\phi_1(s) \quad * \qquad \text{(A 4)}$$

From equations (A2 & A3), $\frac{r}{R} = \frac{s}{s_w}$ (A 5)

which, upon differentiation, becomes $dr = \frac{R\,ds}{s_w}$ (A 6)

But, from equation (A4) $du = -\phi_1(s)\,dr$

which upon substitution of the value of dr from equation (A6) becomes (A 7)

$$du = -\frac{R}{s_w}\phi_1(s)\,ds$$

If the velocity at the tube wall is zero, then integration

---

*The minus sign is inserted for future convenience.

between the limits $u = 0$ at $s = s_w$ and $u = u$ at $s = s$ yields the general relationship between the velocity of the fluid and the shearing stress at a given radius

$$u = \frac{R}{s_w} \int_{s}^{s_w} \phi_1(s)\, ds \tag{A 8}$$

Let the volumetric rate of flow between the cylinders of radii r and $r + dr$ be dQ where $dQ = 2\pi r\, dr\, (u_r)$ (A 9)

Substitution of the values of r from equation (A5) and u from equation (A8) into the expression for dQ yields

$$\frac{dQ}{\pi R^3} = \frac{2}{s_w^3}\, s\, ds \left[\int_{s}^{s_w} \phi_1(s)\, ds \right] \tag{A10}$$

which, upon integration between the limits $s = 0$ at the tube axis and $s = s_w$ at the tube wall yields the total volumetric rate of flow expressed as a function of the radius of the tube and the shearing stress at the tube wall

$$\frac{Q}{\pi R^3} = \frac{2}{s_w^3} \int_{0}^{s_w} s\, ds \left[\int_{s}^{s_w} \phi_1(s)\, ds \right] \tag{A11}$$

or

$$\frac{Q}{\pi R^3} = \phi(s_w) = \phi\left(\frac{PR}{2}\right) \tag{A12}$$

Therefore, a plot of $\frac{Q}{\pi R^3}$ against $\frac{PR}{2}$ will yield a curve which is independent of the dimensions of the tubes when,

a) the data is taken in the laminar flow region

b) the velocity gradient is a unique function of the shearing stress

c) the velocity at the tube wall is zero

Newtonian Fluid.

By definition: $\frac{du}{dr} = \phi_1(s) = \frac{s}{\mu}$ for a Newtonian fluid. Then substitution of $\frac{s}{\mu}$ for $\phi_1(s)$ into equation (A10) and integrating yields,

$$\frac{Q}{\pi R^3} = \frac{s_w}{4\mu} \quad \text{in terms of } s_w \tag{A13}$$

or

$$\frac{Q}{\pi R^3} = \frac{PR}{8\mu} \quad \text{in terms of } P \tag{A14}$$

which is the equation of laminar flow of a Newtonian fluid in

a straight tube of constant circular cross-section.

Bingham Plastic.

By definition, $\frac{du}{dr} = \frac{s-f}{\eta}$ for a Bingham Plastic, where f is the yield value and η is the mobility. Then substitution of $\frac{s-f}{\eta}$ for $\phi_1(s)$ in equation (A11) noting that the function $\phi_1(s)$ is discontinuous at $s = f$ yields

$$\frac{Q}{\pi R^3} = \frac{2}{s_w^3}\Bigg\{\underbrace{\left[\int_0^f s\,ds\left(\int_f^{s_w}\left(\frac{s-f}{\eta}\right)ds\right)\right]}_{\text{plug flow portion}} + \underbrace{\left[\int_f^{s_w} s\,ds\left(\int_s^{s_w}\left(\frac{s-f}{\eta}\right)ds\right)\right]}_{\text{laminar flow portion}}\Bigg\} \qquad \text{(A15)}$$

Integrating and collecting like terms yields

$$\frac{Q}{\pi R^3} = \frac{1}{4\eta}\left\{s_w - \frac{4}{3}f + \frac{1}{3}\frac{f^4}{s_w^3}\right\} \qquad \text{where } s_w > f \qquad \text{(A16)}$$

the latter equation represents the combined effects of plug and laminar flow. The two effects cannot be separated from it. A further substitution of $s_w = \frac{PR}{2}$ yields

$$Q = \frac{\pi R^4}{8\eta}\left\{P - \frac{4}{3}\left(\frac{2f}{R}\right) + \frac{1}{3}\left(\frac{2f}{R}\right)^4\frac{1}{P^3}\right\} \qquad \text{where } \frac{PR}{2} > f \qquad \text{(A17)}$$

which is Buckinghams equation (7) for a Bingham Plastic if no wall slippage occurs.

Evaluation of f and η.

It is possible, though very laborious, to evaluate f and η mathematically from the flow data. Fortunately, a simple graphical method of evaluating the consistency curve of a fluid from flow data through capilliary tubes is available.

Evaluation of the Velocity Gradient as a Function of the Shear Stress.

The following method is applicable for all cases where $\frac{du}{dr} = \phi_1(s)$ only. Consider the velocity distribution in a tube of radius R resulting from pressure gradients P and $P + dP$ as

illustrated in Sketch #6. $P'Q'$ and $P''Q''$ are so drawn that the stress at $P'Q'$ and $P''Q''$ equals the stress at PQ, that is, from equation (A5) $\frac{pR}{2} = \frac{(p+dp)(R-dr)}{2}$ which may be simplified to $\frac{dr}{r} = \frac{dp}{p}$ (A18)

Now $A'A''B''B'$ represents an additional volumetric rate of flow due to the increased pressure gradient, and is the area, πR^2, times the velocity at $R-dr$, which is $\left.\frac{du}{dr}\right)_w dr$, or $dQ' = \pi R^2 \left.\frac{du}{dr}\right)_w dr$ (A19)

But $\frac{dr}{r} = \frac{dp}{p}$, therefore $dQ' = \pi R^3 \left.\frac{du}{dr}\right)_w \frac{dp}{p}$ (A20)

Now from equations (A11) and (A21), it will be shown that the only difference between the curves AOB and $A''OB''$ is their scale, the volume represented by AOB being greater than that represented by $A''OB''$ by a quantity dQ''.

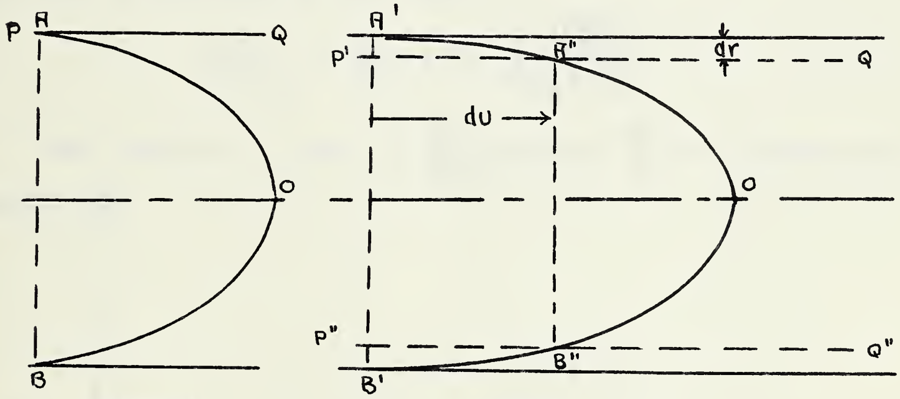

pressure p

pressure p+dp

SKETCH #6. VELOCITY DISTRIBUTIONS IN A CAPILLIARY TUBE AS A RESULT OF PRESSURE GRADIENTS P AND $P+dP$.

From equation (A 11) $\frac{Q''}{\pi r^3} = \frac{2}{s_w^3}\int_0^{s_w} s\,ds \int_0^{s_w} \phi_1(s)\,ds$

and by construction, s_w at $R-dr$, in Sketch #6b, equals s_w at R, in Sketch #6a, in other words,

$\frac{2}{s_w^3}\int_0^{s_w} s\,ds \int_0^{s_w} \phi_1(s)\,ds$ is a constant and equals $\frac{Q_A}{\pi R^3}$ from which $\frac{Q''}{\pi r^3} = \frac{Q_A}{\pi R^3}$ (A21)

Differentiation of equation (A21) yields the value of dQ'' which is,

$$dQ'' = 3\pi r^2 dr \left(\frac{Q_A}{\pi R^3}\right) \tag{A22}$$

Now the net change in the volumetric rate of flow due to an increase in the pressure gradient of dP is $dQ' - dQ''$ which is

$$dQ = \pi R^3 \left.\frac{du}{dr}\right)_w \frac{dP}{P} - 3\pi r^2 dr \left(\frac{Q_A}{\pi R^3}\right) \tag{A23}$$

but $\frac{dP}{P} = \frac{dr}{r}$, from which this equation may be rearranged to

$$\left.\frac{du}{dr}\right)_w = \frac{3r^3}{R^3}\left(\frac{Q_A}{\pi R^3}\right) + \frac{dQ}{\pi R^3}\,\frac{P}{dP} \tag{A24}$$

but $\frac{Q_A}{Q} = \frac{R^3}{R}$ from equation (A21)

Therefore $$\left.\frac{du}{dr}\right)_w = \frac{3Q}{\pi R^3} + \frac{dQ}{\pi R^3}\,\frac{P}{dP} \tag{A25}$$

Since, in the above equation, R is a constant, this equation may also be written in the form

$$\left.\frac{du}{dr}\right)_w = \frac{3Q}{\pi R^3} + \frac{\frac{1}{2}PR\, d\left(\frac{Q}{\pi R^3}\right)}{d\left(\frac{1}{2}PR\right)} \tag{A26}$$

Now consider a plot of $\frac{Q}{\pi R^3}$ against $\frac{PR}{2}$ as illustrated in Sketch #7.

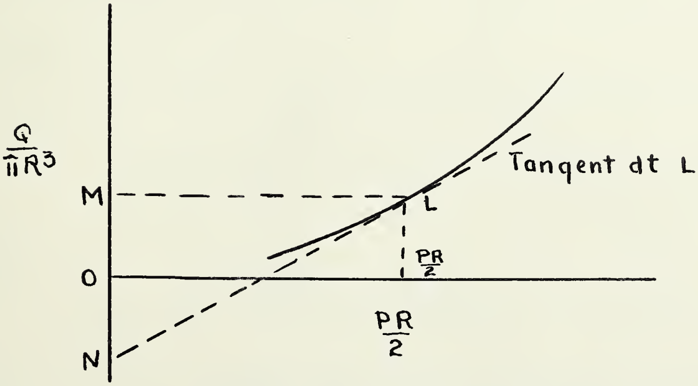

SKETCH #7. PLOT OF $\frac{Q}{\pi R^3}$ AGAINST $\frac{PR}{2}$.

From Sketch #7 and from equation (A26) it is seen that $\frac{3Q}{\pi R^3} = 3OM$

The slope of the tangent at L is $\frac{ON+OM}{OL}$, therefore

$$\frac{1}{2} PR\left(\frac{ON+OM}{OL}\right)$$

therefore

$$\left.\frac{du}{dr}\right)_{w} = 4OM + ON \qquad (A27)$$

And the consistency curve of the fluid may be obtained by plotting $4OM+ON$ against ML since this is a plot of $\left.\frac{du}{dr}\right)_{w}$ against s_{ω}.

This method is valid if,

a) $\frac{du}{dr} = \phi_1(s)$ alone

b) the velocity at the tube wall is zero.

APPENDIX B

THE KINETIC ENERGY CORRECTION IN CAPILLIARY TUBE VISCOMETERS

In practical viscometers, part of the observed pressure drop appears as kinetic energy and part as additional surfaces of shear at the ends of the tube. The following partial analysis of the kinetic energy correction factor is adapted from "Industrial Rheology" by Green (11) and the method of evaluating the end effects is adapted from "The Viscosity of Fluids" by Hatschek (14).

Consider the fluid flowing through the capilliary as illustrated in Sketch #8. The volume of the annulus of fluid of radii r and $r+dr$, passing $A'A$ per unit time, is the velocity times the cross-sectional area, or $2\pi u r dr$ its mass is $2\pi \rho u r dr$ where ρ is the density, and its kinetic energy is therefore $\frac{mu^2}{2} = \pi \rho u^3 r dr$ (B 1)

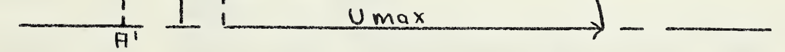

SKETCH #8. FLOW THROUGH A TUBE.

The total kinetic energy produced per second is then the sum of the kinetic energies of all the elements across the tube which is $E_K = \int_0^R \pi \rho u^3 r dr$. But, for a Newtonian fluid the velocity

is, from Poiseuilles equation $U = \frac{P}{4\mu l}(R^2 - r^2)$. Therefore the kinetic energy of the fluid may be expressed in the form

$$E_K = -\frac{1}{2}\int_0^R \pi \rho \left(\frac{P}{4\mu l}\right)^3 (R^2 - r^2)(-2 r\, dr) \tag{B 2}$$

Since $d(R^2 - r^2) = -2 r\, dr$ the equation may be integrated to yield

$$E_K = \frac{\pi \rho P^3 R^6}{8^3 \mu^3 l^3} R^2 \tag{B 4}$$

Then, if $\bar{v}$ is the mean velocity of all the cylinders of fluid, which is the volumetric rate of flow, Q , divided by the cross-sectional area πR^2, then $\bar{U} = \frac{Q}{\pi R^2} = \frac{\pi P R^4}{8\mu} \Big/ \pi R^2$ from poiseuilles equation or

$$\bar{U} = \frac{P R^2}{8 \mu l} \tag{B 5}$$

Substitution of this value of the mean velocity into the equation for E_K yields

$$E_K = \pi \rho \bar{U}^3 R^2 = (\pi R^2 \bar{U})(\rho \bar{U}^2) \tag{B 6}$$

Now the total force acting is $P \pi R^2$, and since this force acts, in one second, along a distance $\bar{U}$, the total energy input per second is $P \pi R^2 \bar{U} = E$. Therefore the energy dissippated as heat, via viscous shear, is

$$E - E_K = \pi R^2 \bar{U} \left(P - \rho \bar{U}^2\right) \tag{B 7}$$

Let P_K be the pressure gradient used in creating kinetic energy. Then $\rho \bar{U}^2 = P_K$. But $\rho \bar{U}^2 = \rho \left(\frac{Q^2}{\pi^2 R^4}\right)$ from equation (B5).

Therefore

$$P_K = \frac{Q^2}{\pi^2 R^4} \tag{B 8}$$

But Poiseuilles equation states that $\mu = \frac{\pi R^4 (P')}{8 Q l}$ where the value of P' is $P - P_K$,

Therefore

$$\mu = \frac{\pi R^4 P}{8 Q L} - \frac{\rho Q}{8 \pi L} \tag{B 9}$$

Green (11) states that Boussinesq has shown that this last term should be modified by a dimensionless constant, b , to yield the relationship

$$\mu = \frac{\pi R^4 P}{8 Q L} - \frac{b \rho Q}{8 \pi L} \tag{B10}$$

The value of b is usually taken as 1.12 but may vary with each tube. For non-Newtonians it may be as high as 1.3.

To account for distortions in the flow patterns at the tube ends, an incremental length, aR , is added to the overall length. The general form of the equation of laminar flow of Newtonian fluids in a capilliary tube viscometer is therefore, (14),

$$\mu = \frac{\pi P R^4}{8Q(L+aR)} - \frac{b e Q}{8\pi(L+aR)} \tag{B11}$$

The value of the constant, , appeared to vary from about 1 to about 3 for square ended capilliaries. It may be obtained experimentally from the data for a given fluid flowing through two short capilliaries of the same radius but of different lengths from the apparent differences in the viscosities which are related by the equations (14)

$$\mu_1 \frac{L_A}{L_A + aR} = \mu_2 \frac{L_B}{L_B + aR} \tag{B12}$$

Then, assuming the value of to be independent of the type of fluid - the error being negligible if $\frac{L}{R}$ is large - the effective value of the constant b may be obtained in a similar manner.

APPENDIX C

THE EQUATIONS OF LAMINAR FLOW IN A ROTATIONAL VISCOMETER.

The following mathematical analyses of the equations of laminar flow of any fluid, which does not exhibit appreciable wall effects, between rotating concentric cylinders are a combination of the works of Reiner and Riwlin (24), Gurney (13), Ambrose and Loomis (1) and Mooney and Ewart (19).

Consider a fluid filling the annular space between two coaxial cylinders, the outer one rotating at a constant angular velocity, Ω, and the inner one stationary. Let the radius of the outer cylinder be R_2 and of the inner cylinder by R_1, the length of the cylinders be h, and the torque on the inner cylinder be T. This is illustrated in Sketch #9.

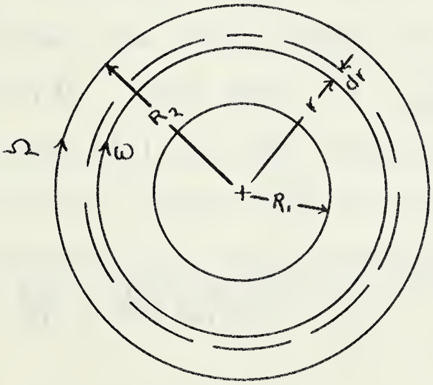

SKETCH #9. LAMINAR FLOW IN A CONCENTRIC CYLINDER ROTATIONAL VISCOMETER.

The tangential velocity of the fluid at radius r is given by $u = r\omega$, at radius $r+dr$ is given by $u+du=(r+dr)(\omega+d\omega)$ from which the change in velocity across the distance dr is $du = \omega\,dr + r\,d\omega$. But, if the angular velocity across the

System were constant, that is, no sliding between the fluid layers occured, the change in velocity would be $du' = (r+dr)\omega - r\omega = \omega\, dr$. Therefore the change is velocity due to the relative sliding of the fluid layers is $r\,d\omega$ and the internal stresses are due only to this term.

Now for the two cylindrical shells of radii r and $r+dr$, if the ratio of the annulus width, dr, to the radius, r, approaches zero, then the corresponding elementary areas on these shells will approach the case of infinite parallel planes. Therefore, for a given shear stress per unit area, s, the velocity gradient between the elementary areas, $\frac{du}{dr}$, is equal to the velocity gradient, $\frac{du}{dh}$, between two infinite parallel planes.

If, over the period of time required for the system to reach a practical equilibrium, the velocity gradient may be considered a unique function of the shearing stress, then $\frac{du}{dr} = \frac{du}{dh} = \phi_1(s)$.

But $du = r\,d\omega$ therefore $r\frac{d\omega}{dr} = \phi_1(s)$ (C 1)

At equilibrium, the torque across the annulus is a constant which is $T = (2\pi r h s)$ from which $s = \frac{T}{2\pi r^2 h}$ (C 2)

Combining equations (C1) and (C2) yields the differential form of the general law of laminar flow of a fluid, obeying the above criteria, between rotating coaxial cylinders:

$$r\frac{d\omega}{dr} = \phi_1\left(\frac{T}{2\pi r^2 h}\right) \qquad \text{(C 3)}$$

The Equations of Flow of a Bingham Plastic.

For a Bingham Plastic, the term $\phi_1(s)$ is by definition, $\frac{s-f}{\eta}$ where f is the yield value and η the mobility, or

$\frac{du}{dr} = r\frac{d\omega}{dr} = \frac{s-f}{\eta}$ from which equation (C3) becomes

$r\frac{d\omega}{dr} = \frac{1}{\eta}\left[\frac{T}{2\pi r^2 h\eta} - f\right]$ which may be rearranged to the form,

$$d\omega = \frac{1}{\eta}\left[\frac{T}{2\pi r^3 h} - \frac{f}{r}\right] dr \qquad \text{(C 4)}$$

Let the velocities of the fluid at the walls of the cylinders be the same as the velocities of the cylinders, i.e. no wall slippage.

Substituting the limits $\omega = 0$ at R_1 and $\omega = \omega$ at r gives

$$\int_0^{\omega} d\omega = \frac{1}{\eta}\int_{R_1}^{r}\left(\frac{T}{2\pi r^3 h} - \frac{f}{r}\right)dr \qquad (C\ 5)$$

which yields upon integration and simplification,

$$T = \left[\omega + \frac{f}{\eta}\ln\frac{r}{R_1}\right]\frac{4\pi h \eta r^2 R_1^2}{r^2 - R_1^2} \quad \text{where } T \begin{array}{l} < 2\pi R_2^2 hf \\ > 2\pi R_1^2 hf \end{array} \qquad (C\ 6)$$

or, when all the material in the annulus is in laminar flow,

$$T = \left[\Omega + \frac{f}{\eta}\ln\frac{R_2}{R_1}\right]\frac{4\pi h \eta R_2^2 R_1^2}{R_2^2 - R_1^2} \quad \text{where } T \geq 2\pi R_2^2 hf \qquad (C\ 7)$$

These equations are illustrated in Sketch #10.

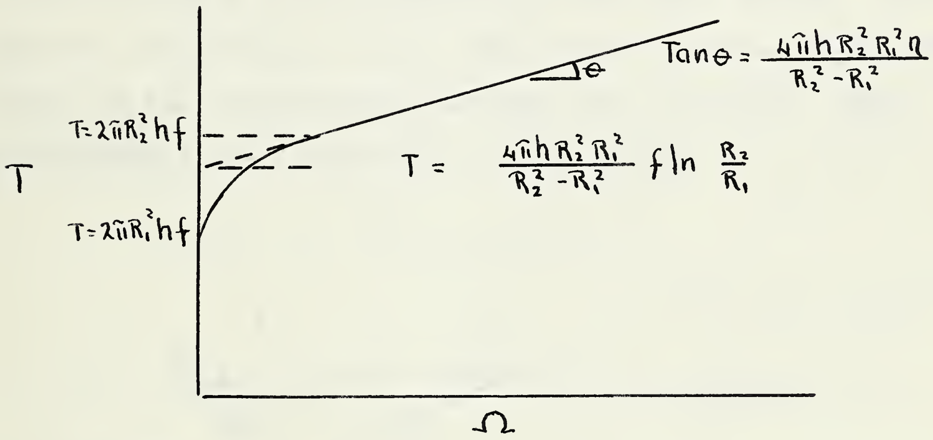

SKETCH #10. THE RELATIONS BETWEEN TORQUE AND ANGULAR VELOCITY FOR A BINGHAM PLASTIC IN A CONCENTRIC CYLINDER ROTATIONAL VISCOMETER.

It is seen that, when $T > 2\pi R_2^2 hf$, the relationship between torque and angular velocity is linear so that it is a relatively simple matter to evaluate the yield value and the mobility.

The yield value is related to the intercept, T', of the linear portion, on the torque axis by the relationship,

$$f = \frac{T'(R_2^2 - R_1^2)}{4\pi h R_2^2 R_1^2 \ln\frac{R_2}{R_1}} \qquad (C\ 8)$$

and the mobility is related to the slope of this line by,

$$\eta^{-1} = 1 \Big/ \frac{\operatorname{Tan}\theta\,(R_2^2 - R_1^2)}{4\pi h R_2^2 R_1^2} \tag{C 9}$$

The Equations of Laminar Flow of any fluid whose rheological properties are such that $\frac{du}{dr} = \phi_1(s)$.

The following analysis involves the approximation that the shearing stress across the annulus is nearly constant. The torque is, at equilibrium, a constant across the annulus. From equation (C2), the shear stress is given by $s = \frac{T}{2\pi r^2 h\eta}$. Therefore, if the ratio of the annulus width to the radius is small, the shearing stress is nearly constant. The velocity gradient is, by definition, a unique function of the shear stress. Define an apparent viscosity, μ^x, such that it is the ratio of the shear stress to the corresponding average rate of shear. These relationships are illustrated in Sketch #11.

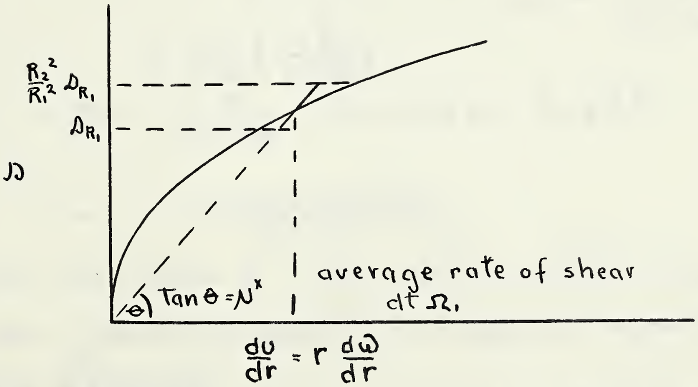

SKETCH #11. THE SHEAR STRESSES AND THE VELOCITY GRADIENTS ACROSS THE ANNULUS.

Therefore, for a given angular velocity, the approximation that $s \doteq \mu^x r \frac{d\omega}{dr}$ may be made. Rearrangement of this relationship yields the differential form of the general equation of flow between concentric cylinders,

[illegible]

$$[illegible]$$

[illegible]

[illegible]

[illegible]

[illegible]

$$\frac{s}{N^x} \simeq r\frac{d\omega}{dr} \simeq \frac{T}{2\pi r^2 h N^x} \qquad \text{where } T > 2\pi R_2^2 h f^x \tag{C10}$$

and f^x is the "effective yield value".

The approxiamte consistency curve may be evaluated by defining and calculating, respectively, the average rate of shear and the shear stress at the radius corresponding to that rate of shear, or the average shear stress and the rate of shear at the radius corresponding to that shear stress.

Gurney (13) defined the average rate of shear as the sum of all the elementary masses of the fluid under shear times their respective rates of shear divided by their total masses. Expressed mathematically, this becomes,

$$r\left.\frac{d\omega}{dr}\right)_{av} = \frac{\int_{R_1}^{R_2} 2\pi r\,dr\left(r\frac{d\omega}{dr}\right)}{\int_{R_1}^{R_2} 2\pi r\,dr} \tag{C11}$$

which, since $r\frac{d\omega}{dr} \simeq \frac{T}{2\pi r^2 h N^x}$ under a given set of conditions, may be written

$$r\left.\frac{d\omega}{dr}\right)_{av} \simeq \frac{\int_{R_1}^{R_2} 2\pi r\left(\frac{T}{2\pi r^2 h N^x}\right)dr}{\int_{R_1}^{R_2} 2\pi r\,dr} \qquad \text{where } T > 2\pi R_2^2 h f^x,\ \Omega = \text{constant}$$

$$\simeq \frac{T}{\pi h N^x}\left(\frac{\ln\frac{R_2}{R_1}}{R_2^2 - R_1^2}\right) \tag{C12}$$

and, since $r\frac{d\omega}{dr} \simeq \frac{T}{2\pi r^2 h N^x}$, $\omega = \Omega$ @ R_2, $\omega = 0$ @ R_1

the value of T is

$$T \simeq \frac{4\pi h N^x \Omega R_2^2 R_1^2}{R_2^2 - R_1^2} \tag{C13}$$

Substituting this value of T into equation (C12) yields the average rate of shear in terms of the angular velocity and the radii of the cylinders,

$$\left.\frac{du}{dr}\right)_{av} \simeq \frac{4\Omega R_1^2 R_2^2}{(R_2^2 - R_1^2)^2}\ln\frac{R_2}{R_1} \qquad \text{where } T > 2\pi R_2^2 h f^x \tag{C14}$$

The radius at which the average rate of shear occurs may be found as follows. Since $s_{av} \simeq \left.\frac{du}{dr}\right)_{av} N^x$ and $T = 2\pi r^2 h s$, then $T = 2\pi r_{av}^2 h\left(\frac{du}{dr}\right)_{av} N^x$ or $r_{av}^2 = \frac{1}{2\pi h}\left[\frac{1}{(du/dr)_{av}}\right]\left[T/N^x\right]$ which, after substituting the values of $\left.\frac{du}{dr}\right)_{av}$ from equation (C14)

and T/μ^x from equation (C13), becomes after simplification

$$r^2_{av} = \frac{R_2^2 - R_1^2}{2\ln\frac{R_2}{R_1}} \qquad (C15)$$

From which the average shear stress is, by definition,

$$s_{av} = \frac{T\ln\frac{R_2}{R_1}}{\pi(R_2^2 - R_1^2)h} \qquad (C16)$$

Mooney (19) defined the average shear stress as the arithmetic mean shear stress, $\frac{s_1 + s_2}{2}$. Using the procedures outlined above, it may be shown that,

$$\left.\frac{du}{dr}\right)_{av} \simeq \frac{\Omega(R_1^2 + R_2^2)}{(R_2^2 - R_1^2)} \qquad \text{where } T > 2\pi R_2^2 h f^x \qquad (C17)$$

$$s_{av} \simeq \frac{T(R_1^2 + R_2^2)}{4\pi R_1^2 R_2^2 h} \qquad (C19)$$

Therefore the approximate consistency curve of a fluid may be evaluated from the Torque - Speed data from a concentric cylinder rotational viscometer if,

a) over the period of time required to measure a given point the system is at a practical equilibrium.

b) the shear stress may be considered a unique function of the velocity gradient over this period.

c) the ratio of the squares of the radii of the cylinders is nearly unity.

c) wall effects are negligible.

by plotting the average shear stress,

$$s_{av} \simeq \frac{T\ln\frac{R_2}{R_1}}{\pi(R_2^2 - R_1^2)h} \quad \text{or} \quad \frac{T(R_1^2 + R_2^2)}{4\pi R_1^2 R_2^2 h} \qquad (C19)$$

against the respective average velocity gradients,

$$\left.\frac{du}{dr}\right)_{av} \simeq \frac{4\Omega R_1^2 R_2^2}{(R_2^2 - R_1^2)^2}\ln\frac{R_2}{R_1} \quad \text{or} \quad \frac{\Omega(R_1^2 + R_2^2)}{R_2^2 - R_1^2} \qquad (C20)$$

where $T > 2\pi R_2^2 h f^x$

APPENDIX D

MEASUREMENT OF THE TORQUE ON THE BASE OF THE INNER CYLINDER BY MEANS OF THE DIFFERENTIAL HEIGHT TECHNIQUE.

The previous analyses of laminar flow in a concentric cylinder rotational viscometer do not take into account the torque on the base of the inner cylinder. The effects of this torque may be determined in two ways.

The first method uses two outer cylinders of the same radius but of different lengths (13). The clearance between the bases of the cylinders is kept constant. This clearance must be large enough to prevent turbulence (20). The fluid is filled, in both cases, to the lip of the rotor.

Since the flow boundaries must be identical at the same velocities, except for the different length of annulus, the difference in the measured torques must be due only to the difference of the height of the fluid in the annulus. The plot of the differences in the torques, considered to act over the differences between the depths of immersion, against the corresponding angular velocities is used to evaluate the absolute consistency curves.

The second method depends on the experimental evidence (11, 15, 20) that, for Newtonian fluids at least, the torque on the base is a constant if some relatively small clearance is exceeded. Lindsley and Fischer (15) found that this torque asymptotically approached this constant value as the clearance increased. For an inner cylinder of say 3 cm. radius or less, the end effect is constant at a clearance of about 1.5 cm.(11,20)

The experimental technique is as follows. The system is

always filled to the rotor lip. The torques on the inner cylinder are measured, at a given depth of immersion relative to the rotor lip, over a fair speed range. The relative depth of immersion is changed and the process is repeated. Normally, more than two depths of immersion are used. Only the data in the laminar flow region is used.

Since this calibration is carried out with a Newtonian fluid, a plot of the torque speed data is linear, over the laminar flow range, and passes through the origin. The best fit straight line is drawn through the data to intersect the origin. The mean torque at some convenient speed is estimated. This is repeated for each depth of immersion. These mean torques, at the chosen speed, are plotted against their respective depths of immersion. Since this plot should be linear (11, 20), the best fit straight line is drawn through this data and is extrapolated to zero torque. This line intersects the depth of immersion axis at some negative value, Δh , The previous procedures are repeated for a series of liquids of different viscosities.

It has been found (11, 15, 20) the value of Δh is independent of the viscosity. In other words, this end effect is equivalent to some constant height of fluid in the annulus. Therefore the equations derived in Appendix C may be used directly if the depth of immersion is increased by this height equivalent to the end effect.

Green (11) indicates, but gives no supporting data, that the height equivalent to the end effect is independent of the type of fluid used.

The relative end effect, from the scanty data in the literature (11, 15, 20) seems to depend on the width of the annulus and varies as the radius raised to a power somewhat greater than

[illegible]

[illegible]

[illegible]

[illegible]

[illegible]

unity. These reported end effects, reduced to a height to diameter ratio of about 1.5 and a diameter of about 1 inch, do not exceed about 10%. Therefore, any variations in the relative end effect for a given system should be unimportant.

The theory behind this approach to a constant relative torque is shown, qualitatively, in Sketch #12 which illustrates the forms the surfaces of constant angular velocity might be expected to take, with a Newtonian fluid, if the outer cylinder rotates and the inner cylinder is motionless.

The velocity gradient, and therefore the shear stress, varies directly as the radius and inversely as the distance between the surfaces. As well, the torque varies directly as the shear stress times the radius.

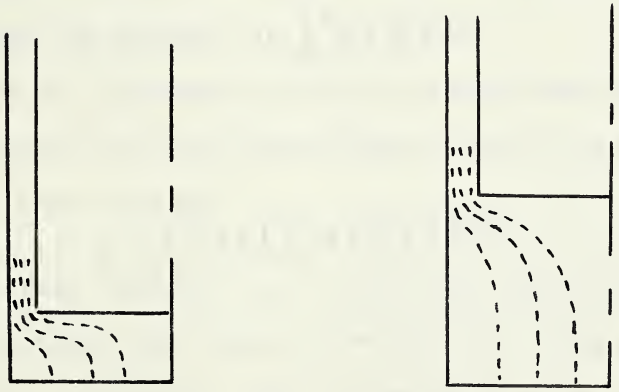

SKETCH #12. THE SURFACES OF CONSTANT ANGULAR VELOCITY IN A ROTATIONAL VISCOMETER.

It is seen that the region of high velocity rapidly approaches the rim of the inner cylinder as the clearance increases. Therefore it might be predicted that the torque on the base would drop off asympototically to a constant value as the clearance increased. This is confirmed experimentally (15).

APPENDIX E

THE CALCULATION OF THE VOLUMETRIC RATE OF FLOW, IN THE LAMINAR FLOW REGION, THROUGH STRAIGHT TUBES FROM THE ABSOLUTE CONSISTENCY CURVE OF A FLUID.

If, for some fluid, the velocity gradient is some known unique function of the shearing stress, it is always possible to develop the equations of laminar flow of the fluid through straight tubes of constant circular cross-section. The general mathematical approach is:

a) determine, from the experimentally obtained absolute consistency curve, a mathematical relationship between the velocity gradient and the shearing stress; $\frac{du}{dr} = \phi_1(s) = \phi_1\left(\frac{pr}{2}\right)$

b) calculate the velocity as a function of the pressure gradient and the radius, $u = \int_R^r \phi_1\left(\frac{pr}{2}\right) dr$ (E 1)

c) sum the products of the velocities and their cross-sectional areas over the whole tube, that is, evaluate the volumetric rate of flow

$$Q = \int_R^0 2\pi r \left[\int_R^r \phi_1\left(\frac{pr}{2}\right) dr\right] dr \qquad \text{(E 2)}$$

Since this method, for fluids other than Newtonians and Bingham Plastics, may prove extremely laborious, a simpler method of attack is desirable. The following section shows how the volumetric rate of flow may be found from the absolute consistency curve by two simple graphical integrations.

Consider the absolute consistency curve, of a fluid whose velocity gradient is a unique function of the shearing stress, shown in Sketch #13.

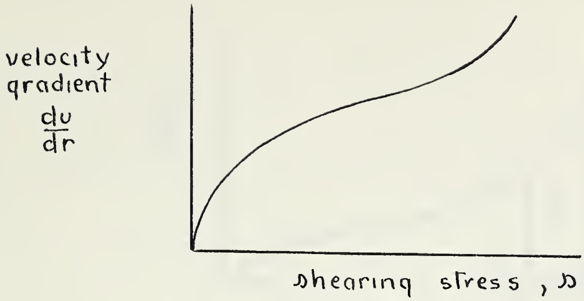

SKETCH #13. AN ABSOLUTE CONSISTENCY CURVE.

It is seen that the area under the curve has the dimensions of power per unit volume. This concept may be extended to the flow through a tube.

Define power per unit volume, ω as the force, acting on an element of fluid of unit length, multiplied by the distance it acts through in unit time, u , and divided by the volume of the element it acts on.

It has been shown (Appendix A) that the shearing stress per unit area in a pipe is equal to half the pressure gradient, p , times the radius to that element, . Therefore the value of s may be replaced by $\frac{pr}{2}$ on the absolute consistency curve.

Now, for the cylindrical element of fluid of radii r and $r+dr$, illustrated on Sketch # 5 , the power per unit volume may be written,

$$\omega_r = \frac{p(2\pi r\,dr)u_r}{2\pi r\,dr} = pu)_r \qquad \text{(E 3)}$$

and the term $pu)_r$ may be written in a more convenient form,

$$pu)_r = p\int_0^u du = p\int_r^R \left(\frac{du}{dr}\right)_r dr = 2\int_{\frac{pr}{2}}^{\frac{pR}{2}} \left(\frac{du}{dr}\right)_r d\left(\frac{pr}{2}\right) \qquad \text{(E 4)}$$

But the integral, $\int_{\frac{pr}{2}}^{\frac{pR}{2}} \left(\frac{du}{dr}\right)_r d\left(\frac{pr}{2}\right)$, represents an area, A , under the consistency curve, between the limits $s = \frac{pR}{2}$ and $s = \frac{pr}{2}$ as illustrated in Sketch #14.

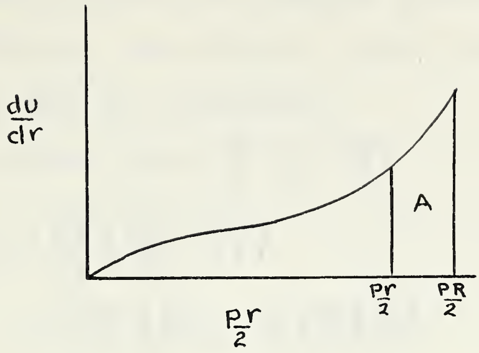

SKETCH #14. POWER PER UNIT VOLUME AT RADIUS R IN A PIPE.

The total power consumption per unit length of pipe is therefore the sum of all the elementary volumes across the tube times the power expended on the respective volumes,

$$w = \int_0^w dw = \int_0^R 2\pi r\,dr \left[2\int_{\frac{pr}{2}}^{\frac{PR}{2}} \left(\frac{du}{dr}\right) d\left(\frac{pr}{2}\right)\right] \qquad \text{(E 5)}$$

$$\frac{\text{Power per unit length}}{\text{pressure gradient}} = \frac{\text{average distance fluid travels} \times \text{cross-sectional area}}{\text{time of flow}}$$

= volumetric rate of flow, Q .

Therefore $$Q = \frac{4\pi}{p}\int_0^R \left[\int_{\frac{pr}{2}}^{\frac{PR}{2}} \left(\frac{du}{dr}\right) d\left(\frac{pr}{2}\right)\right] r\,dr \qquad \text{(E 6)}$$

which integral is presented by the area under the curve formed from a plot of $\frac{4\pi r A}{p}$ against r as illustrated in Sketch #15.

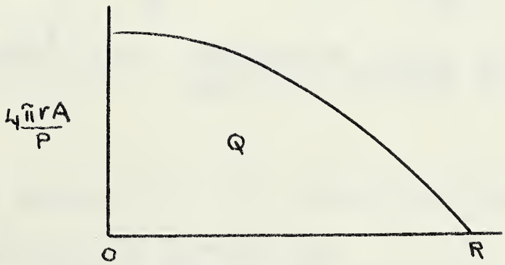

SKETCH #15. EVALUATION OF VOLUMETRIC RATE OF FLOW.

This method of approach must yield the equations of laminar flow of Newtonian fluids or of Bingham Plastics if the appropriate relationships between the shearing stress and the velocity gradient are substituted into the integrals.

For a Newtonian fluid, $\frac{du}{dr} = \frac{1}{\mu}\left(\frac{pr}{2}\right)$

therefore

$$A = \int_{\frac{pr}{2}}^{\frac{pR}{2}} \left(\frac{du}{dr}\right) d\left(\frac{pr}{2}\right)$$

$$= \frac{1}{2}\left(\frac{pR}{2}\right)\left(\frac{du}{dr}\right)_R - \frac{1}{2}\left(\frac{pr}{2}\right)\left(\frac{du}{dr}\right)_r$$

$$= \frac{1}{2\mu}\left(\frac{pR}{2}\right)^2 - \frac{1}{2\mu}\left(\frac{pr}{2}\right)^2$$

$$= \frac{p^2}{8\mu}\left(R^2 - r^2\right) \tag{E 7}$$

and $$\frac{4\pi r A}{p} = \frac{\pi p}{2\mu}\left(R^2 - r^2\right) r$$

Therefore $$Q = \sum_{r=0}^{r=R} \frac{\pi p}{2\mu}\left(R^2 - r^2\right) r = \int_0^R \frac{\pi p}{2\mu}\left(R^2 - r^2\right) r\, dr \tag{E 8}$$

$$= \frac{\pi R^4 p}{8 L \mu} \quad \text{which is Poiseuilles equation} \tag{E 9}$$

For a Bingham Plastic, $\frac{s - f}{\eta} = \frac{du}{dr}$ or $\left.\frac{\frac{pr}{2} - f}{\eta} = \frac{du}{dr}\right)_r$

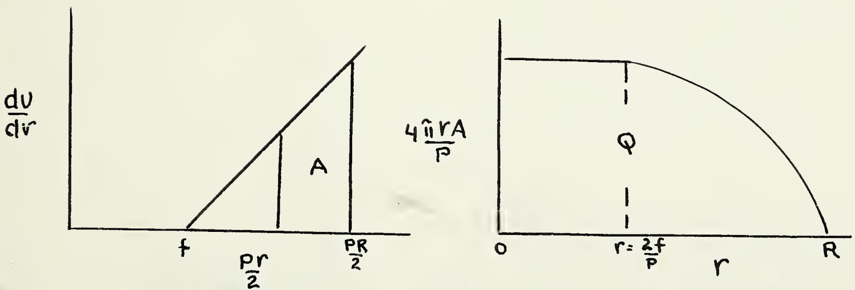

SKETCH #15. EVALUATION OF THE VOLUMETRIC RATE OF FLOW OF A BINGHAM PLASTIC.

From the geometry of the consistency curve of the Bingham plastic illustrated in Sketch #15,

$$A = \frac{1}{2}\left[\left(\frac{pR}{2} - f\right)\left(\frac{du}{dr}\right)_R - \left(\frac{pr}{2} - f\right)\left(\frac{du}{dr}\right)_r\right]$$

$$= \frac{1}{2\eta}\left[\left(\frac{pR}{2} - f\right)^2 - \left(\frac{pr}{2} - f\right)^2\right] \tag{E10}$$

Since the function is discontinuous at $\frac{Pr}{2}=f$, the integration, for Q , must be carried out separately for the two regions of flow, therefore

$$Q = \sum_{r=0}^{r=\frac{2f}{P}} \frac{4\pi r A}{P} + \sum_{r=\frac{2f}{P}}^{r=R} \frac{4\pi r A}{P} \tag{E11}$$

$$= \frac{2\pi}{P\eta}\left\{\int_0^{\frac{2f}{P}} \left(\frac{Pr}{2}-f\right)^2 r\,dr + \int_{\frac{2f}{P}}^{R} \left[\left(\frac{PR}{2}-f\right)^2 - \left(\frac{Pr}{2}-f\right)^2\right] r\cdot dr\right\} \tag{E12}$$

$$= \frac{\pi R^4}{8\eta}\left[P - \frac{8}{3}\frac{f}{R} + \frac{1}{3}\left(\frac{2f}{P}\right)^4 \frac{1}{P^3}\right]$$

which is Buckinghams (E13) equation for a Bingham plastic which exhibits no slippage flow at the walls.

APPENDIX F

ANALYSIS OF THE TORQUE-ANGULAR VELOCITY DATA FOR A MATERIAL APPROXIMATING A BINGHAM PLASTIC

A common approach to the analysis of the consistency curve of a non-Newtonian fluid, particularly in the case of suspensions, is to assume they behave as Bingham plastics.
However, with rotational viscometers which are incapable of high rates of shear in the laminar flow region, the resultant torque - angular velocity curves may exhibit only small "linear portions". This may be due to the fluid properties and, or, to the dimensions of the instrument. It is therefore of interest to investigate the influence of yield value, mobility, and the ratio of annulus width to radius, on the shape of the torque - angular velocity curves for Bingham plastics.

The equations of Reiner and Riwlin (24) may be rearranged into the form, $\omega = \frac{T}{4\pi h\eta}\left(\frac{1}{R_1^2} - \frac{1}{r^2}\right) - \frac{f}{\eta}\ln\frac{r}{R_1}$ where r is the outer radius of laminar flow. Since $T = 2\pi r^2 hf$, the angular velocity, Ω, at which laminar flow across the whole annulus is just reached is given by, $\Omega_d = \frac{fT}{2\eta}\left(\frac{1}{T_f} - \frac{1}{T}\right) - \frac{f}{2\eta}\ln\frac{T}{T_f}$ where T_f is the torque as $\omega \rightarrow 0$.

Holding h, f, η, and R_1 constant, and rearranging into the variable and constant terms yields the general equation,

$$\Omega_d = \frac{f}{2\eta}\left(\frac{T}{T_f} - \ln T\right) - \frac{f}{\eta}\left[\ln 2\pi hf + 2\ln R_1 - 1\right] \qquad \text{(F 1)}$$

Plots of this equation and its first and second derivatives are shown in diagram #26.

Substitution of $a = \frac{r}{R_1}$ into this equation yields,

$$\Omega_d = \frac{f}{\eta}\left[\frac{a^2 - (1 + \ln a^2)}{2}\right] \qquad \text{\_\_\_\_\_\_ curve A} \qquad \text{(F 2)}$$

Differentiation of equation F1 with respect to torque, rearrangement, and sibstitution of $a = \frac{r}{R_1}$ gives

$$\frac{dT}{d\Omega_d} = \left(\frac{2a^2}{a^2-1}\right) 2\pi R_1^2 h \eta \qquad \text{.........Curve B} \qquad (F\ 3)$$

A second differentiation with respect to Ω yields

$$\frac{d^2T}{d\Omega_d^2} = \left[\frac{a^2}{(a^2-1)^3}\right] 8\pi R_1^2 h \frac{\eta^2}{f} \qquad \text{.........Curve C} \qquad (F\ 4)$$

Diagram # 26 shows how the ratio of the cylinder radii $\frac{R_2}{R_1} = a$ influence:

a) the velocity at the end of the curved portion of the torque - angular velocity curves,

b) the slope at the end of the curved portion which is the slope of the linear portion of the torque - speed curves,

c) the rate of change of slope at the end of the curved portion.

The most important point brought out by these curves is the rapidity at which the rate of change of the slope of the torque - speed curves fall off as the value of the ratio of the cylinder radii increases above say 1.1. This is of particular importance in determining the consistency curves of those fluids which only approximate Bingham plastics.

Sketch #17 illustrates the effect of increasing the annulus width, for a given inner cylinder radius, on the torque - speed curves of a Bingham plastic.

FIGURE #26

Effect of Ratio of Cylinder Radii on Torque - Speed Curves for a Bingham Plastic.

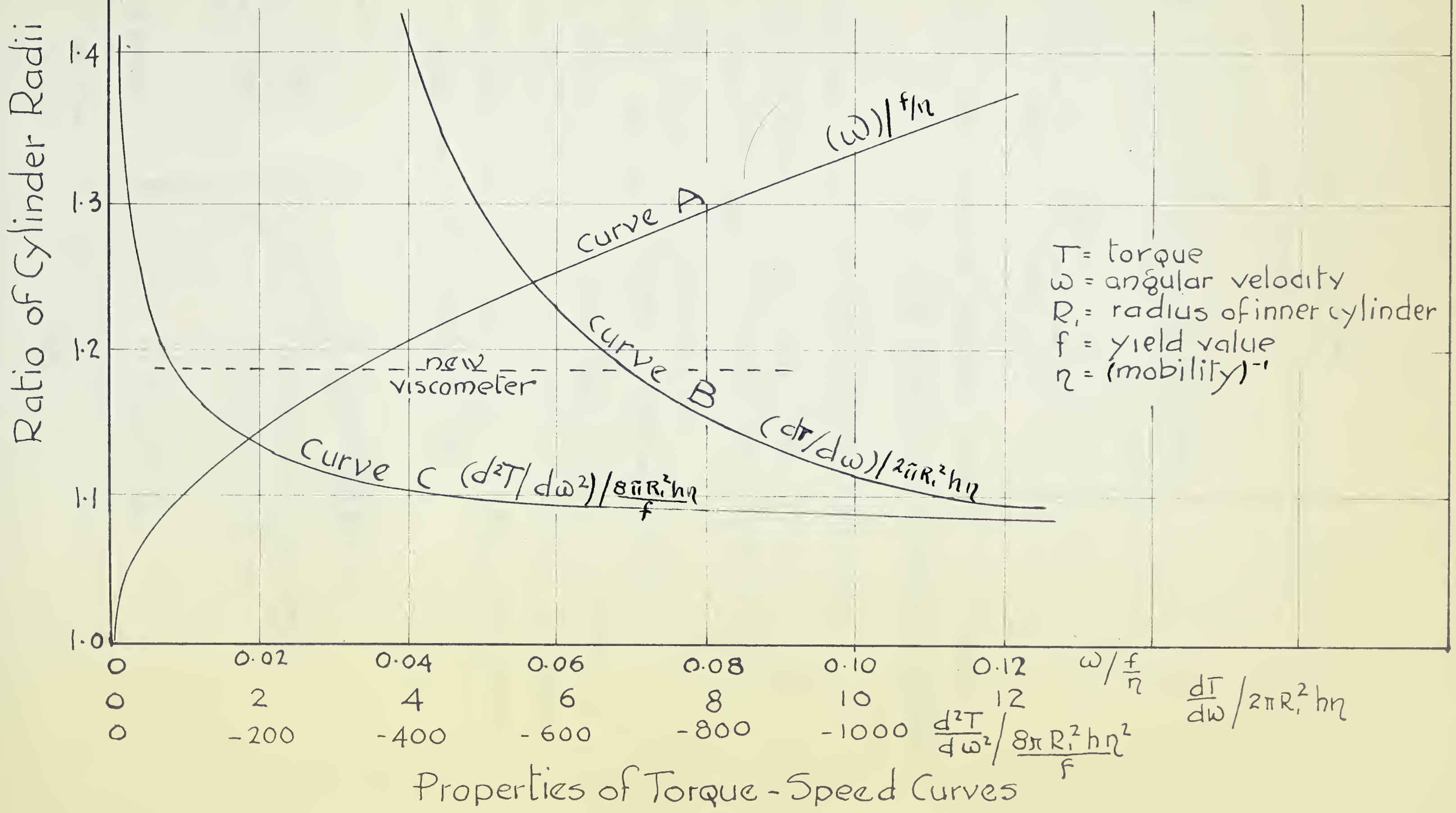

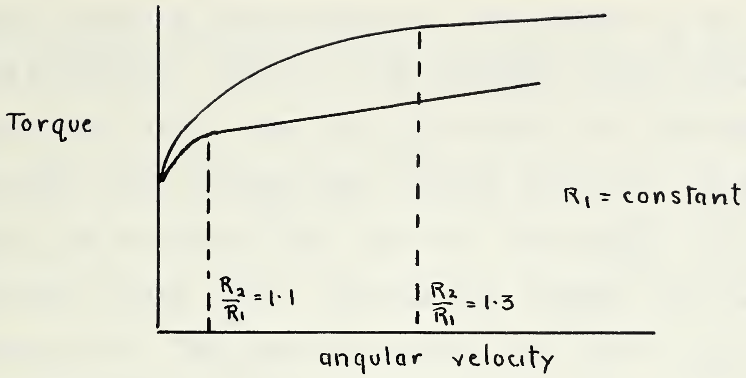

SKETCH #17. THE EFFECT OF ANNULUS WIDTH ON THE TORQUE - ANGULAR VELOCITY CURVES FOR A BINGHAM PLASTIC.

It is evident that increasing the annular width will complicate the interpretation of the data since the end of the linear portion, while it may be determined quite accurately for $\frac{R_2}{R_1} = 1\cdot 1$, is open to question when $\frac{R_2}{R_1} = 1\cdot 3$.

When a material only approximates a Bingham plastic, increasing the annular width greatly complicates the problem of deciding which portion of the curve is to be considered "linear". The absolute consistency curve and the torque - angular velocity curve for such a fluid are shown in Sketch #18.

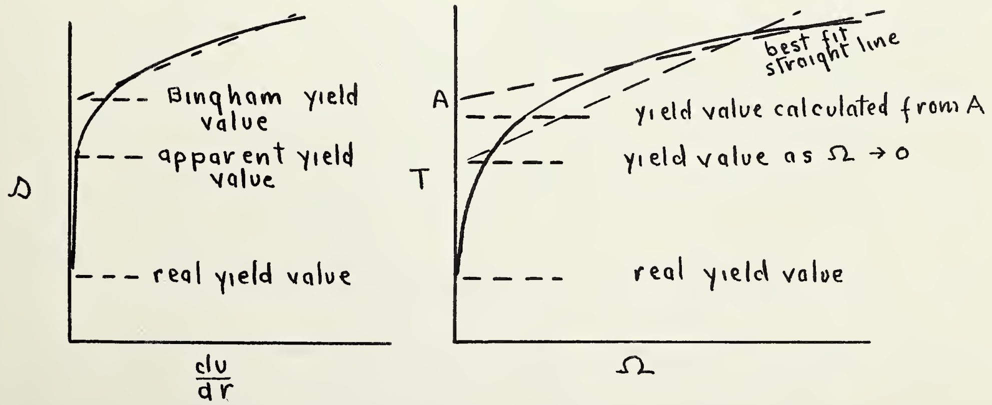

SKETCH #18. THE ABSOLUTE CONSISTENCY CURVE AND THE CORRESPONDING TORQUE - ANGULAR VELOCITY CURVE FOR A MATERIAL APPROXIMATING A BINGHAM PLASTIC.

The existence of a curved portion between the "apparent yield value" and the "Bingham yield value" on the absolute consistency curve causes a large apparent discrepancy in the torque - speed relationships. That is, the apparent yield value, as the speed approaches zero, does not agree with the intercept, of the best straight line through the "linear portion", on the torque axis. Also, the straight line from the intercept, calculated from the apparent yield value, through the "linear portion" does not seem reasonable. The problem becomes even more complicated with a wider annulus.

One method of attack which produces self-consistent results - and tends to remove the nagging doubts regarding the interpretation of the data - is to draw the best straight line through what appears to be the linear portion of the curve, calculate the yield value and the mobility, and find the value of Ω_d corresponding to these values. This angular velocity should correspond to that at the lower end of the curve over which the straight line was drawn.

APPENDIX G

APPROXIMATE MECHANICAL FORCE BALANCE ON A STORMER VISCOMETER

The viscous torque on the rotor, the inner cylinder, of the Stormer Viscometer cannot, as yet, be calculated. The friction in the instrument must be determined by experiment. Consequently, the operating characteristics of this machine can be determined only be experiment. The following approximate mechanical force balance on the Stormer was developed with a view to developing a satisfactory calibration technique.

The rotor is driven, via a gear train, by a falling weight. Experiment shows that the acceleration may be neglected, after about the first ten revolutions, when a liquid is in the system.

In order to simplify the analysis, it is assumed: that there is no acceleration after 25 revolutions; that the force, W_0, required to just keep the system moving is a constant; and that all further friction is directly proportional to the applied load, W, minus the initiating load, i. e. the friction is $(W-W_0)K$.

The thread, which transmits the force of the falling weight, is wrapped around a line drum of radius R_1. This drum is joined to a gear having an effective radius of R_2, i.e. the number of gear teeth is R_2. This gear drives another, of effective radius R_3, which is joined to the rotor shaft. On the basis of the above assumptions regarding the friction, the torque on the rotor is, $(W-W_0)(1-K)\frac{R_1 R_3}{R_2}$.

Assume that the flow pattern, over the lower speed range, is independent of speed and viscosity. Then the viscous torque on the rotor is some constant, b, times the angular velocity, Ω,

[illegible]

[illegible]

[illegible]

[illegible]

[illegible]

[illegible]

[illegible]

[illegible]

times the viscosity, μ , or the torque is $b\Omega\mu$.

Therefore the overall torque balance is

$$(W-W_0)(1-K)\frac{R_1R_3}{R_2} = b\Omega\mu$$

If the above analysis is correct, a plot of net load divided by the angular velocity against viscosity will be a straight line. This plot is the calibration curve of the instrument.

Accordingly, the adopted calibration procedure is:

a) measure the load which just keeps the system moving in air.

b) allow a starting period of 25 revolutions,

c) plot the net load against the angular velocity for each of the standard Newtonian fluids,

d) plot the slopes of these curves, as the angular velocity becomes small, against the viscosity. This is the calibration curve of the instrument.

APPENDIX H

SUMMARY OF DATA FROM ROTATIONAL VISCOMETER.

1) Dimensions of cylinders

a) Radius of outer cylinder	0.882 in.
b) Height of outer cylinder (wall length)	4.656 in.
c) Radius of inner cylinder	0.744 in.
d) Length of inner cylinder (wall length)	4.61 in.
e) Torsion wire length	10.5 in.

2) Calibration of torsion wires with Newtonian oils.

Procedure:

a) The temperature is held constant at 70 ± 0.2 deg F.

b) At zero depth of immersion, the lower rim of the inner cylinder is level with the lip of the outer cylinder.

c) The inner cylinder is lowered a given distance into the outer cylinder.

d) The oil is added until it flows freely over the lip of the outer cylinder.

e) The initial deflection of the protractor is recorded.

f) The number of revolutions are chosen such that the time is measurable within 1%. The timing is repeated.

g) At the end of the run, the deflection is recorded. It must agree with the initial deflection.

Data:

The following tables, #2 to #7, list, for a given viscosity, the number of revolutions, the mean time (secs), the mean deflection (deg), the net deflection (deg) the speed (rps), the depth of immersion (in.).

Table No. 2

CALIBRATION OF TORSION WIRE # 32

5.413 centipoises oil

Revs.	Time (secs)	Deflection (deg)	Net Deflection (deg)	RPS	Immersion (in)	
	initial	282.3	(oil in dash pot)			(2 Mar)
5	41.1	270.7	11.6	0.122	4	
10	44.0	259.2	23.1	0.227		
10	29.6	243.1	39.2	0.337		
15	33.4	229.6	52.7	0.449		
20	35.6	216.3	66.0	0.562		
25	37.5	203.0	79.3	0.667		
25	32.3	189.8	92.5	0.774		
40	36.3	149.5	132.8	1.10	4	
	initial	282.3	(oil in dash pot)			(2 Mar)
5	41.3	275.3	7.0	0.122	2	
10	43.8	268.4	13.9	0.228		
10	29.5	261.3	21.0	0.337		
15	33.3	253.7	28.6	0.450		
20	35.6	246.2	36.1	0.562		
25	32.1	231.0	51.3	0.779		
40	36.3	207.7	74.6	1.10	2	
	initial	206.7	(oil in dash pot)			(6 Mar)
3	44.0	199.0	7.7	0.068	4	
4	32.8	192.7	14.0	0.122		
6	34.4	186.4	20.3	0.174		
8	34.7	179.6	27.1	0.230		
10	35.6	173.6	33.1	0.281		
12	35.4	166.7	40.0	0.339		
14	35.7	160.3	46.4	0.392		
16	35.4	153.4	53.3	0.452		
18	36.0	147.0	59.7	0.500		
20	35.6	139.9	66.8	0.562		
22	35.9	133.5	73.2	0.613		
24	36.0	126.2	80.5	0.667		
25	32.3	113.2	93.5	0.774		
30	33.8	98.9	107.8	0.887	4	
	initial	206.6	(oil in dash pot)			(6 Mar)
3	43.7	200.7	5.9	0.0686	3	
4	32.9	195.9	10.7	0.1215		
8	34.6	186.0	20.6	0.231		
12	35.4	175.7	30.9	0.333		
16	35.3	165.2	41.4	0.450	3	

Revs.	Time (secs)	Deflection (deg)	Net Deflection (deg)	RPS	Immersion (in)	
	initial 206.9		(oil in dash pot)			(6 Mar)
3	44.9	202.9	4.0	0.0668	2	
4	33.1	199.4	7.5	0.121		
6	34.1	196.0	10.9	0.176		
8	34.7	192.5	13.4	0.230		
10	35.6	189.3	16.6	0.281		
14	35.5	181.8	25.1	0.394		
18	35.8	174.5	32.4	0.504	2	
	initial 207.1		(oil in dash pot)			(6 Mar)
3	44.1	206.2	0.9	0.068	1	
4	32.8	205.3	1.8	0.122		
6	33.9	203.1	4.0	0.177		
6	34.5	202.6	4.5	0.174		
8	34.6	200	7.1	0.231		
10	35.5	197.7	9.4	0.282		
14	35.7	192.7	14.4	0.392	1	
	initial 296.0		(no oil in dash pot)			(8 Mar)
3	47.5	288.3	7.7	0.063	4	
3	46.2	288.3	7.7	0.065		
4	34.1	282	14	0.117		
4	33.5	281.6	14.4	0.120		
8	46.4	275.5	20.5	0.172		
8	35.1	269.0	27.0	0.228		
10	36.1	263.0	33.0	0.277		
12	35.7	256.0	40.0	0.336		
14	35.8	249.2	46.8	0.391		
18	39.7	241.5	54.5	0.454		
18	35.9	235.5	60.5	0.501		
20	35.6	228.0	68.0	0.562		
22	35.8	221.8	74.2	0.615		
26	36.0	207.9	88.1	0.723		
28	36.0	201.7	94.3	0.777		
30	35.7	193.8	102.2	0.840		
32	35.7	186.4	109.6	0.895		
34	35.8	179.5	116.5	0.950	4	
	initial 296.0		(no oil in dash pot)			(8 Mar)
3	46.2	290.3	5.7	0.065	3	
4	33.0	285.0	11.0	0.121		
7	40.1	280.1	15.9	0.175		
10	43.6	275.0	21.0	0.229		
10	35.3	270.0	26.0	0.283		
12	35.3	264.8	31.2	0.340		
16	40.1	259.0	37.0	0.399		

[illegible]	[illegible]	[illegible]	[illegible]	[illegible]	[illegible]
[illegible]		[illegible]		[illegible]	
		[illegible]	[illegible]	[illegible]	[illegible]
		[illegible]	[illegible]	[illegible]	[illegible]
		[illegible]	[illegible]	[illegible]	[illegible]
		[illegible]	[illegible]	[illegible]	[illegible]
		[illegible]	[illegible]	[illegible]	[illegible]
		[illegible]	[illegible]	[illegible]	[illegible]
		[illegible]	[illegible]	[illegible]	[illegible]
[illegible]		[illegible]		[illegible]	
	[illegible]	[illegible]	[illegible]	[illegible]	[illegible]
		[illegible]	[illegible]	[illegible]	[illegible]
		[illegible]	[illegible]	[illegible]	[illegible]
		[illegible]	[illegible]	[illegible]	[illegible]
		[illegible]	[illegible]	[illegible]	[illegible]
		[illegible]	[illegible]	[illegible]	[illegible]
	[illegible]	[illegible]	[illegible]	[illegible]	[illegible]
[illegible]		[illegible]		[illegible]	
	[illegible]	[illegible]	[illegible]	[illegible]	[illegible]
		[illegible]	[illegible]	[illegible]	[illegible]
		[illegible]	[illegible]	[illegible]	[illegible]
		[illegible]	[illegible]	[illegible]	[illegible]
		[illegible]	[illegible]	[illegible]	[illegible]
		[illegible]	[illegible]	[illegible]	[illegible]
		[illegible]	[illegible]	[illegible]	[illegible]
		[illegible]	[illegible]	[illegible]	[illegible]
		[illegible]	[illegible]	[illegible]	[illegible]
		[illegible]	[illegible]	[illegible]	[illegible]
		[illegible]	[illegible]	[illegible]	[illegible]
		[illegible]	[illegible]	[illegible]	[illegible]
		[illegible]	[illegible]	[illegible]	[illegible]
		[illegible]	[illegible]	[illegible]	[illegible]
		[illegible]	[illegible]	[illegible]	[illegible]
		[illegible]	[illegible]	[illegible]	[illegible]
		[illegible]	[illegible]	[illegible]	[illegible]
	[illegible]	[illegible]	[illegible]	[illegible]	[illegible]
[illegible]		[illegible]		[illegible]	
	[illegible]	[illegible]	[illegible]	[illegible]	[illegible]
		[illegible]	[illegible]	[illegible]	[illegible]
		[illegible]	[illegible]	[illegible]	[illegible]
		[illegible]	[illegible]	[illegible]	[illegible]
		[illegible]	[illegible]	[illegible]	[illegible]
		[illegible]	[illegible]	[illegible]	[illegible]
		[illegible]	[illegible]	[illegible]	[illegible]

Revs.	Time (secs)	Deflection (deg)	Net Deflection (deg)	RPS	Immersion (in)	
	initial 296.0 (Continued)					
20	39.7	249.0	47.0	0.504		
20	35.5	243.4	52.6	0.564		
20	32.7	238.0	58.0	0.612		
22	32.6	232.0	64.0	0.675		
24	33.0	227.7	68.3	0.727		
26	33.5	222.0	74.0	0.775		
28	33.3	215.7	80.3	0.841	3	
	initial 345.5		(no oil in dash pot)			(9 Mar)
3	44.4	341.5	4.0	0.068	2	
4	32.8	338.1	7.4	0.122		
6	34.6	334.9	10.6	0.173		
8	34.7	331.2	14.3	0.230		
10	35.2	327.9	17.6	0.284		
12	35.5	324.1	21.4	0.338	2	
14	35.6	320.6	24.9	0.393		
18	35.8	313.2	32.3	0.503		
22	35.6	305.6	39.9	0.619		
24	33.1	298.0	47.5	0.728		
10.67 centipoises oil						
	initial 39.3		(castor oil in dash pot)			(2 Mar)
10	86.5	13.4	25.8	0.116	4	
10	45.1	353.7	45.5	0.222		
10	30.1	329.7	69.5	0.332		
20	44.5	303.1	96.1	0.450		
25	44.8	296.1	103.1	0.545		
20	35.7	294.3	104.9	0.561		
30	38.8	232.3	166.9	0.774		
50	50.0	169.1	230.1	1.00		
50	41.5	120.7	278.5	1.20		
50	30.7	18.6	380.6	1.63	4	
	initial 39.0		(castor oil in dash pot)			(2 Mar)
10	87.1	19.4	19.6	0.115	3	
10	45.1	0.8	38.2	0.222		
10	29.9	341.1	57.9	0.334		
20	44.4	321.3	76.7	0.450		
20	35.8	301.7	97.3	0.557		
30	45.0	281.6	117.4	0.667		
50	45.3	202.6	196.4	1.10		
40	45.0	241.1	157.9	0.889		
50	45.5	202.3	196.7	1.10		
50	30.6	102.2	296.8	1.63	3	

Revs.	Time (secs)	Deflection (deg)	Net Deflection (deg)	RPS	Immersion (in)	
	initial 283.5		(castor oil in dash pot)			(2 Mar)
10	85.7	263.0	20.5	0.128	2	
10	44.5	243.3	40.2	0.224		
10	29.7	223.2	60.3	0.336		
20	44.9	202.9	80.6	0.446		
20	35.7	182.7	100.8	0.561		
30	45.2	162.8	120.7	0.665		
30	45.0	120.5	163.0	0.667		
30	36.4	80.6	202.9	0.825	2	
	initial 283.3		(castor oil in dash pot)			(2 Mar)
5	41.8	275.3	8.0	0.119	1	
10	43.8	268.2	15.1	0.228		
15	44.4	260.5	22.8	0.338		
20	44.5	252.4	30.9	0.450		
20	35.8	244.3	39.0	0.561		
25	32.6	227.7	55.6	0.774		
40	36.3	201.7	81.6	1.13		
50	30.5	157.2	126.1	1.64	1	
	initial 265.3		(castor oil in dash pot)			(3 Mar)
5	43.2	239.2	26.1	0.115	4	
10	44.5	214.3	51.0	0.225		
10	29.9	189.3	76.0	0.334		
15	33.5	162.7	102.6	0.448		
20	36.0	137.3	128.0	0.556	4	
	initial 265.0		(castor oil in dash pot)			(3 Mar)
5	41.8	248.7	16.3	0.120	2	
10	43.8	237.0	28.0	0.224		
10	29.7	223.1	41.9	0.334		
15	33.5	209.2	55.8	0.448	2	
	initial 265.5		(no oil in dash pot)			(3 Mar)
5	41.7	257.3	8.2	0.120	1	
10	44.1	250.0	15.5	0.226		
10	29.7	242.6	22.9	0.337		
15	33.4	234.8	31.7	0.449	1	

[illegible]	[illegible]	[illegible]	[illegible]	[illegible]	[illegible]
[illegible]	[illegible]		[illegible]		
	[illegible]	[illegible]	[illegible]	[illegible]	[illegible]
	[illegible]	[illegible]	[illegible]	[illegible]	[illegible]
	[illegible]	[illegible]	[illegible]	[illegible]	[illegible]
	[illegible]	[illegible]	[illegible]	[illegible]	[illegible]
	[illegible]	[illegible]	[illegible]	[illegible]	[illegible]
	[illegible]	[illegible]	[illegible]	[illegible]	[illegible]
	[illegible]	[illegible]	[illegible]	[illegible]	[illegible]
	[illegible]	[illegible]	[illegible]	[illegible]	[illegible]
[illegible]	[illegible]		[illegible]		
[illegible]	[illegible]	[illegible]	[illegible]	[illegible]	[illegible]
	[illegible]	[illegible]	[illegible]	[illegible]	[illegible]
	[illegible]	[illegible]	[illegible]	[illegible]	[illegible]
	[illegible]	[illegible]	[illegible]	[illegible]	[illegible]
	[illegible]	[illegible]	[illegible]	[illegible]	[illegible]
	[illegible]	[illegible]	[illegible]	[illegible]	[illegible]
	[illegible]	[illegible]	[illegible]	[illegible]	[illegible]
[illegible]	[illegible]	[illegible]	[illegible]	[illegible]	[illegible]
[illegible]	[illegible]		[illegible]		
[illegible]	[illegible]	[illegible]	[illegible]	[illegible]	[illegible]
	[illegible]	[illegible]	[illegible]	[illegible]	[illegible]
	[illegible]	[illegible]	[illegible]	[illegible]	[illegible]
	[illegible]	[illegible]	[illegible]	[illegible]	[illegible]
[illegible]	[illegible]	[illegible]	[illegible]	[illegible]	[illegible]
[illegible]	[illegible]		[illegible]		
	[illegible]	[illegible]	[illegible]	[illegible]	[illegible]
	[illegible]	[illegible]	[illegible]	[illegible]	[illegible]
	[illegible]	[illegible]	[illegible]	[illegible]	[illegible]
	[illegible]	[illegible]	[illegible]	[illegible]	[illegible]
[illegible]	[illegible]		[illegible]		
	[illegible]	[illegible]	[illegible]	[illegible]	[illegible]
	[illegible]	[illegible]	[illegible]	[illegible]	[illegible]
	[illegible]	[illegible]	[illegible]	[illegible]	[illegible]
	[illegible]	[illegible]	[illegible]	[illegible]	[illegible]

TABLE No. 3

CALIBRATION OF TORSION WIRE #30

10.67 centipoises oil

Revs.	Time (Secs)	Deflection (deg)	Net Deflection (deg)	RSP	Immersion (in)	
		initial 130.5	(castor oil in dash pot)			(24 Feb)
10	44.8	110.8	19.7	0.223	4	
25	57.8	90.1	40.4	0.432		
25	54.7	89.5	51.0	0.468		
25	37.3	70.5	60.0	0.671		
25	28.4	50.2	80.3	0.880		
50	45.5	30.5	100.0	1.10		
50	30.6	340.6	149.9	1.63	4	
		initial 130.3	(castor oil in dash pot)			(24 Feb)
10	43.7	119.5	10.8	0.229	2	
25	73.7	114.1	16.2	0.339		
25	44.6	103.3	27.0	0.561		
25	31.3	92.4	37.9	0.779		
50	45.5	75.7	54.6	1.10		
50	30.7	47.1	83.2	1.63		
100	36.1	43.8	146.5	2.77	2	
		initial 34.2	(oil in dash pot)			(5 Mar)
10	43.4	13.8	20.4	0.231	3	
10	29.4	3.8	30.4	0.340		
15	33.1	353.5	40.7	0.454		
20	35.6	343.4	50.8	0.562		
20	30.1	333.3	60.9	0.664		
30	38.5	323.3	70.9	0.779	3	
		initial 34.2	(oil in dash pot)			(5 Mar)
10	43.3	23.4	10.8	0.231	2	
10	29.5	18.2	16.0	0.339		
15	33.1	12.5	21.7	0.452		
25	37.2	1.6	32.6	0.672		
30	33.5	350	44.2	0.895	2	
		initial 34.2	(oil in dash pot)			(5 Mar)
10	43.4	28.4	5.8	0.231	1	
15	44.1	25.5	8.7	0.340		
15	26.6	19.2	15.0	0.565		
30	33.8	9.3	24.9	0.888		
40	36.3	2.5	31.7	0.10	1	

Revs.	Time (Secs)	Deflection (deg)	Net Deflection (deg)	RSP	Immersion (in)
20.48 centipoises oil					
		initial 82.3	(castor oil in dash pot) (22 Feb)		
25	44.4	350.3	92.0	0.563	4
50	45.5	259.8	182.0	1.10	
50	30.5	167.7	274.6	1.63	
100	45.8	72.5	369.8	2.18	
100	39.4	12.5	429.8	2.54	4
		initial 81.8	(castor oil in dash pot) (22 Feb)		
25	44.7	10.5	71.3	0.560	3
50	45.6	300.6	141.2	1.09	
100	61.3	229.1	212.7	1.64	
100	45.6	153.8	288.0	2.19	
100	36.0	77.0	? 364.8	? 2.78	3
		initial 81.6	(castor oil in dash pot) (22 Feb)		
25	44.6	33.3	48.3	0.561	2
50	45.6	344.6	97.0	1.10	
50	30.5	293.9	147.7	1.64	
100	45.5	238.8	202.8	2.20	2
		initial 81.8	(castor oil in dash pot) (22 Feb)		
25	44.6	55.9	25.7	0.561	1
50	45.6	28.6	53	1.10	
50	30.5	359.1	82.5	1.64	
100	45.4	326.6	115.0	2.20	
100	36.0	292.4	149.1	2.78	
100	29.9	257.3	184.3	3.34	1
		initial 83.1	(castor oil in dash pot) (23 Feb)		
10	45	47.0	36.1	0.222	4
25	56.5	10.7	72.4	0.443	
30	39.1	317	126.1	0.767	4
		initial 82.3	(castor oil in dash pot) (23 Feb)		
10	44.6	53.6	28.7	0.224	3
25	56.3	25.1	57.2	0.444	
30	38.8	342.5	99.8	0.773	3
		initial 82.1	(castor oil in dash pot) (23 Feb)		
10	44.6	62.3	19.8	0.224	2
25	56.1	42.4	39.7	0.446	
30	38.8	12.6	69.5	0.773	2

Revs.	Time (Secs)	Deflection (deg)	Net Deflection (deg)	RSP	Immersion (in)	
20.48 centipoises oil - continued						
		initial 82.1	(castor oil in dash pot)			(23 Feb)
10	44.7	71.9	10.2	0.224	1	
25	56.1	61.2	21.0	0.446		
25	55.7	60.9	21.2	0.449		
30	39.0	44.5	37.6	0.770	1	
29.49 centipoises oil						
		initial 31.1				(5 Mar)
10	43.5	334.5	56.6	0.230	4	
15	33.5	280.6	110.5	0.448		
20	29.9	226.6	164.5	0.670		
35	39.5	171.6	219.5	0.885		
40	36.4	118.5	272.6	1.10	4	
		initial 31.1				(5 Mar)
10	43.5	348.4	42.7	0.230	3	
15	33.3	306.6	84.5	0.450		
20	29.9	265.2	125.9	0.670		
30	33.9	223.1	168.0	0.886		
40	36.5	182.6	208.5	1.10	3	
		initial 31.1				(5 Mar)
10	43.4	1.7	29.4	0.231	2	
15	33.3	333.3	57.8	0.450		
20	30.0	304.7	86.4	0.668		
30	33.6	275.0	116.1	0.892		
40	35.3	246.7	144.4	1.13	2	
		initial 31.2				
10	43.3	15.2	16.0	0.231	1	
15	33.3	359.7	31.5	0.450		
20	29.9	343.8	47.4	0.670		
30	33.5	327.4	63.8	0.895		
40	36.2	311.5	79.7	1.10	1	

TABLE No. 4

CALIBRATION OF TORSION WIRE #28

20.48 centipoises oil

Revs.	Time (secs)	Deflection (deg)	Net Deflection (deg)	RPS	Immersion (in)	
		initial 14.6				(22 Feb)
25	44.6	328.2	46.4	0.561	4	
50	45.6	281.7	92.9	1.10		
50	30.6	235.5	139.1	1.63		
100	45.6	186.6	188.0	2.19	4	
		initial 14.7				(22 Feb)
25	44.8	350.2	24.5	0.560	2	
50	45.6	325.1	49.6	1.10		
50	30.6	299.2	75.5	1.63		
100	45.7	271.1	103.6	2.19		
50	18.2	242.0	132.7	2.74	2	
		initial 89.2				(23 Feb)
10	44.5	69.7	19.5	0.225	4	
25	56.2	50.0	39.2	0.445		
25	37.9	31.0	58.2	0.660		
50	45.6	352.5	96.7	1.10		
50	38.4	333.5	115.7	1.30		
50	30.7	304.2	145.0	1.63	4	
		initial 89.2				
11	48.7	78.8	10.4	0.226	2	
25	56.0	68.8	20.4	0.447		
25	37.5	58.2	31.0	0.657		
50	50.1	42.5	46.7	1.00		
50	30.8	11.3	77.9	1.62	2	

29.49 centipoises oil

Revs.	Time (secs)	Deflection (deg)	Net Deflection (deg)	RPS	Immersion (in)	
		initial 31.7				(5 Mar)
10	43.3	2.6	29.1	0.231	4	
15	33.2	334.3	57.4	0.450		
20	35.6	320.5	71.2	0.563		
25	37.3	306.7	85.0	0.668		
30	38.5	292.7	99.0	0.779		
30	30.1	264.3	127.4	0.995		
50	30.7	182.6	209.1	1.63		
100	46.4	115.4	276.3	2.16	4	

Revs.	Time (secs)	Deflection (deg)	Net Deflection (deg)	RPS	Immersion (in)	
		initial 31.5				(5 Mar)
10	43.5	9.4	22.1	0.230	3	
15	33.2	348.0	43.5	0.450		
20	30.0	327.0	64.5	0.667		
30	33.8	305.0	86.5	0.887		
40	36.3	283.9	107.6	1.10	3	
		initial 31.5				(5 Mar)
10	43.4	16.6	15.1	0.231	2	
15	33.0	1.7	30.0	0.450		
25	37.4	347.3	44.4	0.668		
30	33.6	332.0	59.7	0.892		
40	36.5	317.4	74.3	1.10	2	
		initial 31.7				
10	43.2	23.4	8.3	0.231	1	
15	33.1	15.3	16.4	0.450		
20	29.7	7.2	24.5	0.674		
30	33.5	358.7	33.0	0.892		
40	30.5	341.9	49.8	1.31		
60	32.3	319.4	72.3	1.86		
80	36.6	305.6	86.1	2.18	1	

39.61 centipoises

		initial 352.8				(5 Mar)
10	44.0	314.3	38.5	0.227	4	
15	33.4	276.5	76.3	0.449		
25	37.5	239.3	113.5	0.667		
30	34.0	201.5	151.3	0.882		
20	35.8	257.7	95.1	0.559	4	
		initial 352.7				
10	44.0	323.4	29.3	0.227	3	
15	33.4	294.4	58.3	0.449		
20	35.7	279.7	73.0	0.560		
25	37.4	265.5	87.2	0.668		
30	33.7	236.1	116.6	0.890		
50	38.1	180.4	172.3	1.31		
100	40.0	20.5	332.2	2.50	3	
		initial 352.7				
10	43.8	332.4	20.3	0.228	2	
15	33.3	312.6	40.1	0.449		
25	44.6	302.7	50.0	0.560		
25	37.4	293.0	59.7	0.668		
30	33.7	272.9	79.8	0.890	2	

Revs.	Time (Secs)	Deflection (deg)	Net Deflection (deg)	RPS	Immersion (in)	
39.61 centipoises - continued						
		initial 352.6				
10	43.4	341.7	10.9	0.231	1	
15	33.3	331.0	21.6	0.449		
20	35.7	325.6	27.0	0.594		
25	37.6	320.2	32.4	0.665		
30	33.6	309.0	43.6	0.890	1	
48.22 centipoises oil						
		initial 17.3				(22 Feb)
25	44.9	267.5	109.8	0.557	4	
50	45.8	161.3	216.0	1.09		
50	30.9	57.0	320.3	1.62		
100	43.6	324.5	413.8	2.30	4	
		initial 16.7				(22 Feb)
30	33.8	292.1	84.6	0.558	3	
50	45.6	209.3	167.4	1.10		
50	30.6	126.8	249.3	1.63		
50	56.3	241.7	135.0	0.887	3	
		initial 16.7				(22 Feb)
25	45.0	319.0	57.7	0.556	2	
50	45.5	261.9	114.8	1.10		
50	30.6	204.5	172.2	1.63		
50	35.4	228.5	148.2	1.41	2	
		initial 16.9				(22 Feb)
25	44.7	346.8	30.1	0.560	1	
50	45.5	315.6	61.3	1.10		
50	30.5	283.3	93.6	1.63	1	

TABLE No. 5

CALIBRATION OF TORSION WIRE #24

48.22 centipoises oil

Revs.	Time (secs)	Deflection (deg)	Net Deflection (deg)	RPS	Immersion (in)	
		initial 68.2				(21 Feb)
25	44.9	83.4	15.2	0.557	4	
50	45.7	82.2(thru 90°)	29.6	1.10		
50	30.8	68.2	43.6	1.62		
100	45.7	53.3	58.5	2.19		
100	35.4	38.0	73.8	2.82	4	
		initial 68.3				
25	45.0	76.3	8.0	0.555	2	
50	45.4	84.0	15.7	1.10		
50	30.8	88.4(thru 90°)	23.3	1.62		
80	36.6	80.2	31.5	2.18	2	

99.51 centipoises oil

Revs.	Time (secs)	Deflection (deg)	Net Deflection (deg)	RPS	Immersion (in)	
		initial 87.5				(21 Feb)
30	54.8	56.7	30.8	0.547	Full	
50	46.0	29.1	58.4	1.09		
50	31.0	- 2.2	89.7	1.61		
100	46.6	-33.4	120.9	2.14		
100	36.5	-64.3	151.8	2.74		
100	30.1	-96.5	184.0	3.32		
100	25.5	-127.0	214.5	3.92	Full	
		initial 87.5				(21 Feb)
25	44.7	63.7	23.8	0.560	Full - 1	
50	45.7	41.0	46.5	1.09		
100	62.4	19.7	67.8	1.60		
100	46.3	-4.5	92.0	2.16		
100	36.5	-29.0	116.5	2.74		
100	30.2	-53.8	141.3	3.31		
100	25.7	-78.7	166.2	3.89	Full - 1	
		initial 39.0				(21 Feb)
25	45	23.7	15.3	0.555	Full - 2	
50	45.6	8.7	30.3	1.10		
50	30.5	-6.0	45.0	1.64	Full - 2	
		initial 37.6				
25	45.4	29.5	8.1	0.550	Full - 3	
50	45.5	21.0	16.6	1.10		
50	30.7	13.3	24.3	1.63	Full - 3	

TABLE No. 6

CALIBRATION OF TORSION WITH #22

99.51 centipoises oil

Revs.	Time (Secs)	Deflection (deg)	Net Deflection (deg)	RPS	Immersion (in)
		initial 82.7			(21 Feb)
25	44.9	70.5	12.2	0.556	Full
50	45.7	58.8	23.9	1.09	
50	36.2	47.8	34.9	1.38	
100	46.2	36.0	46.7	2.16	
100	36.8	24.2	58.5	2.79	
100	30.4	12.5	70.2	3.29	
100	25.6	-0.6	83.3	3.91	Full
		initial 82.7			
35	62.5	76.3	6.4	0.561	Full - 2
50	45.8	70.3	12.4	1.09	
50	36.1	64.5	18.2	1.38	
100	46.4	58.5	24.2	2.15	Full - 2

205.5 centipoises oil

Revs.	Time (Secs)	Deflection (deg)	Net Deflection (deg)	RPS	Immersion (in)
		initial 72.7			(20 Feb)
25	44.9	48.2	24.5	0.558	Full
50	46.0	24.8	47.9	1.09	
50	30.8	0.7	72.0	1.62	
100	46.3	-23.7	96.4	2.16	Full
		initial 73.0			(20 Feb)
25	44.7	54.2	18.8	0.560	Full - 1
50	46.0	36.2	36.8	1.09	
50	30.9	18.5	54.5	1.62	
100	45.7	-0.5	73.5	2.18	
100	36.5	-19.3	92.3	2.74	Full - 1
		initial 72.9			
30	53.5	60.3	12.6	0.561	Full - 2
50	45.8	48.0	24.9	1.09	
100	61.6	36.6	36.3	1.62	
100	46.3	23.0	49.9	2.16	
100	36.5	10.0	62.9	2.74	Full - 2

205.5 centipoises oil - continued

Revs.	Time (Secs)	Deflection (deg)	Net Deflection (deg)	RPS	Immersion (in)
		initial 73.1			
25	44.9	66.1	7.0	0.557	Full - 3
50	46.0	59.5	13.6	1.09	
50	31.0	53.0	20.1	1.61	
100	46.0	46.0	27.1	2.17	
100	36.3	39.0	34.1	2.75	Full - 3

TABLE No. 7

CALIBRATION OF TORSION WIRE #20

205.5 centipoises oil

Revs.	Time (Secs)	Deflection (deg)	Net Deflection (deg)	RPS	Immersion (in)	
		initial 76.4				(22 Feb)
25	44.4	67.8	8.6	0.563	4	
50	45.4	59.7	16.7	1.10		
100	61.7	51.5	24.9	1.62		
100	45.6	43.0	33.4	2.18		
100	36.1	34.1	42.3	2.77		
100	29.7	25.3	51.1	3.36		
100	25.3	16.3	60.1	3.95	4	
		initial 76.4				(22 Feb)
50	45.3	67.6	8.8	1.10	2	
50	30.5	63.6	12.8	1.64		
100	45.7	59.3	17.1	2.18		
100	35.9	54.6	21.8	2.78		
100	29.7	49.7	26.7	3.36		
100	25.4	45.0	31.4	3.94	2	

475.5 centipoises oil

Revs.	Time (Secs)	Deflection (deg)	Net Deflection (deg)	RPS	Immersion (in)	
		initial 92°				(20 Feb)
50	89.2	73.0	19.0	0.560	4	
100	90.7	54.1	37.9	1.10		
100	57.0	31.3	60.8	1.75		
100	44.6	14.8	77.2	2.24		
100	35.0	-4.5	96.5	2.86		
100	30.4	-20.0	112.0	3.29	4	
		initial 92°				
50	85.7	76.6	15.4	0.584	3	
100	90.7	62.7	29.3	1.10		
100	61.4	48.6	43.4	1.63		
100	45.4	33.1	58.9	2.20		
100	35.9	18.6	73.4	2.79		
100	29.6	4.0	88.0	3.38		
100	25.1	-11.0	103.0	3.98	3	
		initial 91.9				(20 Feb)
50	89	81.8	10.1	0.562	2	
50	45.3	72.2	19.1	1.10		
50	30.3	62.5	29.4	1.65		
100	45.5	52.5	39.4	2.20		
100	36.1	42.5	49.4	2.77		
100	29.7	32.3	59.6	3.37	2	

475.5 centipoises - continued

Revs.	Time (secs)	Deflection (deg)	Net Deflection (deg)	RPS	Immersion (in)	
		initial 92.0				(20 Feb.)
50	89.3	86.6	5.4	0.560	1	
50	45.5	81.3	10.7	1.10		
50	30.8	76.2	15.8	1.62		
100	45.6	71.0	21.0	2.20		
100	36.3	65.5	26.5	2.75	1	

The previously listed data are plotted in Figures #2 to #8 inclusive. Figure #9 shows plots of deflection at 1 rps against the absolute depth of immersion for each viscosity and torsion wire. The value of the mean height equivalent to the end effect, obtained from these data by the method outlined in Section Vl, is $\Delta h = 0{\cdot}19$ in . Figure #10 shows plots of the deflection at 1 rps against the relative depth of immersion for the when the absolute depth is unknown.

It has been shown in Section Vl, that the mean torsion wire constant K' may be found from the equation

$$K' = \frac{1}{n}\sum_{1}^{n}\frac{(h+dh)\,\mu\,\Omega}{\theta}$$

where h is the absolute depth of immersion (in.), μ is the viscosity (cp), Ω is 1 rps. and θ is the corresponding mean deflection (deg) obtained from Figures #2 to #6 and #8

The following table, #8, lists, for a given torsion wire and viscosity (cp); the deflections (deg) at 1 rps for each absolute depth of immersion (in.), the corresponding values of K', and the mean value of K' for each viscosity.

Table #8. THE TORSION WIRE CONSTANTS

ION E	VISCOSITY (cp)	DEGREES DEFLECTION AGAINST ABSOLUTE IMMERSION AT 1 RPS				TORSION WIRE CONSTANT AGAINST IMMERSION				MEAN CONSTANT
		4 in	3 in	2 in.	1 in.	4 in.	3 in.	2 in.	1 in.	
	5.413	119.4	92.4	62.0	-	0.190	0.187	0.192	-	0.192
		118.0	89.2	59.6	-	0.192	0.193	0.200	-	
	10.67	228.8	176.4	123.2	68.4	0.196	0.193	0.207	0.185	0.194
	?	211.0	172.6	125.0	68.4	-	0.197	0.204	0.185	
	10.67	90.0	70.5	48.3	-	0.495	0.483	0.483	0.500	0.490
		90.0	-	48.3	-	0.495	-	0.483	-	
	20.48	162.8	129.0	90.0	25.3	0.526	0.507	0.467	0.503	0.501
	29.49	245.7	187.0	129.0	48.3	0.502	0.502	0.500	0.497	0.500
	20.48	88.5	-	46.6	-	0.970	-	0.962	-	0.966
	29.49	127.8	97.2	66.6	36.2	0.966	0.967	0.968	0.967	0.967
	39.61	171.3	131.0	89.6	48.8	0.967	0.964	0.966	0.964	0.965
	48.22	198.4	152.7	104.6	-	1.015	1.01	1.01	-	1.01
	48.22	26.8	-	14.4	-	7.53	-	7.30	-	7.46
	205.5	15.3	-	7.7	-	56.2	-	56.8	-	56.5
	475.5	34.3	25.1	17.8	9.7	58.1	60.4	58.5	59.5	59.1

The following table, #9, lists, for a given torsion wire and viscosity: the deflections (deg) at 1 rps for each relative depth of immersion (in), the slope of the depth of immersion vs. degrees deflection plot, and the mean torsion wire constant for each viscosity.

Table #9. The Torsion Wire Constants.

ION RE	VISCOSITY (cp)	DEGREES DEFLECTION AGAINST RELATIVE IMMERSION AT 1 RPS				SLOPE OF IMMERSION VS. DEFLECTION PLOTS	MEAN CONSTANT
		4 in.	3 in.	2 in.	1 in.		
	48.22	26.8	-	14.4	-	0.178	7.23
	99.51	55.4	42.5	27.4	15	0.0726	8.60
	99.51	21.4	-	11.3	-	0.204	20.3
	205.5	44.4	33.7	22.8	12.4	0.0933	19.1

where the dimensions of the torsion wire constant are

$$\frac{(\text{in})(\text{cp})(\text{rps})}{(\text{deg deflection})}$$

3) The Measurement of the Properties of Clay-Water Slurries.

Procedure:

The procedure is generally similar to that outlined for the Newtonian oils. However, in view of the settling characterisitcs of the muds, rapidity of measurement is of prime importance. The important new details are:

a) The initial deflection is read when the rotor is empty

b) The freshly mixed slurry is pumped in through the filling tube, the inner cylinder being held on centre during the operation. The system is full when the slurry flows freely over the lip of the lip of the rotor.

c) Measurements are commenced as soon as possible after filling.

d) The speed may be determined by the dial setting on the transmission.

e) The deflection is read when the system is empty. It should correspond to the initial deflection.

Data:

a) Since the lower concentration slurries settle readily, a correction for this settling is advisable. The relationship between the stator deflection and the time the slurry is under shear is determined at some rate of shear near the average rate under normal operation. This data is shown on Figure #12 as a plot of % change in torque against time in minutes. The slopes of the linear portion of these curves are the correction factors.

The following table, #10, lists, for a given % solids (wet basis) and depth of immersion (in), the deflection (deg), the time from the initial application of shear (min), the % change in deflection based on the initial deflection, and the correction factor (% change in torque per min).

SETTLING CHARACTERISTICS OF CLAY-WATER SLUVRIES

Deflection (deg)	Time from Application of shear (min)	% Change of Deflection	% Change per min.
20.6% solids (wet basis)			(29 Mar)
4 in. absolute immersion		(Dial setting 5.0)	
141.1	-3		
151.4	0	(basis) 0	
152.6	4.5	0.8	
151.4	6.5	0	
149.4	9.5	-1.3	
147.4	11.5	-2.6	
146.1	14.0	-3.5	
143.7	16.5	-5.1	0.47%
2 in. absolute immersion			
78.9	0	(basis) 0	
79.2	3	0.4	
78.7	4	-0.3	
77.7	6	-1.5	
76.0	9	-3.7	
74.7	11	-5.2	
73.2	13	-7.2	0.67%
17.7% solids (wet basis)			
4 in. absolute immersion		(Dial setting 5.0)	
89.2	0	(basis) 0	
90.2	1	1.1	
88.0	7	-1.3	
86.2	9	-3.4	0.71%
2 in. absolute immersion			
43.6	0	(basis) 0	
43.5	1.5	0	
42.6	3.5	-2.3	
41.8	5.5	-4.1	
40.3	8.5	-7.6	1.1%
14.6% solids (wet basis)			
4 in. absolute immersion		(Dial setting 5.0)	
99.9	0 (basis)	0	
99.0	2	-0.9	
98.2	3.5	-1.7	
95.8	6	-4.1	
93.8	9	-6.2	0.79%

14.6% solids (wet basis) - cont'd. (4 Apr.)

Deflection (deg)	Time from Application of shear (min)	% Change of Deflection	% Change per min.
2 in. absolute immersion			
52.3	0	0	
51.7	2	-1.2	
49.2	5.5	-5.9	
47.8	8.5	-8.6	1.2%

The height equivalent to the end effect is assumed to be the same as that determined for the Newtonian oils. The torque is given by $T = 1 \cdot 83 \times 10^{-6} K'\theta$ (lb force ft) where K' is the torsion wire constant $\frac{\text{(in)(cp)(rps)}}{\text{(deg deflection)}}$ and θ is the deflection (deg).

The following tables, #11 to #13, list, for a given slurry and absolute immersion (in), the number of revolutions, the time (sec), the deflection (deg), the net deflection (deg), the speed (rps) and the torque per inch of immersion (lb force ft).

CLAY-WATER SLURRIES

TABLE No. 11

29.4% solids (wet basis), Torsion Wire #24 (26 Mar.)

Immersion (in)	Revolutions	Time (sec)	Deflection (deg)	Net Deflection (deg)	RPS	Torque per in. (lb.force-ft.)
4			initial - 271.0			
	1	31.3	229.5	41.5	0.032	13.5x10-5
	4	31.7	220.1	50.9	0.126	16.4
	6	25.5	215.3	55.7	0.235	17.9
	10	29.5	211.8	59.2	0.339	18.9
	16	35.1	208.6	62.4	0.456	20.0
	20	35.7	205.9	65.1	0.559	20.8
	25	37.4	203.5	67.5	0.668	21.6
	30	33.8	199.7	71.3	0.888	22.8
	20	35.6	204.2	66.8	0.562	21.4
	10	42.9	212.5	58.5	0.234	18.8
4	4	32.5	218.2	52.8	0.122	16.9
			initial 271.0			
4	1	16.9	224.7	46.3	0.059	14.9x10-5
	5	28.5	217.9	53.1	0.175	17.0
	10	35.2	213.6	57.4	0.284	18.4
	15	38.1	210.5	60.5	0.394	19.3
	20	32.7	205.5	65.5	0.614	20.9
	25	30.2	201.8	69.2	0.829	22.1
	20	32.5	205.0	66.0	0.616	21.1
	15	32.9	208.3	62.7	0.454	20.1
	4	31.4	218.7	52.3	0.128	16.7
	4	28.0	218.8	52.2	0.143	16.7
4	15	32.8	210.3	60.7	0.458	19.5
2			initial 271.2			
	1	52.2	250.7	20.5	0.019	13.4x10-5
	4	31.6	243.0	28.2	0.126	17.3
	10	42.3	240.5	30.7	0.236	18.8
	10	29.3	238.7	32.5	0.341	19.8
	15	33.2	237.0	34.2	0.462	20.9
	20	35.7	235.5	36.7	0.560	22.5
	30	33.8	232.5	38.7	0.889	23.7

TABLE No. 12

25.1% solids (wet basis), Torsion Wire #28 27 Mar.

Immersion (in	Revolutions	Time (sec)	Deflection (deg)	Net Deflection (deg)	RPS	Torque per in. (lb.force ft.)
4		initial	247.8			
	1	30.1	71.5	176.3	0.033	7.45x10-5
	4	32.4	19.5	228.3	0.123	9.65
	8	34.3	355.5	253.3	0.233	10.7
	12	35.2	339.9	267.9	0.341	11.3
	14	30.7	327.2	280.6	0.456	11.9
	18	32.0	316.9	290.9	0.562	12.3
	22	32.8	305.3	301.5	0.671	12.8
	30	38.7	294.5	313.3	0.775	13.2
	30	33.8	284.0	323.8	0.887	13.7
	34	34.1	275.1	332.7	0.996	14.1
	40	36.2	267.5	340.3	1.10	14.4
	28	31.7	280.7	327.1	0.884	13.8
	22	32.9	303.0	304.8	0.668	12.9
	19	43.2	328.0	279.8	0.440	11.8
	8	34.2	355.0	252.8	0.234	10.7
4	4	31.3	19.0	228.8	0.128	9.7
2		initial	247.2			
	1	25.9	147.0	100.2	0.039	8.07x10-5
	4	31.8	126.7	120.5	0.126	9.74
	8	34.6	116.3	130.9	0.231	10.55
	12	35.3	108.7	138.5	0.340	11.2
	14	30.8	102.3	144.9	0.455	11.7
	18	32.1	96.9	150.3	0.560	12.2
	22	32.7	90.8	156.4	0.673	12.65
	30	38.7	85.9	161.3	0.775	13.05
	30	33.9	81.3	165.9	0.883	13.4
	12	11.0	74.5	172.7	1.10	13.9
	26	33.4	85.5	161.7	0.779	13.1
	20	35.6	97.2	150.0	0.562	12.1
2	1	8.4	140	107.8	0.119	8.7

TABLE No. 13

21.9% solids, (Wet Basis), Torsion wire #28 29 Mar.

Immersion In	Revolutions	Time (Sec)	Deflection (deg)	Net Deflection (deg)	RPS	Torque per in. (lb.force-ft)
4			initial 247.2			
	4	32.3	114.8	132.4	0.124	5.6x10-5
	8	34.4	100.3	146.9	0.232	6.20
	12	35.4	85.4	161.8	0.339	6.83
	14	31.2	77.0	170.2	0.449	7.37
	18	32.4	69.3	177.9	0.556	7.50
	22	33.1	62.0	185.2	0.664	7.81
	24	30.9	55.2	192.0	0.777	8.12
	28	31.6	48.8	198.4	0.887	8.39
	32	32.5	43.5	203.7	0.985	8.60
	36	32.8	38.7	208.5	1.10	8.80
	30	34.0	44.5	202.7	1.13	8.57
	36	33.0	24.4	212.8	1.09	8.95
	24	31.1	49.0	198.2	0.772	8.38
	22	39.3	63.2	184.0	0.560	7.80
	12	35.2	79.8	167.4	0.341	7.06
	4	31.4	104.6	132.6	0.127	5.60
	2	28.4	119	128.2	0.070	5.41
4	1	24.5	132	115.2	0.041	4.86
2			initial 247.0			
	4	31.8	174	73.0	0.126	5.54
	12	35.1	162.5	84.5	0.342	6.81
	16	28.7	154.2	91.8	0.558	7.40
	26	33.7	147.0	100.0	0.772	8.07
	34	34.4	141.4	105.6	0.987	8.51
	24	35.5	150.2	96.8	0.675	7.82
	14	30.9	160.0	87.0	0.453	7.03
2	8	34.4	170.8	76.2	0.232	6.15

The settling rate correction is assumed to be directly proportional to the depth of immersion and to depend only on the past time under shear. The height equivalent to the end effect is assumed to be that determined for the Newtonian oils. The torque is given by $T = 1.83 \times 10^{-6} K'\theta$ (lb force ft) where K' is the torsion wire constant $\frac{(in)(cp)(rps)}{(deg\ deflection)}$ and θ is the deflection (deg).

The following tables, #14 to #16, list, for a given slurry and absolute depth of immersion (in), the dial setting, the deflection (deg), the reference time (hr), the net deflection (deg), the speed (rps) and the torque per inch of immersion (lb force ft) corrected for settling.

Clay-Water Slurries

Table #14

20.6% solids (wet basis), Torsion wire #28

Immersion (in)	Dial Settling	Deflection (deg)	Time (hr)	Net Deflection (deg)	RPS	Torque per in (lb force ft)
4	Initial 257.1		1056			
	1.0	143.0	1058	114.1	0.126	4.84x10-5
	3.0	122.5		124.6	0.341	5.31
	5.0	108.1		149.0	0.560	6.34
	7.0	96.3	1101	160.8	0.777	6.90
	9.0	86.1		171.0	0.991	7.35
	11.0	77.5	1103	179.6	1.21	7.71
	7.0	93.7	1104	163.4	0.777	7.10
	4.0	110.5		146.6	0.454	6.36
	1.0	138.7		118.4	0.126	4.97
4	0.5	148.7	1106	108.4	0.075	4.75
3	Initial 257.3		1144			
	1.0	167.3	1145	90.0	0.126	5.0x10-5
	3.0	154.0		103.3	0.341	5.77
	5.0	143.5		113.8	0.560	6.37
	8.0	130.7	1148	126.6	0.885	7.15
	11.0	120.2		137.1	1.21	7.80
	8.0	129.2		128.1	0.885	7.32
	4.0	145.5	1150	111.8	0.454	6.37
3	1.0	167.5	1151	89.8	0.126	5.15
	Initial 256.7		1358			
2						
2	1.0	198.0	1401	58.7	0.126	4.75x10-5
	3.0	187.3		69.4	0.341	5.65
	5.0	180.2	1402	76.5	0.560	6.24
	7.0	174.0		82.7	0.777	6.76
	9.0	168.6		88.1	0.991	7.26
	11.0	164.1		92.6	1.21	7.69
	7.0	172.7		84.0	0.777	7.00
	3.0	185.7	1406	71.0	0.341	5.92
	1.0	196.8		59.9	0.126	5.05
2	0.5	202.5	1407	54.2	0.075	4.55

Table #15

17.7% solids (wet basis). Torsion wire #28 (2 Apr)

Immersion (in)	Dial Settling	Deflection (deg)	Time (hr)	Net Deflection (deg)	RPS	Torque per in (lb force ft)
4	Initial 344.2					
	0.5	285.0	1617.5	59.2	0.075	2.57x10-5
	1.0	279.5		64.7	0.126	2.81
	3.0	266.0		78.2	0.341	3.44
	5.0	256.2		88.0	0.560	3.90
	8.0	244.6		99.6	0.885	4.44
	11.0	234.7	1623	109.5	1.21	4.92
	8.0	243.6		100.6	0.885	4.67
	3.0	264.6		79.6	0.341	3.61
4	1.0	278.5	1625	65.7	0.126	2.97
	Initial 344.2		1648			
3	0.5	298.0		46.2	0.075	2.56x10-5
	1.0	294.0		50.2	0.126	2.80
	3.0	283.4	1650	60.8	0.341	3.43
	5.0	275.7		68.5	0.560	3.91
	8.0	266.6		77.6	0.885	4.47
	11.0	259.0	1653	85.2	1.21	4.95
	8.0	265.7		78.5	0.885	4.60
	5.0	274.3		69.9	0.560	4.14
	3.0	282.0		62.2	0.341	3.68
3	1.0	292.7	1656	51.5	0.126	3.08
2	Initial 340.0		1702			
	0.5	312.4		27.6	0.075	2.23x10-5
	1.0	309.3	1705	30.7	0.126	2.50
	3.0	302.3		37.7	0.341	3.12
	5.0	296.9	1707	43.1	0.560	3.60
	8.0	290.3		49.7	0.885	4.20
	11.0	284.6	1709	55.4	1.21	4.73
	8.0	289.6		50.4	0.885	4.32
	5.0	295.6		44.4	0.560	3.82
	3.0	301.3	1711	38.7	0.341	3.36
	1.0	309.4	1712	30.6	0.126	2.69

Table #16

14.6% solids (wet basis). Torsion wire #30 (4 Apr)

Immersion (in)	Dial Settling	Deflection (deg)	Time (hr)	Net Deflection (deg)	RPS	Torque per in (lb force ft)
4	Initial 348.5		1414			
	1.0	279.0	1415	69.5	0.126	1.52x10-5
	3.0	262.3		86.2	0.341	1.91
	5.0	249.4	1418	99.1	0.560	2.23
	8.0	233.4		115.1	0.885	2.60
	11.0	218.8	1420	129.7	1.21	2.92
	8.0	231.9		116.6	0.885	2.64
	5.0	247.3	1422	101.2	0.560	2.34
	1.0	278.2		70.3	0.126	1.62
4	0.5	285.7	1423	54.8	0.075	1.27
	Initial 348.4		1444			
3	1.0	294.4		54.0	0.126	1.55x10-5
	3.0	281.8	1447	66.6	0.341	1.94
	5.0	272.4	1448	76.0	0.560	2.14
	8.0	259.7		88.7	0.885	2.62
	11.0	248.5	1450	99.9	1.21	2.98
	8.0	258.7		89.7	0.885	2.72
	3.0	281.4	1452	67.0	0.341	1.94
3	0.5	300.5	1452.5	47.9	0.075	1.47
	Initial 348		1556			
2	1.0	312.7	1558	35.3	0.126	1.47x10-5
	3.0	303.7		44.3	0.341	1.87
	5.0	297.0	1600	51.0	0.560	2.18
	8.0	288.1		59.9	0.885	2.59
	11.0	280.1	1601.5	67.9	1.21	2.94
	8.0	287.6		60.4	0.885	2.64
	5.0	296.5		51.5	0.560	2.28
	1.0	313.2		34.8	0.126	1.55
	0.5	317.4	1605	30.6	0.075	1.38
2	0.25	320.4		27.6	0.055	1.25

4) Miscellaneous

Table #17

Torsion Wire Diameters

#20	0.0324 in.
#22	0.0251
#24	0.0199
#28	0.0120
#30	0.0101 in.

Table #18

Onset of Oscillation of Stator

Viscosity (cp)	Onset of Oscillations at Immersions of 4 in.	3 in.	2 in.	1 in.
10		2.8 RPS		
20	2.2 RPS	2.8	2.8 RPS	
40		2.5		
50	2.8		2.2	
100	3.1 RPS		2.2	1.6 RPS
200			3.1	3.1
475		4.0 RPS	3.4 RPS	2.7 RPS

APPENDIX I

SUMMARY OF DATA FROM STORMER VISCOMETER #48715

(1) Dimensions of Stormer Viscometer

Dimensions of instrument

a) Radius of line drum plus the radius of the 5 lb. test braided nylon cord (only one layer is permitted)	0.568 in.
b) Effective radius of large gear	274 teeth
c) Effective radius of small gear	25 teeth
d) Radius of rotor shaft	0.121 in.
e) Radius of inner baffle	0.554 in.
f) Inside radius of cylinder	0.594 in.
g) Outside radius of cylinder	0.623 in.
h) Radius of outer baffle	0.697 in.
i) Length of inside baffle opposing inner cylinder	0.91 in.
j) Length of outside baffle opposing outer cylinder (equals length of outer cylinder)	1.38 in.

From Appendix F, gross torque on rotor is $0.052(w-w_0)$ (in. gm) where w is in grams.

(2) Calibration with Newtonian oils

Procedure:

a) The instrument is filled with oil until the upper surface of the rotor is covered with a layer about 1/16 in. deep.

b) The temperature is held constant at 70 ± 0.2 deg. F.

c) A 25 revolutions start-up period is allowed.

d) The time for the next 100 revolutions is measured. Duplicate runs are made.

e) The initiating load (Appendix F) is measured daily.

Data:

The following tables, #19, lists for a given viscosity, the applied load (gm), the time (sec), the number of revolutions, and the speed (rps).

Table #19 Calibration of Stormer Viscometer

2.654 centipoises oil (24 Jan)

LOAD (gm)	REVS.	TIME (secs)	RPS
4.8	100	50.7	1.97
5.8	100	41.4	2.42
6.8	100	35.6	2.81
7.8	100	31.6	3.18

5.41 centipoises oil (24 Jan)

LOAD (gm)	REVS.	TIME (secs)	RPS
4.8	50	37.5	1.33
5.8	100	62.2	1.61
6.8	100	51.3	1.95
7.8	100	44.1	2.27
10.8	100	39.1	2.55
11.8	100	30.3	3.31

Initiating load about 2 gm

10.67 centipoises oil (24 Jan)

LOAD (gm)	REVS.	TIME (secs)	RPS
5.8	50	49.3	1.01
6.8	100	81.0	1.22
8.8	100	60.1	1.67
10.3	50	24.7	2.02
11.8	100	43.9	2.29
16.8	100	32.0	3.12

20.48 centipoises oil (24 Jan)

LOAD (gm)	REVS.	TIME (secs)	RPS
6.8	50	72.5	0.69
8.8	50	52.1	0.96
11.8	50	35.8	1.40
13.8	100	29.7	1.69
16.8	100	48.8	2.06
21.8	100	38.8	2.63
31.8	100	26.8	3.73

29.41 centipoises oil (23 Jan)

LOAD (gm)	REVS.	TIME (secs)	RPS
8.8	50	70.0	0.72
9.8	50	60.6	0.83
11.8	50	49.3	1.01
13.8	100	80.6	1.24
16.8	50	32.9	1.52
21.8	100	50.5	1.98
26.8	100	40.7	2.45
31.8	100	34.7	2.88
36.8	100	30.3	3.30

39.64 centipoises oil (23 Jan)

LOAD (gm)	REVS.	TIME (secs)	RPS
8.8	50	96.0	0.52
11.8	50	65.4	0.77
13.8	50	55.4	0.90
16.8	50	43.3	1.15
21.8	100	66.4	1.50
26.8	100	53.2	1.88
31.8	100	44.5	2.24
36.8	100	38.4	2.60
41.8	100	33.5	2.97

Initiating load is 2.0 gms.

Newtonian oils contd.

48.22 centipoises oil (23 Jan)

LOAD (gm)	REVS.	TIME (secs)	RPS
11.8	50	82.0	0.61
21.8	100	80.5	1.24
26.8	50	32.1	1.56
31.8	100	54.0	1.88
41.8	100	40.5	2.47
51.8	100	32.4	3.08
61.8	100	27.7	3.61

73.51 centipoises oil (23 Jan)

LOAD (gm)	REVS.	TIME (secs)	RPS
16.8	50	87.0	0.58
21.8	50	63.0	0.79
31.8	100	83.3	1.20
41.8	100	61.1	1.64
51.8	100	48.3	2.09
61.8	100	40.3	2.48
71.8	100	34.5	2.90
91.8	100	27.0	3.74

Initiating load is 2.2 gm

99.51 centipoises oil (22 Jan)

LOAD (gm)	REVS.	TIME (secs)	RPS
21.8	100	15.8	0.63
41.8	100	78.7	1.27
51.8	100	62.6	1.60
61.8	100	52.5	1.91
71.8	100	45.3	2.21
81.8	100	40.2	2.49

149.8 centipoises oil (22 Jan)

LOAD (gm)	REVS.	TIME (secs)	RPS
16.8	50	15.7	0.32
26.8	50	90.7	0.55
36.8	50	68.2	0.73
46.8	50	52.7	0.95
56.8	50	42.8	1.17
66.8	100	73.4	1.36
76.8	100	62.7	1.58
86.8	100	55.3	1.80

Initiating load is 2 gm

3) Measurement of friction factor

Procedure:

a) Equal opposing loads are applied to the rotor shaft to counterbalance the load applied to the line drum.

b) The net load on the line drum, $W_f - W_o$, which just keeps falling for a given load on the rotor shaft, W, is measured.

The applied net torque on the line drum is $0{\cdot}052\,(W_f - W_o)$ in. gm. where W is in grams. The counter torque on the rotor shaft is $0{\cdot}121W$ in. gm. The friction factor, $1-K$, is therefore $\frac{0{\cdot}121\,W}{0{\cdot}052\,(W_f - W_o)}$.

The following table, #20, lists the applied loads (gm) and the friction factors.

Table #20 Stormer Friction Factor

Net load on line drum (gm.)	Load on rotor shaft (gm.)	Friction factor
33.75	13.6	0.942
59.75	23.6	0.921
110.75	43.6	0.917

mean friction factor is 0.93

4) Measurement of the properites of Clay-Water Slurries

Procedure:

The procedure is the same as the procedure for Newtonian oils. However, in view of the high settling rates of the slurries and of the danger of appreciable evaporation, the data were taken as rapidly as possible.

Data:

From Appendix F, the net torque on the rotor is given by $9.5 \times 10^{-6}(W - W_0)$ (lb. force ft.) where W is in grams.

The following table, #21, lists for a given % solids (wet basis) the applied load, the number of revolutions, the time (secs.), the net torque (lb. force ft.) and the speed (rps.).

Table #21

Clay-Water Slurries

29.4% Solids (wet basis) (26 Mar)

LOAD (gm)	REVS.	TIME (secs)	TORQUE (lb force ft)	RPS
46	50	57.4	3.81x10-4	0.87
51	100	62.6	4.23	1.60
56	100	42.9	4.70	2.33
58	100	31.4	4.87	3.18
61	100	27.3	5.14	3.66
66	100	21.6	5.58x10-4	4.63

Initiating load 3 gm

25.1% Solids (wet basis) (27 Mar)

LOAD (gm)	REVS.	TIME (secs)	TORQUE (lb force ft)	RPS
31	100	69.1	2.48x10-4	1.45
34	100	44.0	2.74	2.27
36	100	35.7	2.92	2.80
38	100	29.9	3.10	3.34
40	100	25.9	3.28	3.86
42	100	22.9	3.45	4.36
46	100	19.2	3.80	5.2
41	100	23.9	3.36	4.18
36	100	33.1	2.93	3.02
31	100	54.5	2.48	1.83

Initiating load 3 gm

21.9% Solids (wet basis) (29 Mar)

LOAD (gm)	REVS.	TIME (secs)	TORQUE (lb force ft)	RPS
21	50	26.7	1.66x10-4	1.82
24	100	36.5	1.93	2.74
26	100	30.0	2.10	3.33
28	100	25.7	2.28	3.89
31	100	22.0	2.54x10-4	4.55

Initiating load 2¼ gm

20.6% Solids (wet basis) (30 Mar)

LOAD (gm)	REVS.	TIME (secs)	TORQUE (lb force ft)	RPS
16	100	88.8	1.24x10-4	1.13
18	100	56.0	1.42	1.79
20	100	40.1	1.59	2.49
22	100	32.2	1.77	3.10
24	100	27.5	1.95	3.64
26	100	24.5	2.12	4.08
28	100	21.9	2.30x10-4	4.56

Initiating load 2 gm

17.7% Solids (wet basis) (2 Apr)

LOAD (gm)	REVS.	TIME (secs)	TORQUE (lb force ft)	RPS
10.75	100	77.1	0.78x10-4	1.30
12.75	100	48.8	0.95	2.05
13.75	100	42.3	1.04	2.36
14.75	100	36.9	1.13	2.71
15.75	100	33.2	1.22	3.01
16.75	100	30.3	1.31	3.30
18.75	100	26.4	1.48	3.79
21.75	100	22.5	1.75	4.45

Initiating load 2 gm

14.6% Solids (wet basis) (4 Apr.)

LOAD (gm)	REVS.	TIME (secs)	TORQUE (lb force ft)	RPS
6.7	50	55.8	0.407x10-4	0.90
8.7	100	52.3	0.584	1.91
9.7	100	42.2	0.672	2.37
10.7	100	36.8	0.760	2.79
11.7	100	33.8	0.850	3.00
13.7	100	28.3	1.03	3.53

Initiating load 2.1 gm

NOMENCLATURE

ARABIC

A	area
b	constant
c	constant
d	diameter
D	diameter of flow boundary
E	kinetic energy
f	yield value
g	acceleration due to gravity
h	height
l	length
n	number of revolutions per second
p	pressure gradient
P	pressure drop
Q	volumetric rate of flow
r	radius
R	radius of flow boundary
s	shear stress per unit area
t	time
T	torque
U	velocity
V	volume
W	power per unit volume of flowing fluid

SUBSCRIPTS

I	inside
2	outside
w	flow boundary

nomenclature continued

GREEK

η	coefficient of rigidity
ϕ	function of; friction
ρ	density
θ	angle
μ	viscosity
ω	angular velocity
Ω	angular velocity at flow boundary

BLUE PRINTS

Copies of the blue prints of the new viscometer are available on request to the Department of Chemical Engineering at the University of Alberta.

B29763